THESIS
2

MICHIGAN STATE UNIVERSITY LIBRARIES
3 1293 01566 0909

LIBRARY
Michigan State
University

This is to certify that the

dissertation entitled

TECHNOLOGY OF CVD DIAMOND THERMISTOR AND
THIN FILM HEATER

presented by

Gwo-Shii Yang

has been accepted towards fulfillment
of the requirements for

Ph. D. degree in Electrical Engineering

Dr. Han
Major professor

Date 7/25/96

MSU is an Affirmative Action/Equal Opportunity Institution

O-12771

PLACE IN RETURN BOX to remove this checkout from your record.
TO AVOID FINES return on or before date due.

DATE DUE	DATE DUE	DATE DUE
NOV 0 2 1998		
1222 00		

MSU is An Affirmative Action/Equal Opportunity Institution
c:\circ\datedue.pm3-p.1

TECHNOLOGY OF CVD DIAMOND THEMISTOR AND THIN FILM HEATER

By

Gwo-Shii Yang

A DISSERTATION

Submitted to
Michigan State University
in partial fulfillment of the requirements
for the degree of

DOCTOR OF PHILOSOPHY

Department of Electrical Engineering

1996

ABSTRACT

TECHNOLOGY OF CVD DIAMOND THEMISTOR AND THIN FILM HEATER

By

Gwo-Shii Yang

Due to the extended operational environments of modern sensors, it becomes necessary to investigate new materials for optimal sensing performance, especially under harsh environments. The unique intrinsic properties of diamond make it an excellent material for modern sensors.

In the present work, an improved nucleation technique was developed to enhance the diamond nucleation density up to 1.1 x 10^{11} cm^{-2} on Si and oxidized Si wafers. 1 μm thick films were obtained with a mean surface roughness of 30 nm. The ultrahigh nucleation density technique is helpful to reduce the deposition time for obtaining continuous films.

The temperature sensing properties of diamond were studied on single crystal substrates and polycrystalline samples with different grain sizes in the temperature range of 300 - 1000 K. An average difference between temperatures determined by diamond thermistors and those measured by thermocouples was in the range of 0.3289 - 4.8759% (1.4270 - 25.8909 K). The sensitivity factor β of diamond thermistors ranged from 350 - 2200 K with a corresponding room temperature resistance of 0.977 - 509.5 KΩ. It has been found that the effect of doping level on the thermistor sensitivity (β) is less prominent in the case of polycrystalline films. A better linearity of log(ρ) vs. 1000/T relation was obtained for polycrystalline samples. The results suggest that polycrystalline films are preferable to single crystal samples for thermistor application. The maximum

heating temperature and powder density of 950 K and 93 watt/cm^2, respectively, were achieved for heating application. Due to its high thermal conductivity, the substrate temperature was isothermal.

By using a single structure diamond resistor, heat generation and temperature sensing were achieved simultaneously. The average difference between temperatures determined by self-sensing of diamond thin film heaters and reference temperatures measured by thermocouples was in the range of 1.05 - 3.6%. The single structure diamond sensor/ heater device is reported for the first time.

Copyright by
Gwo-Shii Yang
1996

to my family

ACKNOWLEDGMENTS

I would like to express my deep gratitude to my advisor, Prof. D. M. Aslam, for his guidance and support throughout the present work. I am grateful for the opportunity to learn from his example as both a research and an engineer.

I would like to thank Prof. D. Reinhard, Prof. J. Asmussen, and K. P. Kuo for their supply of specimen in the study of nucleation density effects. I also would like to thank Prof. J. V. Beck, Prof. J. J. McGrath, and M. White for their expertise in thermodynamics and optical temperature measurement. Many thanks go to Prof. T. Grotjohn and J. Mossbrucker for the assistance in Raman analysis and L. Hoffman, Prof. B. Golding, and A. Engebretson for their assistance in metal evaporation.

I would also like to thank the members of my research group, S. Sahli, D. Hong, I. Taher, Dr. Kwon, and U. S. Kim, for their assistance and helpful discussion.

Last but not least, I would like to thank my parents for providing me with the opportunity to complete this study. A special thank goes to my wife, Yuh-pyng, for everything I can possibly think of.

TABLE OF CONTENTS

LIST OF TABLES

LIST OF FIGURES

CHAPTER 1

RESEARCH MOTIVATION AND GOALS

1.1 Introduction

The great progress of microelectronics technology has changed many aspects of the life of humanity. Due to advanced integrated circuit technologies, microprocessors and related memory units have become available at relatively low cost not only for professional usages, but also for consumer or household usages. Widespread applications of microprocessors and related memory units, which are able to handle and store information, have created the need for low cost and high performance sensors and actuators in large quantities. Thus, the application areas of sensors and actuators have shifted from the conventional purposes, such as measurement, testing, and/or automation, to more consumer oriented ones (e.g., domestic and automotive electronics, household, safety, comfort, and pleasure) and highly advanced scientific areas (e.g., medicine, environment protection, research, etc.). In order to incorporate modern sensors and actuators into microprocessor-based systems for a variety of applications, the requirements for the sensor and actuator materials are now focused on long-term reliability, compatibility with IC batch fabrication, environmental stability, and capability of micromachining. Materials that are widely used or under investigation for modern

sensor/actuator applications include semiconductors, ceramics, glasses, optical fibers, and polymeric materials [1,2].

Temperature sensors are widely utilized in a variety of areas, such as aerospace, manufacturing industries, medical and biological applications, and household usages [3]. Due to a strong demand in modern automation of machinery and process control, great scientific and technological efforts are necessary to produce temperature sensors with a wide range of temperatures, good measurement accuracy, excellent sensitivity, good stability under various environments, and fast dynamic response. Common types of temperature sensors include thermocouples, resistance temperature detectors (RTD), thermistors, integrated circuit (IC) sensors, diodes and transistors [4,5,6]. Among those different types of temperature sensors, thermistors are not only used to measure temperature but also suitable for a wide range of applications. In the use of temperature sensing, thermistors are reported to be very sensitive but non-linear in the range of -100 to 500 ^{o}C [5]. Other applications of thermistors include flowmeters, liquid level sensors, pressure and vacuum gauges, which are mainly based on the measurements of heat dissipation [3]. For these applications, thermistors with self-heating capability are essential. At present, metal-oxide based materials are commonly used in the commercially available thermistors. The first commercial thermistor was made of UO_2 in Germany in 1932 [3]. The typical maximum operation temperature of those metal-oxide thermistors is somewhat limited to 250 - 300 ^{o}C.

Heat generation is also required in a wide variety of areas. Depending upon the applications, heaters with different element materials, shapes, and configurations are developed to enhance the performance in certain ways. Different heater elements include strip heaters, cartridge heaters, tubular heaters, immersion heaters, and so on. Among all of them, the thick/thin film heater offers the advantages of small sizes and direct deposition on the object to be heated to achieve precise heating. The thick/thin film

heaters commonly available today are based on nickel, aluminum, or carbon steel alloy [7,8]. The maximum operation temperature and power density for those heaters are in the range of 300 - 1300 ^{o}C and 0.8 - 40 watt/cm^{2}, respectively [9,10,11].

In most real life heating applications, temperature sensing and control are essential. For liquid level sensors, mass flow meters, and vacuum and pressure gauges which are based on measurements of heat dissipation, the capabilities of heat generation and temperature sensing are required simultaneously. Since the materials commonly used as heating elements lack high sensitivity to the temperature change, different materials are utilized for heating and temperature sensing. In such a configuration, thermal and chemical properties of materials involved, if not carefully considered, may cause problems. It is also important to minimize the response time and uncertainties in the measurements associated with heat dissipation and placement of sensing and heating elements. The use of a single element as a heater and a temperature sensor may help eliminate such problems. The desired material properties for such an element include high thermal conductivity, ability to be used as an electrical conductor and insulator, high sensitivity to temperature, micromachining capability, resistance to chemical attack, and mechanical stability.

1.2 Objective of This Work

Due to a unique combination of its mechanical, physical, chemical, and electrical properties, diamond has been recognized as an excellent material for high temperature electronics applications [12]. The properties of diamond are well-understood, but the use for active electronic device applications is not feasible at this time because of the difficulties associated with its economical growth and n-type doping. Therefore, the current prognosis for diamond is primarily as a protective coating [13,14], a thermal

management film [15], and a material for electron-emitting cathodes [16,17]. The temperature sensors and thin film heaters, which do not need n-type doping and single crystal diamond, seem to be suitable applications to fully benefit from the excellent properties of diamond. Recent progress in the technology of chemical vapour deposited (CVD) diamond has led to inexpensive high-quality intrinsic or p-type polycrystalline films on various non-diamond substrates. Due to its large band gap, high thermal conductivity, and chemical and mechanic stability, diamond is an excellent material for high temperature sensing and heating applications, especially under harsh environments.

Early work on diamond thermistors has successfully demonstrated the excellent sensing properties of diamond thermistors [18,19]. However, this also revealed some problems mainly associated with the relatively low nucleation density of 10^8 cm^{-2}. There are also some limitations due to the seeding and patterning techniques used today, such as poor selectivity and reproducibility, and restriction to two dimensional structures. In order to utilize diamond for real world temperature sensor/heater applications, it is necessary to develop mature device infrastructure and characterization technologies. Figure 1.1 shows a number of essential techniques needed to be developed. First, a diamond device infrastructure technology is required to successfully fabricate the sensor/heater structures. Then a development in the characterization methods for an emerging material is also important to fully calibrate and evaluate the devices.

The present research mainly focuses on the following issues:

(1) Enhancement in the diamond nucleation density to effectively reduce the grain size, surface roughness, and deposition time for continuous films.

(2) Development of a seeding and patterning technique, which is compatible with standard IC fabrication processes, capable to enhance the selectivity, and

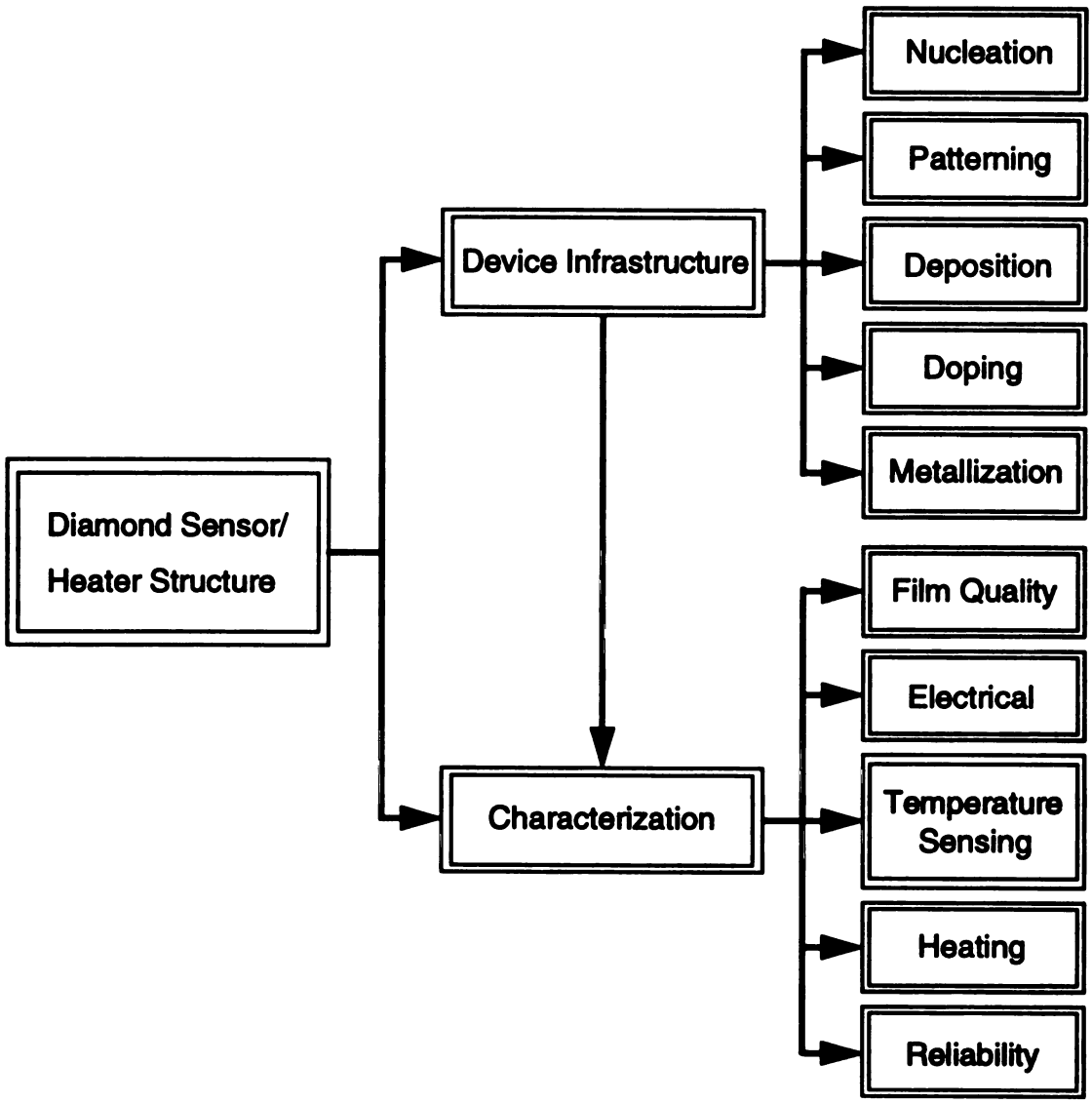

Figure 1.1 Realization of diamond sensor/heater structure.

adaptable to 3-D patterning.

(3) Fabrication of diamond sensor/heater test structures to optimize the device performance.

(4) Study of the sensing and heating properties of diamond.

1.3 Dissertation Organization

In addition to research motivation and goals (chapter 1) and conclusions and future research (chapter 5), this dissertation consists of three major parts, namely, background, diamond device infrastructure, and single element diamond sensor/heater structures. They are described in the chapter 2, 3, and 4, respectively.

In chapter 2, overviews of the current technologies of temperature sensors and thin film heaters are presented. The diamond properties, thin film deposition techniques, and diamond-based sensors are also described in this chapter. Chapter 3 deals with the development of infrastructure technologies for fabrication of diamond sensor/heater devices, which includes thin film deposition, ultrahigh nucleation density, and device fabrication. Chapter 4 focuses on the characterization of diamond sensor/heater test structures. The temperature sensing and heating properties of CVD diamond are discussed.

CHAPTER 2

BACKGROUND

2.1 Introduction

This chapter presents an overview of materials related to the present research. First, a report of current technologies of temperature measurement and thin film heater is presented. The properties of diamond are then examined to illustrate the advantages of diamond for electronic applications. This follows a comprehensive description of the CVD diamond technologies. Toward the end of this chapter, the current status of various diamond sensors are reported.

2.2 Temperature Sensors

Temperature has been defined in a qualitative way as the level of thermal energy, and it has been identified as a state function, one that must be specified in order to characterize the state of a material or system. A variety of material properties have been utilized to determine the temperature and are summarized in Table 2.1. In this section, an overview of the most commonly used thermometers is presented.

TABLE 2.1 Material properties used to measure temperature

Property	Example
Thermal expansion	
Liquid	Mercury thermometer
Solid	Piezoelectric crystal resonant frequency
Gas	Gas thermometer
Electrical resistance	
Metal	Platinum resistance temperature detector
Semiconductor	Thermistor, transistor
Thermoelectric	Thermocouple
Vapor pressure	Liquid hydrogen
Light intensity	Optical pyrometer
Heat emission	Total radiation or infrared pyrometer

2.2.1 Liquid-in-Glass Thermometers

The liquid-in-glass thermometer was the first true temperature measuring instrument [6]. It generally consists of a thin walled glass bulb attached to a glass stem with the bulb and stem system sealed against its environment. The portion of the bulb-stem space that is not occupied with the thermometer liquid usually is filled with a dry inert gas under sufficient pressure to prevent separation of the thermometer liquid. A scale is provided to indicate the height to which the liquid column rises in the stem, and this reading is made to indicate closely the temperature of the bulb. A contraction chamber (an enlargement of the capillary) often is provided below the mail capillary to avoid the need for a long length of capillary or to prevent contraction of the liquid column into bulb. An expansion chamber (an enlargement of the capillary) often is provided above the main capillary to protect the thermometer in the case of overheating. A reference point (usually ice point) should be provided as a check against changes in the bulb volume [4,5,6].

The operation of a liquid-in-glass thermometer thus depends on the coefficient of expansion of the liquid being greater than that of the containing glass bulb. Any increase in the bulb temperature cause the liquid to expand and rise in the stem, with the difference in volume between the bulb and stem serving to magnify the change in volume of the liquid. The most commonly used thermometer liquid is mercury, though mercury-thallium and organic liquids are also used under the circumstance of temperature below 0 ^{o}C. The accuracies of this type of thermometers were reported to be in the range of 0.01 to 1 or 0.1 to 2 ^{o}C, depending on the type of immersion, in the operation temperature range of -328 to 500 ^{o}C [5,6].

2.2.2 Resistance Thermometry

A resistance thermometer generally consists of four major portions as follows [6]:

(1) A sensor, an electric circuit element whose resistance varies with temperature;

(2) A framework on which to support the sensor;

(3) A sheath by which the sensor is protected;

(4) Wires by which the sensor is connected to a measuring instrument (usually a bridge), which is used to indicate the effect of variation in the sensor resistance.

This type of thermometer can be divided conveniently into two basic groups, resistance temperature detectors (RTD) and thermistors, based on the construction materials of metals and semiconductors, respectively. Resistance thermometers provide temperature directly in the sense that no reference junction are involved, and no special extension wires are needed to connect the sensor with measuring instrument. The advantages of resistance thermometers are simplicity of circuits, sensitivity of measurement, and stability of sensors.

2.2.2.1 Resistance Temperature Detector

The RTDs are generally made of platinum (Pt), nickel (Ni), and copper (Cu). The Pt RTD has a quite linear and stable resistance-temperature relation over a wide temperature range and is used exclusively for precise temperature measurement. However, it is extremely sensitive to contamination and to strains. Thus a complex mounting and careful packaging are essential for Pt RTDs. The RTDs made of Cu or Ni are much cheaper than those made of Pt, but the operation temperature ranges are limited.

The dependence of resistance on temperature for most metals above the Debye temperature can be written as a power series [5],

$$R = R_0(1 + At + Bt^2 + Ct^3) \qquad \text{.....(2.1)}$$

Here A, B, C are constants of material. The Callendar equation defined as

$$t = 100\left(\frac{R_t - R_0}{R_{100} - R_0}\right) + \delta\left(\frac{t}{100}\right)\left(\frac{t}{100} - 1\right) \qquad \text{.....(2.2)}$$

is most commonly used for relating platinum resistance to temperature. Here t is degrees Celsius, R is resistance, and δ is a constant representing the small departure from linearity that is appropriate to the particular thermometer. The subscripts on R indicate the resistance at 0 °C, at 100 °C, and at the measured temperature [5,6].

Generally speaking, the RTDs possess a positive temperature coefficient and offer precise temperature measurement over a fairly large temperature range (an accuracy of $\pm$ 0.001 °C is routinely achieved using Callendar equation in laboratory usage [5]). Since the resistance change in temperature of RTDs is small, very accurate measuring instruments are required. Table 2.2 summarizes the characteristics of RTDs made of Pt, Cu, and Ni.

2.2.2.2 Semiconductor Thermistor

A thermistor is a special type of semiconductor with a predictable variation in resistance as temperature is changed. Thermistors can have either negative or positive temperature coefficients of resistance. The former are particular useful for temperature

TABLE 2.2 The characteristics of resistance temperature detectors

	Platinum	Copper	Nickel
Average temperature coefficient (α) of resistance over 0 to 100 °C ($°C^{-1}$)	0.00385 - 0.003927	0.0042	0.0067
Resistivity (Ωcm)	9.81×10^{-6}	1.529×10^{-6}	5.91×10^{-6}
Linearity of resistance versus temperature	Excellent	Excellent	Poor
Useful temperature range (°C)	-260 to 800	-100 to 150	-100 to 500

compensation of electronic circuits and are widely used for this purpose [5]. Most thermistors are compound semiconductors which are usually ceramic compositions of transition metal oxides, such as Cu_2O, Co_2O_3, SnO, TiO_2, Fe_2O_3, NiO, U_2O_3, and Mn_2O_3 [5]. In this case of thermistors, the exactly electrical conduction mechanism is complex and poorly understood. At present, two models are used to provide an explanation for the resistivity-temperature behavior of metal oxide thermistors. One model for electrical conduction theory involves the hopping mechanism which is observed in ferrites and manganites that have a spinel crystal structure. In this model, conduction occurs when charge carriers hop from one ionic site in the spinel lattice to an adjacent site. The other model is based upon a consideration of energy bands. According to this model, the charge carriers are the results of physical impurities rather than chemical impurities, and occur from either an excess or a deficiency of oxygen atoms in the crystal lattice. Regardless of

the mechanism, the resistivity can be described by

$$\rho = \frac{1}{\sigma} \cong \frac{1}{n_i e^{-\Delta E/(kT)} q\mu} = C_0(e^{\Delta E/(kT)}) \quad \text{..... (2.3)}$$

where n_i, k, q, and μ are intrinsic carrier concentration, Boltzmann's constant, electronic charge, and carrier mobility, respectively, and $\Delta E = E_i - E_f$ and $\Delta E = E_f - E_i$ for p-type and n-type semiconductors, respectively. Because the exponential term usually dominates, the resistivity of a thermistor can be approximated by

$$\rho = \rho_0 e^{\frac{\beta}{T}} \quad \text{..... (2.4)}$$

where ρ_0 is the resistivity at infinite temperature and β is a material constant for the device. The resistance R of a resistor is given by

$$R = \rho \frac{L}{A} \quad \text{..... (2.5)}$$

where L is the length and A is the cross-sectional area of the resistor. Using Eq. (2.4) and Eq. (2.5), the resistance can be expressed as

$$R = R_0 e^{\beta\left(\frac{1}{T} - \frac{1}{T_0}\right)} \quad \text{..... (2.6)}$$

In Eq. (2.6), R_0 is the resistance measured at T_0. In semiconductor thermistor technology,

T_0 is often taken at 25 °C. If temperature is the parameter to be determined from resistance measurement, then Eq. (2.6) can be rewritten as

$$T(K) = \left\{ \frac{1}{\beta}\left(\ln\left(\frac{R}{R_0} \right) \right) + \frac{1}{T_0} \right\}^{-1} \qquad \text{..... (2.7)}$$

Due to the non-linearity of ln(R) versus 1/T characteristic of semiconductor thermistors, Eq. (2.7) is valid only for small temperature spans for which the ln(R) versus 1/T characteristic approximates a straight line. Various empirical equations were used to describe the relation between resistivity (or resistance) and temperature of thermistors, which is better than Eq. (2.7). Among those equations, the third order Steinhart-Hart equation [20], defined by

$$\frac{1}{T} = a + b(\ln\rho) + c(\ln\rho)^2 + d(\ln\rho)^3 \quad , \qquad \text{..... (2.8)}$$

is determined to be the best mathematical expression of resistivity-temperature relation for thermistors with negative temperature coefficient [5,6,20].

The sensitivity of temperature response of thermistor is usually characterized by the constant β [3,5,20], defined as

$$\beta = \frac{\ln(R_0/R)}{(1/T_0 - 1/T)} \qquad \text{..... (2.9)}$$

The typical value of β for conventional metal-oxide thermistors ranges from 2000 to 4000 K over a temperature range of 25 to 400 °C [5,20]. Another commonly used parameter of

sensitivity of temperature sensors is the temperature coefficient α, which is defined as

$$\alpha = \frac{1}{R}\frac{dR}{dT} \qquad \text{..... (2.10)}$$

It is usually expressed in terms of percentage change in resistance per degree. In the case of thermistor, α is a strong function of temperature. From Eq. (2.6) and (2.10), α can be represented by

$$\alpha = \frac{-\beta T^{-2} R_0 e^{\beta\left(\frac{1}{T}-\frac{1}{T_0}\right)}}{R_0 e^{\beta\left(\frac{1}{T}-\frac{1}{T_0}\right)}} = -\beta T^{-2} \qquad \text{..... (2.11)}$$

Thermistors offer a variety of applications. For temperature measurement, thermistors are extremely sensitive to temperature change. They may be 1000 to 1 million times more sensitive than a platinum RTD. Figure 2.1 shows the comparison of typical resistance-temperature relation of Pt RTD and thermistors [6]. However, they are less stable and nonlinear as compared to platinum RTD. In addition, the current flowing through a thermistor should be small to minimize Joule heating, which introduces error for temperature reading. For other applications, such as switching, temperature control, and flow measurement, sufficient current to cause Joule heating is desirable. The nonlinear nature of thermistors is undesirable in many applications. For electronic circuitry as well as temperature measurement, the resistance is often modified by combining one or more thermistors with other resistors to enhance the measurement resolution, sensitivity, or linearity. Widely used circuits for correction of non-linearity of thermistors are Wheatstone bridge, Callendar-Griffiths bridge, Smith bridge, and Mueller bridge [3,4,20].

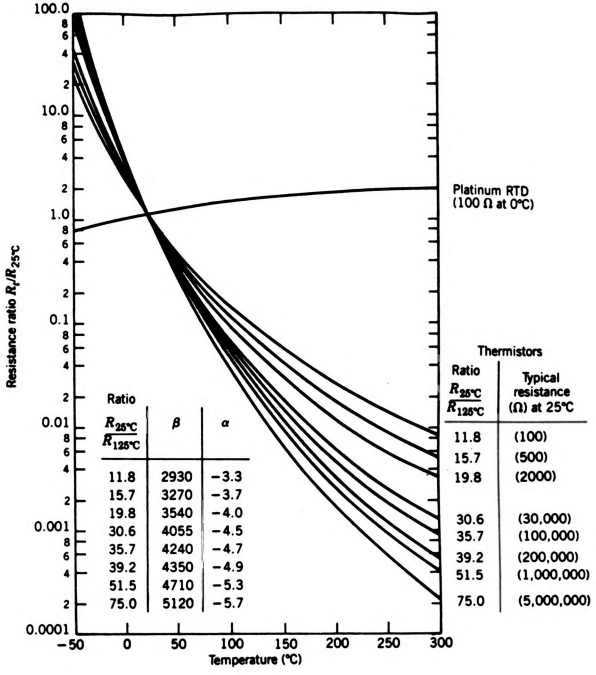

Figure 2.1 Comparison of R-T characteristics for thermistors and Pt RTD.

2.2.3 Thermoelectric Thermometry

Thermoelectric effects have been employed for over 100 years as a practical tool for the measurement of temperature [21]. Thermoelectric temperature measurements are made with thermocouples. Thermocouples are usually made from two dissimilar metal wires connected so that one junction is held at a reference temperature and the other junction serves as the temperature sensing device. The operation principle of thermocouples are known as Seebeck effect, which a temperature difference is converted into an electromotive force called Seebeck voltage. A thermoelectric temperature measurement system usually consists of a sensing element, electrical lead wires, and a voltage measuring instrument.

Different combination of metals or metal alloys are reported to manufacture thermocouples to enhance the performance in a certain temperature range. In general, thermocouples [22] offer a large measuring temperature range and linear response but are less sensitive. Table 2.3 summarizes the compositions, operation temperature range, and limits of error of some commercially available thermocouples [5,6,21]. A plot of Seebeck voltage versus temperature for some common types of thermocouples is shown in Figure 2.2 [5,23].

2.2.4 Optical Pyrometry

The radiation from a hot body may be used as a measure of its temperature. Theoretically either the total radiation emitted or that emitted at a single wavelength can be used. In most cases, it is difficult to ensure the measurement of total radiation due to the strong absorption of infrared band in the atmosphere. In addition, the single wavelength is also difficult to achieved. In the practical application, a narrow band of wavelength is established by a red filter so that calculation of temperature can be made on the basis of an

TABLE 2.3 Summary of important parameters of thermocouples

Type	Positive Wire	Negative Wire	Temperature Range (°C)	Limits of Error (°C or %) Standard	Special
B	$Pt_{70}Rh_{30}$	$Pt_{94}Rh_6$	871 to 1705	0.5%	
E	$Ni_{90}Cr_{10}$	$Ni_{45}Cu_{55}$	0 to 316	1.667	1.25
			316 to 871	0.5%	0.375%
J	Fe	$Ni_{45}Cu_{55}$	0 to 277	2.222	1.111
			277 to 760	0.75%	0.375%
K	$Ni_{90}Cr_{10}$	$Ni_{95}Mn_2Al_2Si_1$	0 to 277	2.222	1.111
			277 to 1260	0.75%	0.375%
N	$Ni_{84.5}Cr_{14.2}Si_{1.4}$	$Ni_{95.5}Si_{4.4}Mg_{0.1}$	0 to 277	2.222	1.111
			277 to 1260	0.75%	0.375%
R	$Pt_{87}Rh_{13}$	Pt	0 to 538	1.389	
			538 to 1482	0.25%	
S	$Pt_{90}Rh_{10}$	Pt	0 to 538	1.389	
			538 to 1482	0.25%	
T	Cu	$Ni_{45}Cu_{55}$	-184 to -101		1%
			-101 to -59	2%	1%
			-59 to 93	0.833	0.417
			93 to 371	0.75%	0.375%

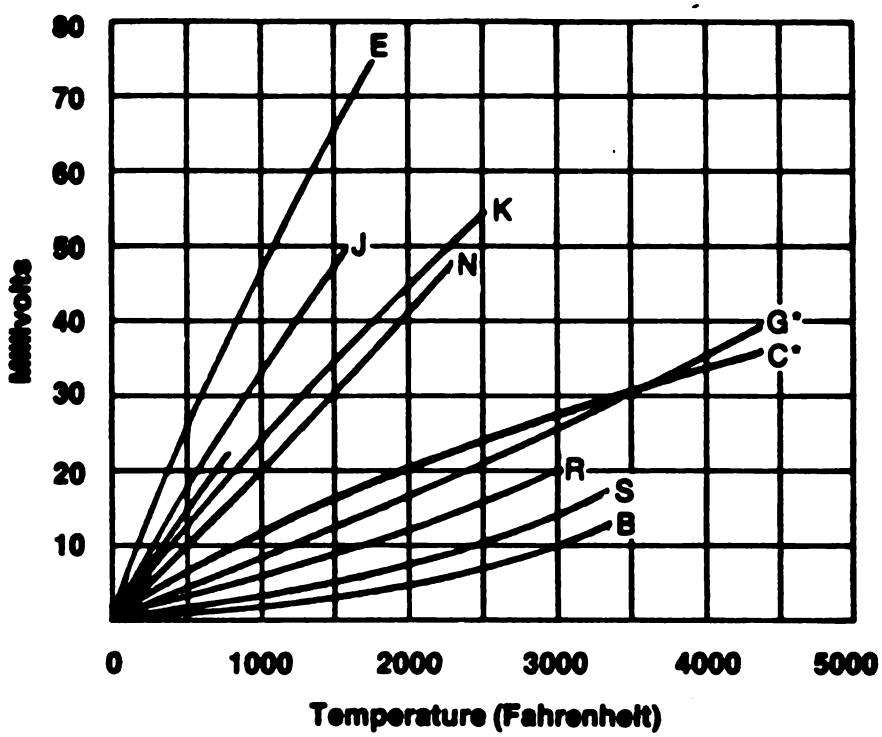

Figure 2.2 Seebeck voltage of various thermocouples listed in Table 2.3.

effective wavelength. The particular wavelength is usually taken as 0.655 μm [4,5]. However, the emissivity of the object is a function of wavelength and temperature. A careful consideration of emissivity is essential to obtain an accurate temperature reading of non-black body. An alternate design of two-color pyrometer, which employs two wavelengths, offers a convenient measurement of temperature without the need of emissivity correction. The operation principle is that energy radiated at one color increases with temperature at a different rate from that at another color [6]. Generally speaking, temperature obtained by single wavelength pyrometer with careful emissivity correction is closer to the actual temperature than that by two-color pyrometer. The temperature

measured by two-color pyrometer is accurate only when the emissivity at two wavelengths is equal. Accuracies obtainable with commercial automatic optical pyrometers are on the order of $\pm$ 3.89 °C for 816 to 1232 °C and of $\pm$ 6.67 °C for 1232 to 1760 °C [5,6].

2.3 Thick/Thin Film Heaters

In order to fulfill a wide variety of applications, heaters with different heating elements, shapes and configurations were developed, such as strip heaters, cartridge heaters, tubular heaters, immersion heaters, and thick/thin film heaters. The thick/thin film heaters offer the advantages of small sizes and direct deposition/attachment on the heated objects. In general, the thick film technique involves screen printing pastes onto substrates and firing procedure in the temperature range of 850 - 1000 °C to remove the organic materials in the pastes. The thin film technique is referred to those produced by chemical vapor deposition methods.

The performance of most commercially available thick/thin film heaters based on nickel, aluminum, or carbon steel alloy [7,8] are heavily dependent on the substrate materials used. The alumina (Al_2O_3) and boron nitride (BN) are commonly used as a substrate when high temperature heating (>600 °C) is required. Silicone rubber is the most widely used substrate material in flexible heaters. BeO, high density mulcorit (HDM), porcelain enamelled steel (PES), Kapton, and Mylar are also used as heater substrates under different occasions [8,9,10,11]. The maximum operation temperature and power density for those heaters are in the range of 300 - 1300 °C and 0.8 - 40 watt/cm^2, respectively.

In some special applications, heaters with special materials and structures are designed

and fabricated. For example, a polysilicon heater structure was realized using standard CMOS technology to supply temperatures necessary for the operation of most semiconductor gas sensors [24]. A doped tungsten wire was used as a heater operated at 2500 °C to enhance the energy of exhaust gases of thrusters. This was reported to extend a satellite's life by 30% [25].

2.4 Diamond Properties

Diamond is well known as a tetrahedral network of carbon atoms in which each atom is at the center of four other atoms. The carbon building unit is ordered in a cubic lattice and interconnected by strong bonds. This makes diamond unique in many of its physical properties.

The best known and most utilized property is the fact that diamond with a hardness of 10^4 kg/mm^2 is number one in all materials [26]. In addition, the combination of low coefficient of friction (when terminated with hydrogen), highest Young's modulus, low thermal expansion, and high thermal conductivity make it an excellent material for numbers of mechanical applications, such as cutting, bearing, heat spreading, and abrasion applications [26,27,28,29]. Its optical index of refraction (2.41 at 591 nm) and transmissivity (225 from nm to far IR) make it an ideal anti-reflection coating for infrared detectors [26,30,31].

Diamond is commonly regarded as an inert material that cannot be etched by boiling acids or bases [32,33]. Its immunity of chemical attack makes utilization under chemical harsh environments become possible. It has been known that diamond oxidizes in an oxygen environment at temperatures over 600 °C [19,34]. Molten potassium and sodium nitrides are reported to attack the diamond surface at a temperature in the range of 427 - 827 °C [30,35].

The electrical properties of large crystals found in nature or synthesized by high-temperature high-pressure anvil machines were well understood [36,37]. The understanding of CVD diamond, especially polycrystalline diamond, however is inferior. Table 2.4 compares some important properties of commonly used semiconductor materials for electronics applications. Diamond is known as an indirect-gap semiconductor, with an energy gap of 5.5 eV at room temperature [36,37,38]. A calculated band diagram is shown in Figure 2.3 [33,39].

The properties of carrier mobility and dopant ionization energy are major factors as to the ultimate practicality of diamond devices. A lot of efforts were made to determine the carrier mobility for different types of diamonds. Williams et al. (1970) determined the hole mobility in natural semiconducting diamond in the range of 700 - 2000 cm^2/Vs at room temperature by Hall effect measurement. In similar measurement as Williams, the carrier mobility of synthetic type IIb diamond was determined lower ~300 cm^2/Vs by Collins at 1989. Vavilov et al. (1974) and Fujimori et al. (1990) measured hole mobility in boron doped diamond of 200 - 700 cm^2/Vs and 850 cm^2/Vs, respectively, which are comparable with 1300 cm^2/Vs calculated for doping at 10^{16} cm^{-3} by Osmam et al. (1989). For ion implanted diamonds, values in the range of 200-700 cm^2/Vs were observed (Vavilov et al. 1989). The highest value measured in boron doped CVD single crystal homo-epitaxial diamond was 1000 - 1430 cm^2/Vs [40]. For the highly oriented diamond films, a mobility of 165 cm^2/Vs was reported by Stoner et al. [41]. It is generally expected that mobility in polycrystalline diamond films will be less than that in single crystal films [42]. The Hall mobility of boron-doped polycrystalline diamond films are reported in the ranges of less than 1 up to ~100 cm^2/Vs [43,44,45]. The combined electron-hole mobility of undoped polycrystalline CVD diamond films, as measured by transient photoconductivity at low carrier density, are in the range of 50 - 4000 cm^2/Vs,

TABLE 2.4 Properties of semiconductor materials

PROPERTIES	Diamond	β-SiC	GaAs	Si
Lattice Constant (A)	3.567	4.358	5.65	5.430
Thermal Expansion ($x10^{-6}$ °C)	1.1	4.7	5.9	2.6
Density (g/cm^3)	3.515	3.216		2.328
Melting Point (°C)	4000	2540	1238	1420
Band Gap (eV)	5.45	3.0	1.43	1.1
Saturated Electron Velocity ($x10^7$ cm/s)	2.7	2.5	1.0	1.0
Carrier Mobility (cm^2/Vs)				
Electron	2200	400	8500	1500
Hole	1600	50	400	600
Breakdown ($x10^5$ V/cm)	100	40	60	3
Dielectric Constant	5.5	9.7	12.5	11.8
Resistivity (Ω cm)	10^{13}	150	10^8	10^3
Thermal Conductivity (W/cm K)	20	5	0.46	1.5
Absorption Edge (μm)	0.2	0.4		1.4
Refractive Index	2.42	2.65	3.4	3.5
Hardness (Kg/mm^2)	10,000	3500	600	1000
Johnson Figure of Merit ($x10^{23}$ $W\Omega/s^2$)	73,856	10,240	62.5	9.0
Keyes Figure of Merit ($x10^2$ W°C/cm s)	444	90.3	6.3	13.8

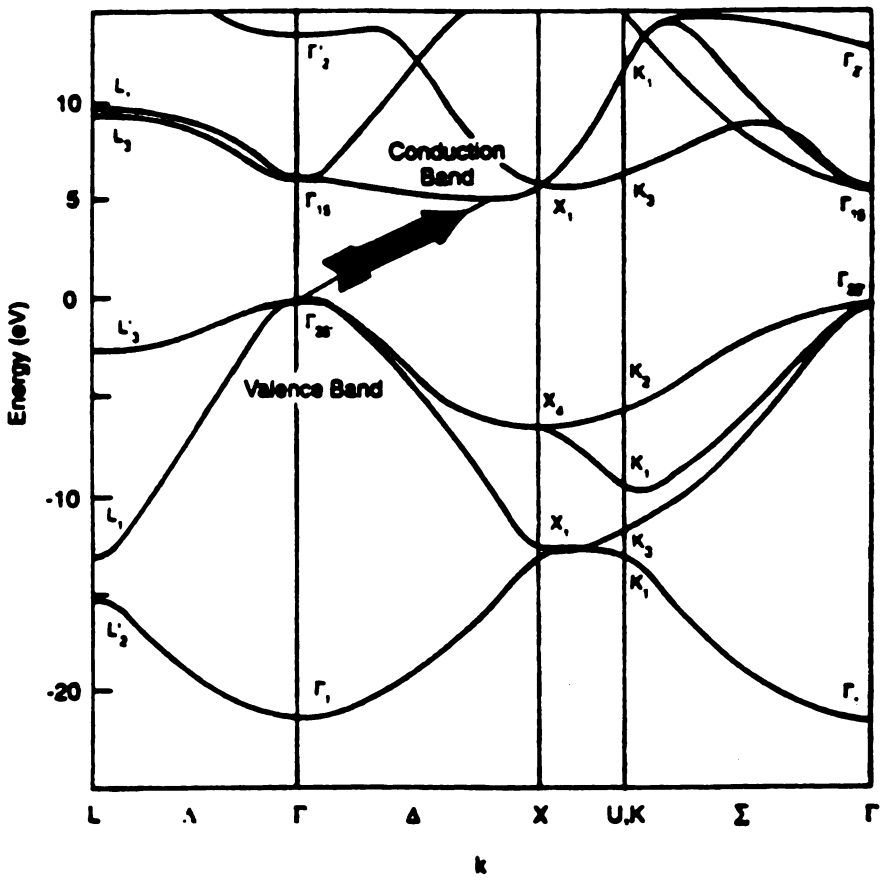

Figure 2.3 Band diagram of diamond.

respectively [46,47], which is comparable to that of the best single-crystal IIa natural diamonds [48].

The activation energies for boron, computed from the slopes of measured ρ versus 1/T curves assuming no compensation, are in the range of 0.22 - 0.34 eV for samples without annealing. These values correspond to hole concentration values in the range of 10^{18} - 2.0 x 10^{15} cm^{-3} [18]. In the case of highly doped diamond films with a boron concentration on

the order of 10^{20} cm^{-3}, the resistivity and activation energies of less than 0.01 Ωcm and 0.02 eV were observed [49].

2.5 CVD Diamond Technology

This section reports the current CVD diamond technologies needed for electronic devices and/or sensor applications. First, diamond film deposition technologies, such as nucleation enhancement methods, deposition reactors, and film structure characterization, are presented. To achieve semiconductor sensor devices in diamond, processing capabilities such as patterning, doping, and metal contacts are critical. They are also described in this section.

2.5.1 Nucleation

Diamond has been shown to nucleate on a wide variety of materials. Due to the low nucleation density of diamond on non-diamond materials (~ 10^4 cm^{-2}), substrate surfaces are, in most cases, treated to enhance nucleation density. Diamond powder [50,51], c-BN powder [52] or other types of abrasive polishing, as well as ultrasonic agitation with diamond powder suspension [53,54,55,56] are the most commonly utilized pre-treatment techniques. Bias enhanced nucleation (BEN) has also been reported for effectively creating nucleation sites on silicon substrates [57] and preparing highly oriented diamond (HOD) films [58,59]. Although those methods successfully enhanced the nucleation density into the range of 10^7 to 10^{10} cm^{-2}, an improvement over those existing techniques is still desired in terms of the reproducibility, maximum nucleation density, and efficiency. A brief description of the nucleation pre-treatment methods is given here.

• **Abrasive polishing**

It is well known that diamond nucleation density may be increased several orders of magnitude simply by scratching or abrading the substrate surface prior to placing it into the growth chamber. Diamond powder [50,51], c-BN, and SiC [52] powders of various grain sizes were commonly utilized to polish the substrates for nucleation enhancement. A rinse of organic solvents or cleaning by ultrasonic bath were sometimes followed to remove the redundant powder sticking on substrates. It was reported that a nucleation density of 3 X 10^{10} cm^{-2} is achieved by polishing with 10 nm diamond powder [50]. However, abrasive polish will cause damage of substrate surface and has a poor uniformity and reproducibility.

• **Ultrasonic treatment**

In this method, diamond particles with a wide range of sizes were suspended into hydrocarbon fluids. With substrates placed inside, the diamond powder solution was agitated by ultrasonic bath for a certain period of time [53,54]. The substrates were usually followed by an organic solvent cleaning procedure. It is believed that the residual of diamond powder bombarding on the substrate surface contributes to the nucleation of diamond. By utilizing ultrasonic treatment, the nucleation density in the range of 10^7 to 10^{10} cm^{-2} was reported [54,60]. A non-uniformity of growth nucleation was also observed [52].

• **Bias enhanced nucleation (BEN)**

In stead of ex-situ pretreatment for nucleation enhancement, the in situ negative DC biasing potential of -100 to -300 V [57,58,59] relative to the plasma is performed while the substrate is immersed in a methane-hydrogen plasma. A thin layer of amorphous

carbon found to deposit during the biasing treatment is believed to contribute to the enhancement of nucleation. A high density of up to 5 X 10^{10} cm^{-2} was reported [41]. However, a long treatment period of 2 hours was required for a high nucleation density.

• **Diamond powder loaded photoresist**

This method to enhance nucleation density for diamond growth is based on the idea of spreading diamond seed crystals, suspended in photoresist, on the substrate surface. Diamond powder loaded photoresist (DPR) is spin-coated on the substrate surface before diamond deposition. The sample is subsequently placed in the diamond deposition reactor and the photoresist evaporates at high deposition temperature leaving behind the diamond powder particles which act as seeds for diamond growth. The DPR was prepared by suspending fine diamond powder particles with a mean size of 0.101 μm into photoresist [18,61]. The uniform and reproducible nucleation density of ~10^{8} cm^{-2} was achieved. The advantages of DPR method include simplicity of application, compatibility with standard IC fabrication processes, good reproducibility, and no damage of substrates.

2.5.2 Deposition methods

The motivation and interest for the diamond synthesis started since the discovery by Tennant in late 18 century [62] that it is simply a crystalline form of carbon. The early attempts which were mostly based on unscientific approaches were unsuccessful. The real breakthrough came in 1955 at General Electric by using a high temperature high pressure (HPHT) process to synthesize diamond from graphite [63]. Simultaneously methods for synthesizing diamond at low pressure have been under development since early 1950s. Since then, lots of efforts were made to improve the growth rate, film quality, and reproducibility due to the potential applications and advantages of diamond. In the

following section, a brief review of various chemical vapor deposition (CVD) methods for growth of diamond films is given.

• **Thermally enhanced CVD methods**

Among numbers of thermal enhanced CVD methods, the hot filament assisted CVD process is the most commonly utilized one. It was first successfully achieved by Matsumoto and coworkers in 1982 [64,65]. In this method, the diamond film is deposited on a heated substrate from a gas mixture of methane and hydrogen [66] activated by a hot filament made of tungsten (W), tantalum (Ta) or rhenium (Re) placed close to the substrate. A schematic diagram of this deposition reactor is shown in Figure 2.4. Table 2.5 outlines the deposition parameters reported by various workers.

The role of hot filament is to thermally dissociate the gas mixture of methane and hydrogen to form hydrocarbon radicals, for example CH, CH_2, C_2H_2, CH_3, and atomic hydrogen. These radicals lead to preferential growth of diamond against graphite on substrate. The main advantages of HFCVD method are its relative simplicity, inexpensiveness and easy to scale up to large substrate areas. However, various components in the system can add impurity into the films due to increased vapor pressure in the presence of hot filament at very high temperature. Some variety of thermal enhanced CVD methods are also reported, such as, electron-assisted and laser assisted thermal CVD [67].

• **Plasma enhanced CVD methods**

Another widely utilized method of diamond growth is plasma enhanced CVD of carbon containing species mixed in low concentration with hydrogen. The role of plasma is to generate atomic hydrogen and to produce the proper carbon precursors for the growth of diamond films [66]. In such processes, atomic hydrogen is produced by electron impact

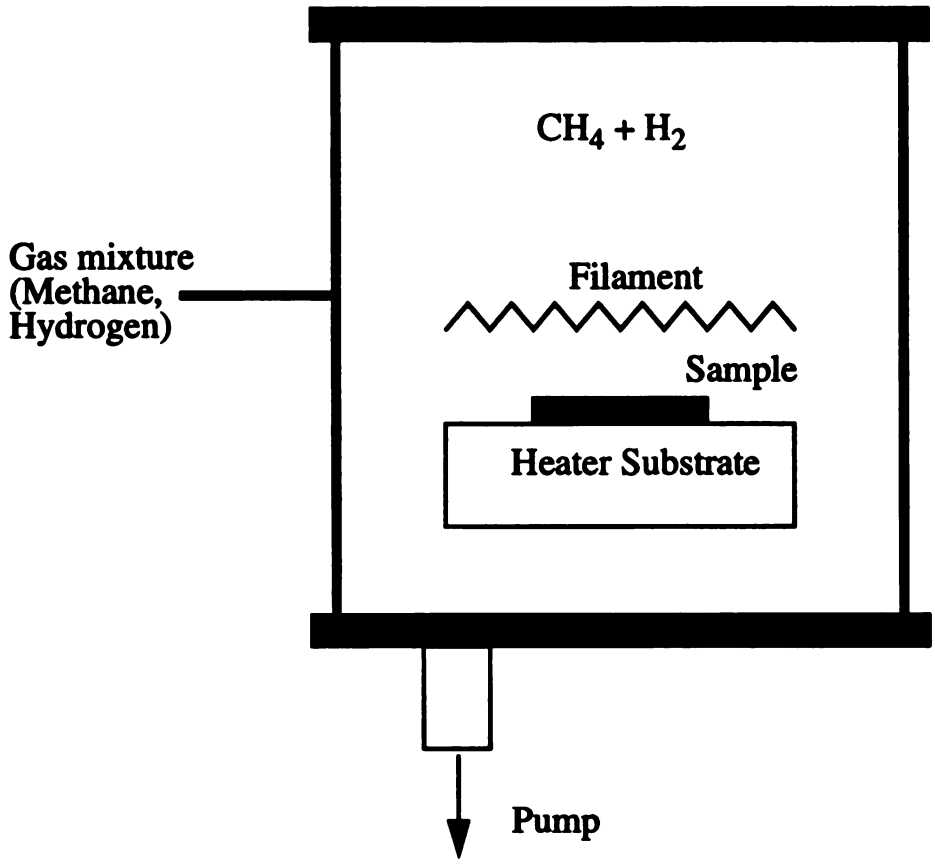

Figure 2.4 Schematic diagram of a hot filament-assisted CVD deposition system for growth of diamond thin films.

TABLE 2.5 Deposition Parameters Used in the Growth of Diamond Films by Hot Filament-Assisted CVD

Gas Mixture (CH_4/H_2)	Operating Pressure	Substrate Temperature	Filament Temperature
0.5 - 2%	10 - 100 torr	700 - 1000 °C	1900 - 2300 °C

dissociation of molecular hydrogen. Similarly, electron impact dissociation processes are responsible for the formation of carbon-containing neutral or ionic radicals. The absolute concentration of atomic hydrogen and neutral radicals depends on the pressure of the plasma. In low pressure plasma, the electrons acquire high kinetic energy from the electric field. However, due to the high mean free path, they do not transfer much energy to molecular species. As a result, the gas temperature is relatively low, and thus atomic hydrogen and neutral radicals are produced in low concentrations by collisions with high energy electrons only. In the case of high pressure, due to the small mean free path, the gas and electron temperature are about the same. Thus, the concentrations of atomic hydrogen and neutral radicals are much higher, because both electron and molecular collisions contribute to their formation. The accounts for the significantly higher growth rates reported in high pressure plasma.

Plasma generated either by various forms of electrical discharges or induction heating have been used. Table 2.6 summarizes typical deposition condition reported by works for three most commonly used plasma sources.

In DC-plasma assisted CVD method, a plasma in a H_2-hydrocarbon mixture is excited by applying a DC bias across two parallel plates, one of which is the substrate. A growth rate of 20 μm per hour was reported by Suzuki et al. [68]. Diamond films produced by DC plasma were reported to be under high stress and to contain high concentrations of hydrogen. Additionally, they may contain impurities resulting from plasma erosion of the electrodes [67]. As implied by the name, a RF discharge at 13.56 MHz is used to excite the plasma in RF-plasma-assisted CVD. This method was reported to prepare diamond films with small crystal grains and well adhered to a variety of substrates [69]. In this method, high power in the discharge was found necessary for efficient diamond growth, which frequently caused contamination of films due to sputtering from the walls of the reactor [67]. Microwave-plasma-assisted CVD methods have been used much more extensively

TABLE 2.6 Deposition Parameters used in the Growth of Diamond Films by Plasma enhanced CVD

Method	Gas Mixture (CH_4/H_2)	Operating Pressure	Substrate Temperature	Input
DC-plasma	0.5 - 5%	200 torr	600-800 °C	Discharge (V/I): 1000/4(V/A-cm^2)
RF-plasma	0.5 - 2%	1 - 30 torr	800-1000 °C	RF power: 500-1000 W
Microwave-plasma	0.5 - 2%	5 - 100 torr	700-1000 °C	100-700 W

than any other methods and have a number of advantages over any other methods for growth of diamond films, such as no contamination due to lack of electrode erosion, higher concentration of atomic hydrogen and hydrocarbon radicals due to higher plasma density. An additional advantage is that the plasma is confined in the center of deposition chamber thus prevents carbon deposition on the walls of reactors [67].

- **Combustion flame-assisted CVD**

Diamond deposition by combustion flame assisted CVD was first reported at 1988 by Hirose and Kondo and triggered a worldwide activity partly because of the simplicity and low cost of the experimental apparatus and partly because of the high growth rates of 150 μm per hour [70].

A typical set up of combustion flame-assisted CVD reactor is shown in Figure 2.5. It

basically consists of an oxygen acetylene torch supplied with oxygen and acetylene with a mass flow control system. The main combustion reaction leads to the formation of CO and H_2 with a number of reactive intermediates (H, OH, C_2 and C_2H) [67]. Hydrogen addition to the oxygen-acetylene flame was found to reduce the amount of amorphous carbon in diamond films. A torch operated in an argon filled chamber was found to improve the purity of diamond films by Doverspike et al. [67].

2.5.3 Diamond film structure characterization

In order to use the CVD diamond in the practical applications, a careful characterization is necessary to control and enhance the quality of diamond films deposited by CVD methods. However, the uality of diamond can be defined in terms of numbers of ways, such as, elemental composition, structure, bonding state, surface morphology, and defect density [71], depending upon the applications. Secondary ion mass spectrometry (SIMS) [60], Auger electron spectroscopy (AES) [72], and X-ray photoelectron spectroscopy (XPS) [58] can be used to determine the elemental composition. Transmission electron diffraction (TED) and X-ray diffraction (XRD) [50,59] allow the determination of crystal structure and lattice spacing. Raman spectroscopy is very popular for determining true diamond bonding throughout the bulk of the films. Scanning electron microscopy (SEM), scanning tunnelling microscopy (STM) [54], and atomic force microscopy (AFM) [50,73] are utilized to examine the surface morphology and growth nucleation of diamond films. Transmission electron microscopy (TEM) [71] can be used to observe the defect microstructure in the bulk films and to determine the defect density. Furthermore, the localized bonding can be observed via electron energy loss spectroscopy (EELS) of TEM [57]. A brief review of commonly used tools is given below.

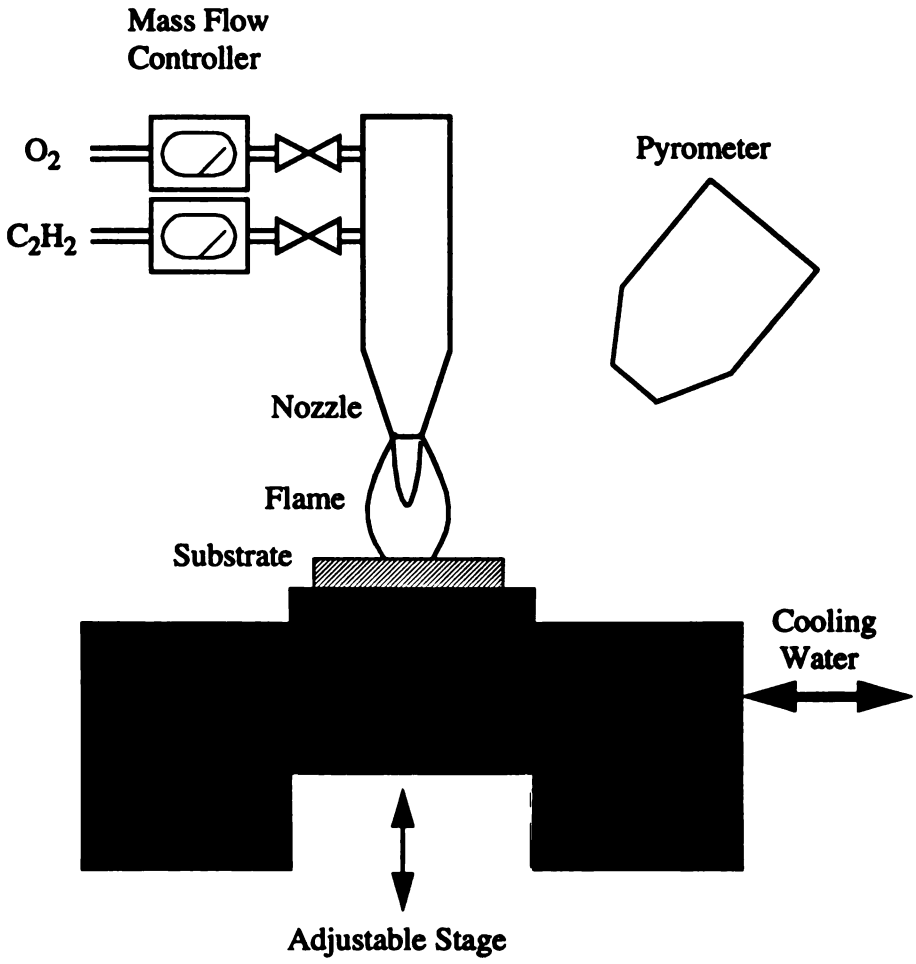

Figure 2.5 Schematic diagram of an oxygen-acetylene apparatus for the growth of diamond films. (From Hanssen et al. (1991))

• **Raman spectroscopy**

In Raman effect, discovered by physicist Sir Chandrasekhara Venkata Raman of India, light is scattered by an atom or a molecule that changes its state. There is a corresponding discrete decrease in the frequency of scattered radiation. Raman spectroscopy is widely used in the analysis of materials, and the identification of trace elements. In the diamond related researches, Raman spectroscopy is a powerful tool to identify the presence of sp^2 and sp^3 bonding in diamond films [74]. However, a great difference in the scattering efficiency for graphite (sp^2) and diamond (sp^3) needs to be considered to make a valuable evaluation. The wave number shift of 1332 corresponds to sp^3 diamond peak.

• **Scanning electron microscopy (SEM)**

SEM consists of an electron gun in a vacuum chamber column and images by collecting the secondary electrons emitted from samples due to the incident electron beam. The image then is displayed on a cathode ray tube (CRT) for directly vision [75]. Because of the large magnification range of 10 X to 300,000 X [76] and great depth of field, SEM is a very powerful tool for studying the morphology and visual analysis of diamond films. It is widely utilized to inspect the surface morphology, crystal orientation, the grain sizes and film thickness, and to monitor the nucleation densities and patterning. The need for a conducting specimen somewhat limits its utility for undoped films on insulating substrates.

• **Atomic force microscopy (AFM)**

Atomic force microscopy is another useful tool for studying the nucleation density, crystal structure and surface morphology of CVD diamond films. In an AFM, a very fine tip, mounted on a cantilever, is scanned through the sample to obtain the surface profile.

The sample is mounted on a piezoelectric device which provides the movement of the sample during scanning. The advantages of AFM are higher resolution of 0.1 nm or less and greater sensitivity to define profile differences of vertical variations in sample [75]. The vertical resolution of AFM is in the sub-A range, better than that of other profilometers [77], which make AFM ideal for study of surface roughness of diamond films. In addition, no vacuum is needed for the operation of AFM, and it can be used on non-conducting surfaces.

2.5.4 Patterning

In order to fulfil a variety of applications and desirable structures, various techniques have been developed to pattern diamond thin films. Patterning techniques are, in general, distinguished into two categories, selective deposition and selective etching. In addition, the ArF excimer lasers with a photon energy of 6.4 eV and wave length of 193 nm was reported to prepare free-standing single crystal diamond microstructures from homoepitaxial films [78]. The feature sizes prepared by this method are in the range of 200 - 400 μm with a thickness of ~15 μm.

- **Selective deposition**

The selective deposition is achieved by pre-deposition nucleation on the desired area, or by masking the undesirable area during the diamond deposition. Hirabayashi et al. used Ar sputtering in undesired growth regions to suppress nucleation after substrates were pretreated by ultrasonic method [56]. Ma et al. reported selective deposition onto SiO_2 stripes patterned on a Si substrate [53]. The Ar^+ ion beam was used to suppress the nucleation on both Si and SiO_2 except in the shadows cast by the downwind edge of the SiO_2 stripes. The selective nucleation was successfully achieved by standard

photolithography in DPR method, developed at Michigan State University, or by masking substrates during the ultrasonic treatment by Masood et al. [61]. Leksono and coworkers reported successfully the patterning of diamond films by lift off process on Si wafer. Thin ZnO film and amorphous silicon were used as sacrificial layers for lift off processes [79]. SiO_2 or Si_3N_4 as a masking layer during the diamond deposition was successfully reported by Masood et al. [61] and Roppel and coworkers [80].

- **Selective etching**

The patterning of continuous diamond films by selective etching was reported by Masood et al. [19,61]. Using a rapid thermal processor (RTP), diamond films were successfully etched in oxygen environment at 700 °C. The SiO_2 or Si_3N_4 were used as masks to block the undesirable area during etching process.

2.5.5 Doping

As a wide band gap semiconductor material, E_g=5.5 eV, diamond offers advantages for electronic applications under extreme environmental conditions. Realization of those applications requires a control over the ability to dope it p- and n-type. CVD diamond films deposited without intentional doping are usually good insulators. To achieve the semiconducting diamond films, one should be able to incorporate controlled amounts of impurities into diamond films. In general, doping of semiconductors could be achieved by diffusion, ion implantation, or in situ doping. Because of the low diffusibility of most elements in diamond, diffusion is impractical. Although ion implantation can achieve active doping, the damages of crystal structure were introduced [81]. Therefore, in situ doping was commonly utilized in preparing semiconducting diamond films. Boron (B), aluminum (Al), phosphor (P), lithium (Li), and nitrogen (N) are potential dopants of

diamond. P-type diamond films were successfully prepared by using boron as an in situ dopant. However, all attempts to obtain n-type doping were unsuccessful until now [82,83].

A number of in situ doping techniques involving gaseous, liquid and solid sources to incorporate boron into CVD diamond films have been successfully used to produce the p-type semiconducting diamond films. Solid sources (B_2O_3 [84,85], boron powder [18]) have the advantages of chemical stability and simplicity. However, non-uniformity of doping are observed and it easily contaminates deposition chamber. Gaseous source (B_2H_6 [41]) has a better controllability, but is poisonous and explosive. Liquid source ($B(CH_3O)_3$ [84,86]) is also used to prepare p-type diamond and is reported to be nonpoisonous, stable, and controllable.

2.5.6 Metallization

Metallic contacts are essential for achieving electronic devices. For thermistor applications, it is desirable that the resistance of devices be determined mainly by the resistivity of the bulk material and that the influence of contact resistance be minimized. In addition, the good adhesion and high temperature stability are essential for developing the contact structure for high temperature device applications.

It is found that Ti and Mo form carbides with diamond at high temperatures which provide good ohmic contact with diamond [87]. The contact resistance is found to decrease with an increase in the doping level [88]. A contact resistivity ($\rho_c=R_c^2/R_\square$) of ~ $1 \times 10^{-6}\ \Omega\ cm^2$ was reported upon annealing at 600 °C for highly doped (~ $10^{20}\ cm^{-3}$) diamond films [89], where R_c is the contact resistance measured by transmission line method (TML) and $R_\square$ is the sheet resistance of bulk diamond film. Ti/Au, Ta/Au, Ti/Pt

and Ti/Mo/Au were reported by several workers to provide good contacts with diamond films [18,89,90,91]. With the presence of passivation layer, the Ti/Au and Ti/Mo/Au contacts were reported stable for extended periods at 500 and 670 °C, respectively, in ambient environment [91,92]. It is also found that the Ti/Pt bi-layer provided a good contact up to 1000 °C under high vacuum of 10^{-7} torr and a good adhesion between diamond and SiO_2 [18,19].

2.6 Diamond Sensors

According to physical quantities to be measured, sensors can be roughly grouped into temperature sensors, mechanical sensors (pressure sensors, accelerometers, vibrometers, etc.), acoustic sensors (microphones, ultrasonic sensors, hydrophones), radiation sensors, humidity sensors, gas sensors, ion-selective sensors, sensors in medicine and biology, and others (liquid component sensors, material identification, etc.). Many known physical phenomena are used in the design of those sensors [93].

Diamond with an excellent combination of properties has been studied by many investigators for sensing applications. This section reports the current status of various diamond sensors found in literatures.

2.6.1 Diamond temperature sensors

In order to utilize diamond for real world temperature sensor applications, characterization of the temperature response, the sensitivity, the operation temperature range, the reproducibility, and reliability are important. The temperature dependence of a diamond temperature sensor is generally characterized in terms of resistivity (or resistance) by two-point, four-point probe, and Van der Pauw [94] methods. The carrier

concentration and mobility determined by Hall effect measurement [81,95] or by transient photoconductivity measurement [96] are found important to further understand the conduction mechanisms of diamond at different temperatures.

The resistivity of diamond was studied as a function of temperature for different structures, doping levels, and geometry by a number of researchers. It is found that the CVD polycrystalline diamond has a negative temperature coefficient (NTC) of resistivity and temperature coefficient α of -0.005 to -0.02 K^{-1} over the temperature range of -73 to 1273 K in vacuum [18]. The typical beta (β) factors of polycrystalline diamond thermistors are in the range of ~1000 to 5500 K [97,98] as compared to 2000 to 4000 K of conventional metal-oxide thermistors over 298 - 673 K [20]. However, the high sensitivity (β value) is achieved at low doping level where the corresponding resistance values are unacceptably high (i.e. greater than 1 MΩ) for practical applications. As reported by Fox and coworkers, the polycrystalline films are preferable to highly oriented and homo-epitaxial diamond films for thermistor application due to their improved linearity with inverse temperature [91]. The Figure 2.6 shows the temperature dependence of resistivity, carrier concentration, and mobility for homoepitaxial, highly oriented, and polycrystalline diamond reported by Fox et al. [91].

The effects of high temperature annealing on the diamond films and metal contacts were studied to make reliable and reproducible sensors. It is well known that diamond films oxidize at temperatures > 600 °C in oxygen presented environments. Oxidation of diamond by oxygen plasma was observed even at lower temperatures. In oxygen ambient, the maximum operation temperature, therefore, is limited by the oxidation temperature of 600 °C. The use of diamond thermistors in oxidizing ambient at high temperatures may be possible if the diamond film is passivated, which may, however, reduce the sensitivity of the thermistor. Chalker et al. reported that non-passivated diamond films became non-conducting at 610 °C in air, while silica coated devices operated up to marginally higher

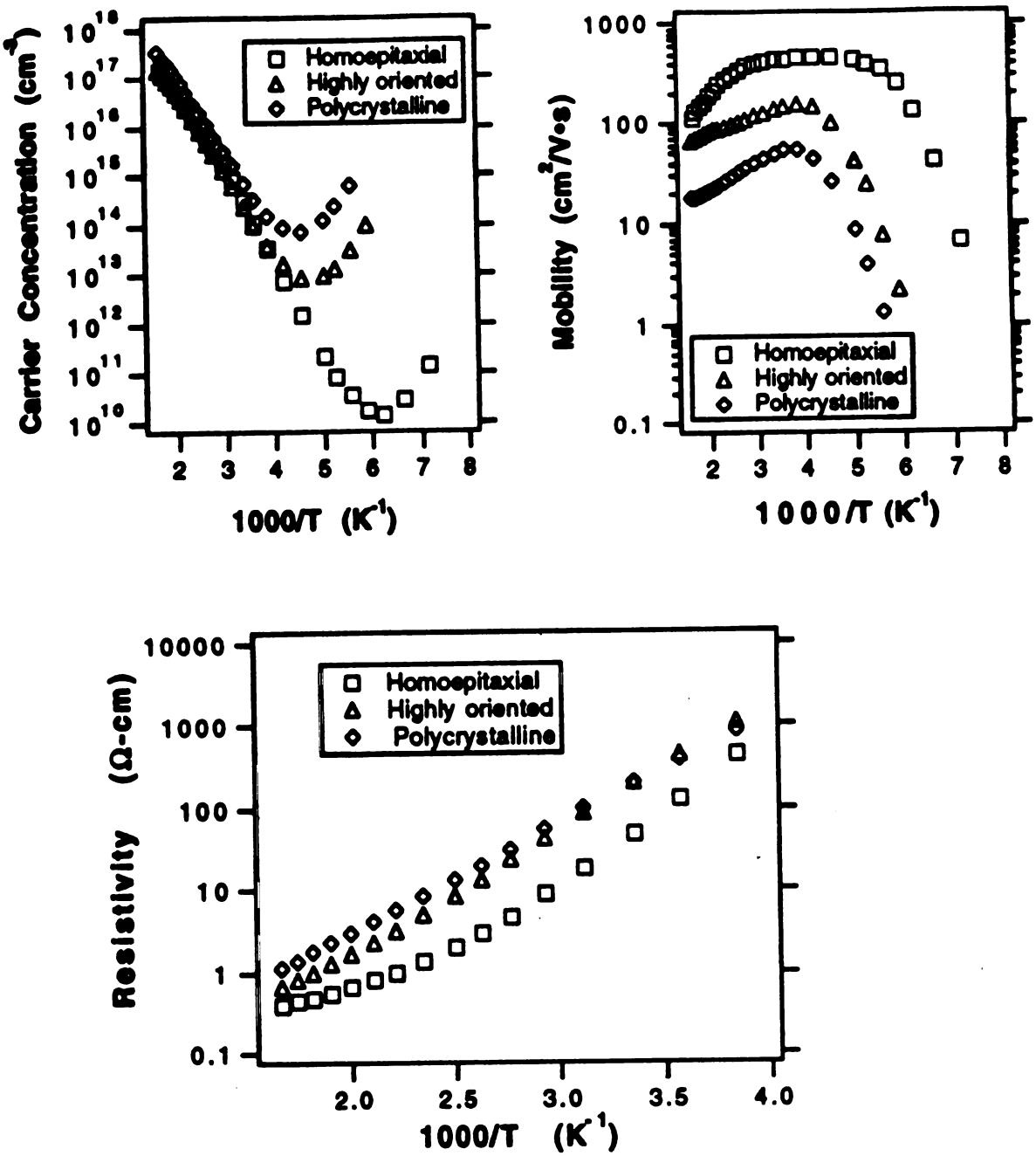

Figure 2.6 **The temperature dependence of properties for different diamond structures.**

temperature of 670 °C due to the crack of coating material [92]. A degradation of metal contact (Ti/Mo/Au) was also observed via a combination of oxidation and carburization. The long term stability at 500 °C for 200 hours was reported by Fox et al. It is also found that presence of a silicon nitride passivation layer allowed stable operation in 800 °C [91].

2.6.2 Radiation sensors

Sensors for electromagnetic radiation may be classified as quantum sensors and thermal sensors. Quantum sensors are based on photoemission, photoconduction, or photovoltaic effects. Thermal sensors operate in two steps: first, an incident photon flux is converted into a temperature variation, which then can be determined [93].

Diamond has been used for various radiation detection purposes. The diamond radiation detectors reported to date are mainly simple metal-insulator-metal (MIM) devices based on photoconductive effect. Electrons that absorbed a photon with energy greater than bandgap (5.5 eV) raised from the valence band to conduction band. The presence of the photon-induced electron in the conduction band gives an increase in the conductivity. This type of diamond photodetectors are reported to detect the ultraviolet, X-rays, γ-rays, neutrons, high-energy electrons, and charged particle with high sensitivity [99,100,101,102,103]. The MIM structure has been successfully used as a switching device which is activated by electron beam bombardment [104]. The diamond diodes are reported to be used as UV detectors by Marchywka et. al. [105]. By characterizing the photocapacitance, diamond surface channel p-type MIS capacitors are reported to be utilized as an UV radiation detector with low leakage [106].

Due to the excellent combination of properties, diamond detectors can be operated under extremely high radiation fields with a large dynamic range in both response and speed.

2.6.3 Piezoresistive Sensors

The piezoresistive effect of HPHT synthetic diamond was reported by Larsa et al. at early eighties [107,108]. The resistance was characterized as a function of stress in <100> and <111> directions with excellent sensitivity over the pressure range of 0 to 2000 $kg.cm^{-2}$. The results suggest that diamond is an excellent material for micromechanical sensors. However the diamond sensors have never been promoted mainly due to the high cost.

The observation of significant piezoresistive effect was first reported in both polycrystalline and homoepitaxial CVD p-type diamond layers of 2 μm thick by Aslam et al. in 1992 [109]. In addition, the ability to micromachine diamond films into miniature beams and membranes, the applications of polycrystalline diamond films in the strain gauges, pressure sensors, and accelerometers then were studied by various researchers [110,111,112].

The diamond cantilever beam and free standing diaphragm structure are commonly used to study the gauge factor of diamond films. The room temperature piezoresistivity gauge factors of homoepitaxial and polycrystalline diamond films are reported in the range of 200 - 550 and 5 - 100, respectively [110,111]. The diamond film gauge factors are reported to increase with the temperature [110], grain size [111], and resistivity [110,111]. The electrical field dependence of polycrystalline diamond gauge factors are also investigated by Sahli et al. [112]. Figure 2.7 (a) shows the gauge factors of diamond and silicon as a function of strain and (b) shows the doping dependence of gauge factors as a function of strain reported by Taher et al. [110].

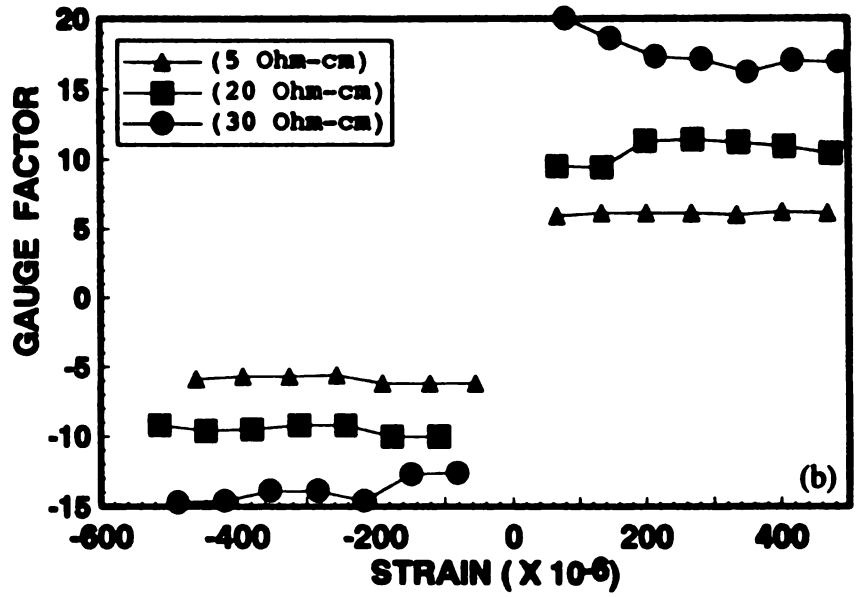

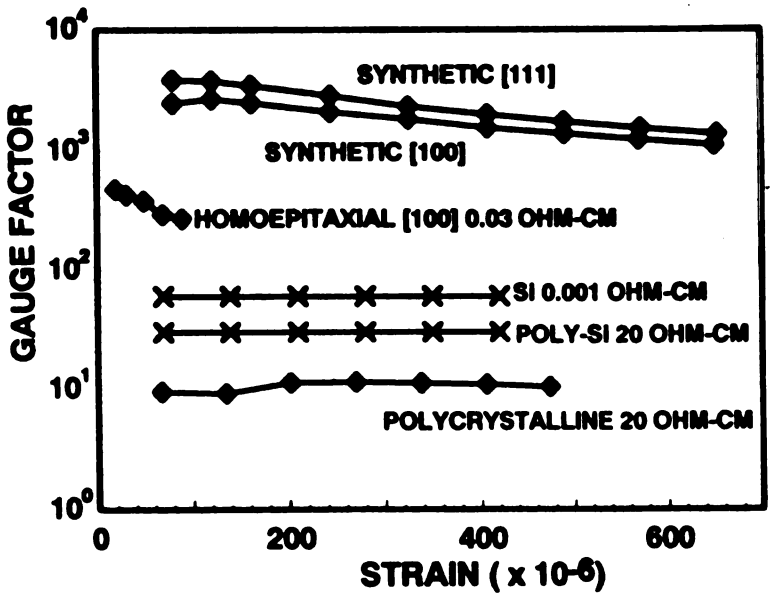

Figure 2.7 Results of gauge factors study by Taher et al.

2.6.4 Gas sensor

A Pd/i-diamond/p-diamond (MIS) structure was used for hydrogen sensing by Y. Gurbuz et al. [113]. The I-V characteristics of diamond based MIS structure shifts from near ohmic to rectifying behavior after exposure to 0.01 torr of H_2 gas at 27 ^oC. The capacitance is reported to decrease upon H_2 absorption. This structure is reported to have a high sensitivity, good reproducibility, and fast response.

2.7 Summary

A comprehensive report on the temperature measuring instruments and thin film heaters is presented in this chapter. The diamond properties, CVD diamond technologies, and current status of diamond sensors are also discussed.

CHAPTER 3

DIAMOND DEVICE INFRA-STRUCTURE

3.1 Introduction

To realize reliable and reproducible diamond micro-sensors and thin film heaters, it is necessary to develop diamond infrastructure technologies. The technologies developed or used in the present study can be grouped into thin film deposition, nucleation density enhancement, and device fabrication. In this chapter, current efforts of development, improvement and implementation of those technologies for realizing the diamond devices are described in detail.

3.2 Thin Film Deposition Technology

The ability to grow high quality films is essential for the realization of diamond sensor/heater application. With the exception of MPCVD samples used in the nucleation enhancement study, all diamond films used in the present research were prepared by a hot filament chemical vapour deposition system (HFCVD) [65]. The MPCVD samples were supplied by professors Asmussen and Reinhard [114,116]. In addition to the description of HFCVD, the design and construction of a new MPCVD system are described in this

section.

3.2.1 Film Growth

3.2.1.1 Hot Filament Chemical Vapour Deposition System

- **Description of reactor**

The HFCVD reactor used in this work was designed and constructed at Michigan State university by A. Masood, S. Sahli, and D. S. Hong. Some modifications and optimizations were incorporated during the course of this work to improve the reproducibility, deposition uniformity, growth rate, and film quality.

A simplified schematic diagram of this system is shown in Figure 3.1. The HFCVD reactor consists of an 18-inch diameter stainless steel vacuum chamber with a 10 inch access door. Ten 5 inch long tantalum (Ta) filaments in a series configuration are horizontally mounted on a 4.5 X 5 inch^2 frame via 20 molybdenum (Mo) hooks. The supporting frame consists of the combination of 2 BN bars and 2 Mo bars which also serve as electrodes. The 4.5 X 5 inch^2 filament array is utilized to ensure a uniform deposition over a 4 inch wafer. The filament typically draws 20 - 23 Amp current at nominal temperature of 2300 ^{o}C. The filament temperature is monitored by an optical pyrometer through a 6 inch glass view port.

The reactant gas mixture consists of ultra-pure grade (99.995%) methane (CH_4) and hydrogen (H_2). The flow rates of these gases are independently controlled by MKS type 1159B mass flow controllers. The operation pressure is monitored through a MKS type 122A baratron pressure gauge and is controlled by a MKS type 250 pressure controller via a type 248A upstream valve. The base pressure is measured by a MDC thermocouple

vacuum gauge with a range of 1 - 1000 mtorr. A Varian SD-200 rotary pump is used for evacuation. In addition, nitrogen is used to purge and backfill the chamber.

Either 4 inch Si wafer or graphite plate is used as sample holder. The supporting frame is specially designed with a vertical movement mechanism to adjust the separation of filament array and substrate in the range of 0.5 - 1 cm. Type K thermocouples are used to monitor the both top and back side of substrate temperatures during the deposition process. Since enough amount of heat is generated by a relatively large filament array, no additional substrate heating is required to maintain the nominal substrate temperature of 900 °C for diamond deposition.

- **Deposition Parameters**

Since CVD growth of diamond is essentially in metastable phase, the selection and consistency of processing parameters are very important to achieve reproducible high quality diamond films [62]. The ranges and typical values of deposition conditions used throughout this research are summarized as follows:

(1)	Gas composition:	$CH_4 : H_2 = 0.5\% - 1\%$ (1%)
(2)	Gas Flow rate:	CH_4 : 1 - 5 sccm (4 sccm)
		H_2 : 200 - 500 sccm (400 sccm)
(3)	Filament temperature:	2200 - 2350 °C (2300 °C)
(4)	Substrate temperature[1]:	850 - 950 °C (900 °C)

1. A temperature profile of 4 inch substrate was characterized by measuring temperatures at several points of substrate using thermocouples during a test deposition. A ~100 °C difference was found between the temperatures measured at the center and the edge of the top side of substrate. The substrate temperature then was monitored at the edge in the actual deposition to minimize the blocking area by thermocouples.

vacuum gauge with a range of 1 - 1000 mtorr. A Varian SD-200 rotary pump is used for evacuation. In addition, nitrogen is used to purge and backfill the chamber.

Either 4 inch Si wafer or graphite plate is used as sample holder. The supporting frame is specially designed with a vertical movement mechanism to adjust the separation of filament array and substrate in the range of 0.5 - 1 cm. Type K thermocouples are used to monitor the both top and back side of substrate temperatures during the deposition process. Since enough amount of heat is generated by a relatively large filament array, no additional substrate heating is required to maintain the nominal substrate temperature of 900 °C for diamond deposition.

• **Deposition Parameters**

Since CVD growth of diamond is essentially in metastable phase, the selection and consistency of processing parameters are very important to achieve reproducible high quality diamond films [62]. The ranges and typical values of deposition conditions used throughout this research are summarized as follows:

(1)	Gas composition:	$CH_4 : H_2 = 0.5\% - 1\%$ (1%)
(2)	Gas Flow rate:	CH_4 : 1 - 5 sccm (4 sccm)
		H_2 : 200 - 500 sccm (400 sccm)
(3)	Filament temperature:	2200 - 2350 °C (2300 °C)
(4)	Substrate temperature[1]:	850 - 950 °C (900 °C)

1. A temperature profile of 4 inch substrate was characterized by measuring temperatures at several points of substrate using thermocouples during a test deposition. A ~100 °C difference was found between the temperatures measured at the center and the edge of the top side of substrate. The substrate temperature then was monitored at the edge in the actual deposition to minimize the blocking area by thermocouples.

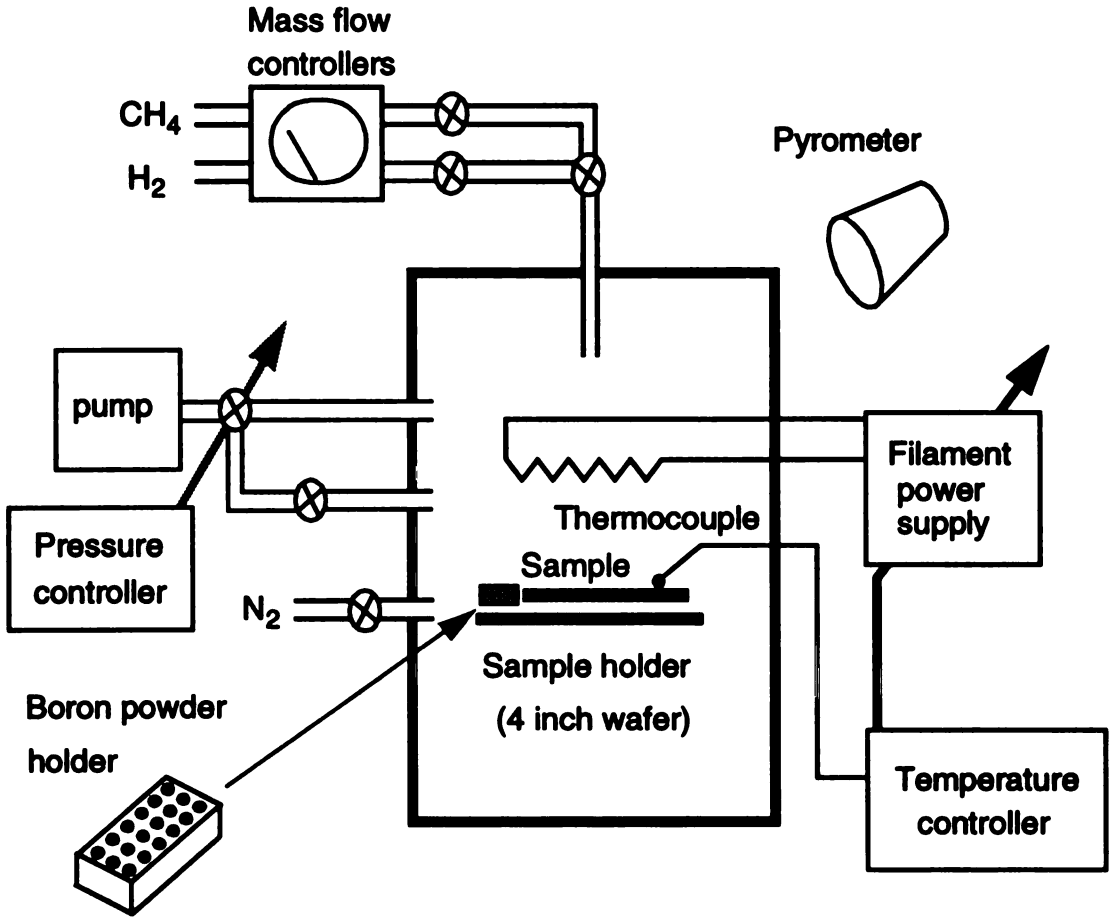

Figure 3.1 The simplified schematic diagram of HFCVD system.

(5) Operation pressure: 40 - 50 torr (50 torr)

(6) Substrate to filament distance: 0.5 - 1.5 cm (1 cm)

(7) Doping source: Boron powder or B_2O_3 plana boron source

• Operation Procedure

The operation sequence of HFCVD is reported to have a great influence on the deposited film quality [19]. The operation steps used through out this research are described as follows.

Start up procedures:

(1) Samples to be deposited and doping sources (if any) are loaded on sample holder. The distance of filaments and substrate is adjusted to be ~1 cm. (The distance varies with the sag of filaments.)

(2) Process chamber is evacuated down to a base pressure of less than 10 mtorr.

(3) Hydrogen is then introduced into the process chamber.

(4) When the chamber pressure reaches > 20 torr, the filament temperature is brought up slowly to the nominal temperature of 2300 °C. The slow adjustment of filament current is desired to avoid any damage.

(5) CH_4 is switched on only after the substrate temperature reaches desired temperature of 900 °C.

Shut down procedures:

(1) The CH_4 is turned off to terminate the deposition processes, while the H_2 remains

on for another 5 to 10 minutes. During this period, the hydrogen is the preferential etchant to remove a thin conducting carbonaceous layer on the surface of CVD diamond films [19]. No conduction is found in the case of undoped films after this treatment.

(2) The applied filament current is decreased slowly down to zero. The chamber is then evacuated. Samples are unloaded after the system is cool down.

3.2.1.2 Film Quality Analysis

The quality of both doped and undoped diamond films were monitored by secondary electron microscopy (SEM) and Raman spectroscopy. The SEM provided a direct vision of film surface morphology. Only samples with well faceted diamond crystals were used for electrical measurement in this research. The Raman spectroscopy was also used to ensure a diamond characteristic peak of 1332 cm^{-1}.

3.2.2 Microwave Plasma Assisted Chemical Vapor Deposition Reactor

In addition to the HFCVD reactor, a microwave plasma assisted chemical vapor deposition (MPCVD) reactor is designed and constructed using a microwave cavity donated by professor Asmussen. This reactor, which became operational in June 1996, could not be used for researches reported in this dissertation.

Based on the operational function, a MPCVD reactor can be categorized into the following five major subsystems.

(1) Microwave cavity

(2) Process chamber

(3) Microwave power supply

(4) Gas flow and vacuum system

(5) Computer monitor system

• **Microwave cavity**

The cross sectional view of the cavity is shown in Figure 3.2. As shown, the cavity wall is formed from a 7 inch I.D., water cooled, copper cylinder. The top end is formed from a copper sliding short, which is electrically connected to the cavity walls via the silver finger stock. By moving the sliding short vertically up and down, the electrical and physical height of the cavity can be changed to fine tune the microwave operating electromagnetic mode. The cavity sits on a stainless steel, water-cooled base-plate. Reactive gases flow into the discharge zone, which is confined by a 4 inch I.D. quartz dome at the lower part of cavity, via the gas input tunnel inside the base plate. A 3 inch high, stainless steel, water-cooled sample stage is attached to the bottom of the base plate to hold samples up to 2 inch diameter. The water cooling capability is incorporated for deposition at low temperature. As shown in Figure 3.3, three circular blades are designed to ensure the uniformity of cooling effect. Microwave power is coupled into the cavity through an adjustable coupling probe from the side of cavity. By adjusting the length of the coupling probe, the microwave reflected power can be minimized for efficient deposition. The cavity used in this research is developed by J. Asmussen et al. [115].

• **Process chamber**

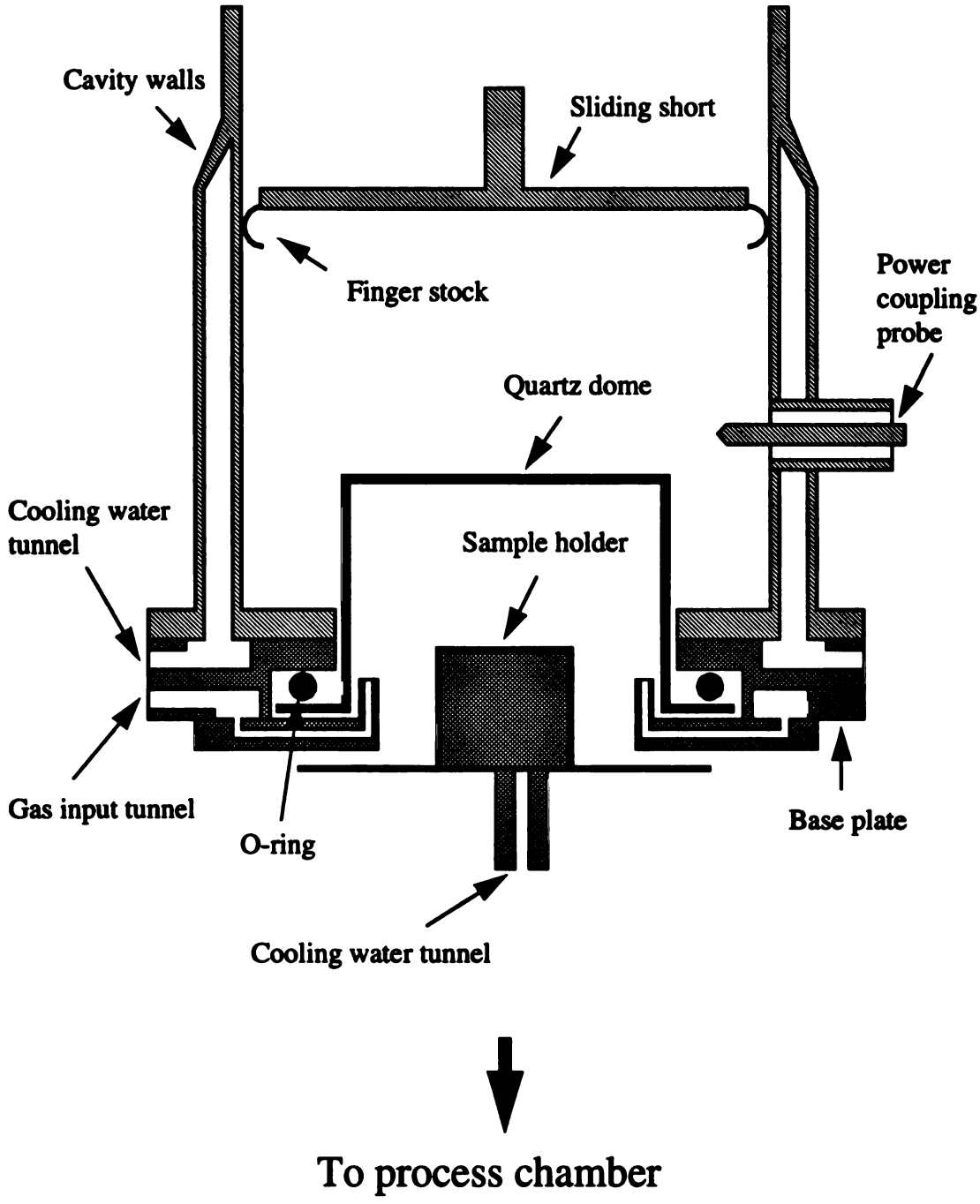

Figure 3.2 The cross sectional view of microwave cavity.

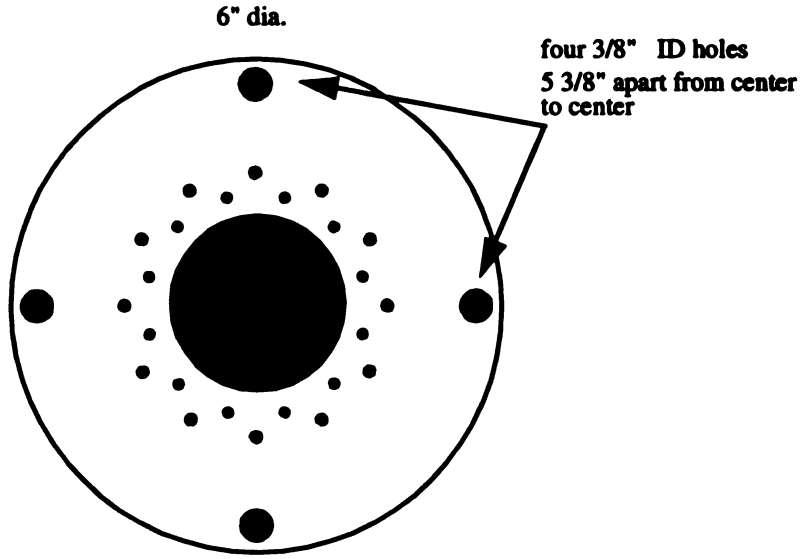

(a) Top view

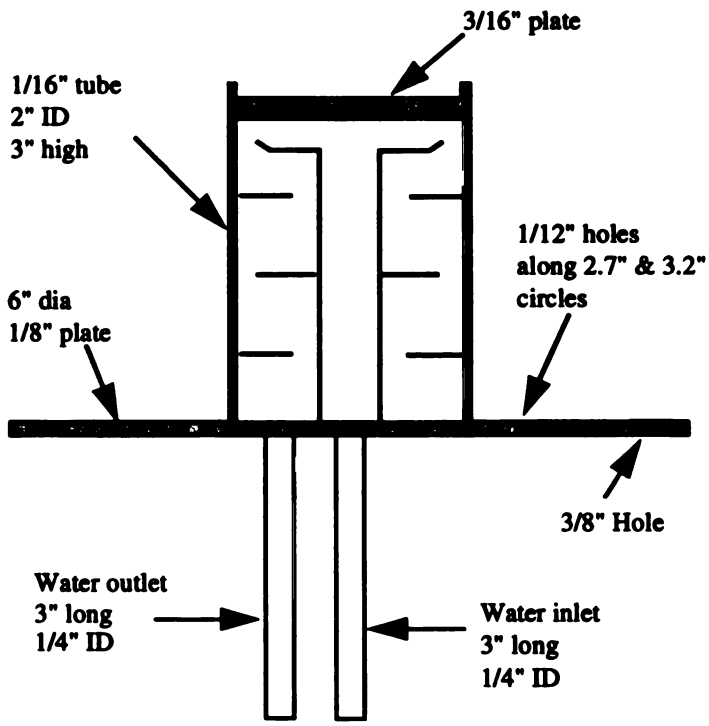

(b) Cross sectional view

Figure 3.3 The design of water cooled sample stage.

MPCVD diamond deposition reactor consists of a 17 inch high, 18 inch O.D. stainless steel process chamber. The samples can be loaded and unloaded through a 10 inch access door. The sample stage attaches to the base plate through a 7 inch opening at the top of the chamber. Cooling water of the sample stage, vacuum gauges, and all electrical feedthroughs are assembled through 2.75 inch Del-Seal ports.

• **Microwave power supply**

An ASTeX model S-1000 power supply is used to generate up to 1 KW of 2.45 GHz microwave power for diamond deposition. The configuration of power supply circuit is shown in Figure 3.4. A rack mount control unit contains the compact switching power supply and control electronics which operates a separate magnetron head. Directional coupler and circulator are used to monitor the reflected power.

• **Gas flow and vacuum system**

Figure 3.5 shows the schematic drawing of the flow control and vacuum system. The reacting gases consist of ultra pure grade (99.995% purity) of H_2 and CH_4 supplied by cylinder tanks. The MKS type 247C 4 channel flow controller along with two MKS type 1159B mass flow controllers are used to control the CH_4 and H_2 flow rates in the ranges of 0 - 20 and 0 - 1000 sccm, respectively. Source gases are mixed before reaching the inlet on the base-plate.

A Varian SD-300 mechanical pump with a base pressure of 1×10^{-4} torr is used for pumping. Two MKS type 622A Baratron pressure transducers along with a MKS type PDR-C-2C 2 channel read out are used to monitor the chamber pressure at the range of 1 - 1000 torr and under 1 torr, respectively. During the deposition process, the operation pressure are measured and controlled by a MKS type 622A baratron gauge with full scale of 100 torr, a MKS type 651 exhaust valve controller, and a MKS type 653A throttle

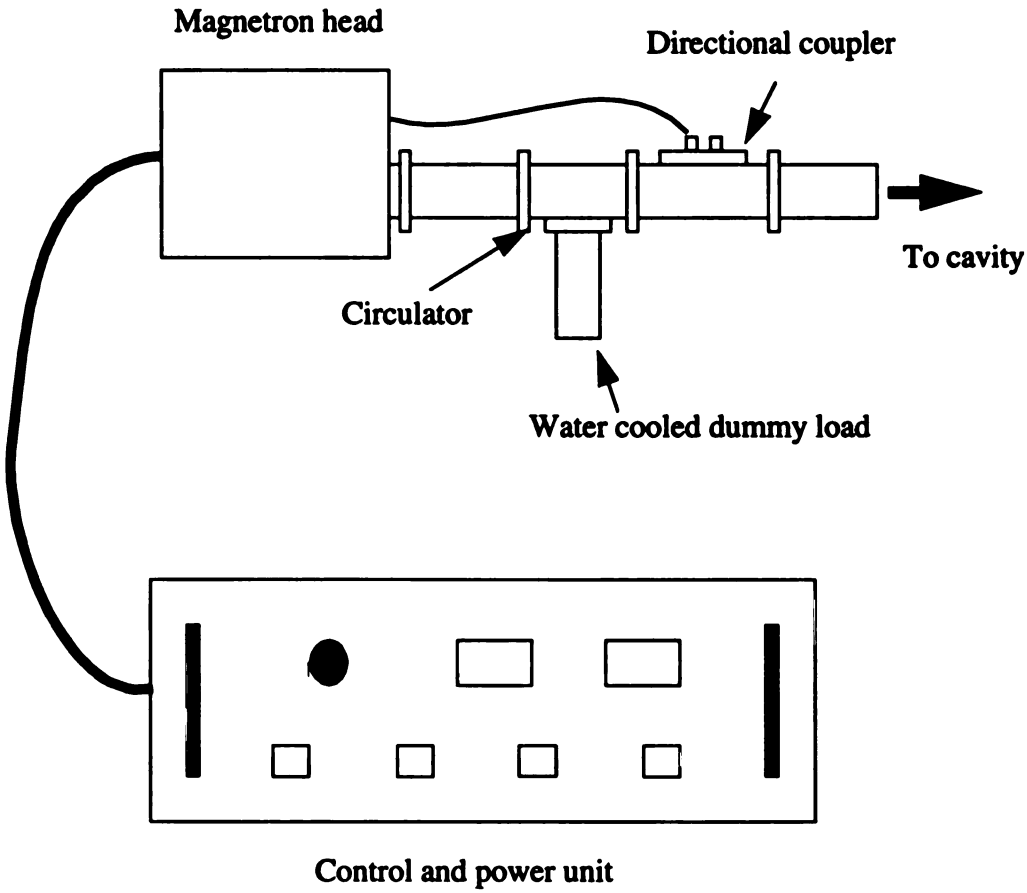

Figure 3.4 The configuration of microwave power supply.

valve. Nitrogen is used for system vent and exhaust purge.

- **Computer monitor system**

A computer monitor system is incorporated in the design of MPCVD system based on both safety and film quality control considerations. The primary goals of this monitor system are to monitor the operation parameters during the deposition process and to control the shut down procedure. A block diagram of this system is shown in Figure 3.6. During the deposition process, the operation pressure of main chamber, flow rates of reactant gases, input and reflected power of microwave, and temperatures of system at several critical points are monitored by a personal computer along with read-out units of according parameters. The proper procedure to turn off the gases flow, microwave power, and throttle valve will take place at the end of deposition process or whenever a fault is detected.

3.3 Nucleation Enhancement Technology

Diamond has been shown to nucleate on a wide variety of materials. Due to the low nucleation density on non-diamond materials (~ 10^4 cm^{-2}), substrates are, in most cases, treated to enhance nucleation density into the range of 10^7 - 10^{10} cm^{-2} [117]. The commonly used pre-treatment techniques are described in previous chapter (2.5.1). Because of low nucleation density, long deposition time is required to prepare continuous diamond films. Consequently, rougher film surface is resulted due to large grain sizes. The surface roughness of 0.5 - 2 μm was observed for 1.5 to 4 μm thick films prepared using an initial nucleation density of ~ 10^8 cm^{-2}. The rough surface problems become more pronounced for sensor/device application, since highly smooth film surfaces are essential in post-deposition lithography and etching of metal contacts. There are also some

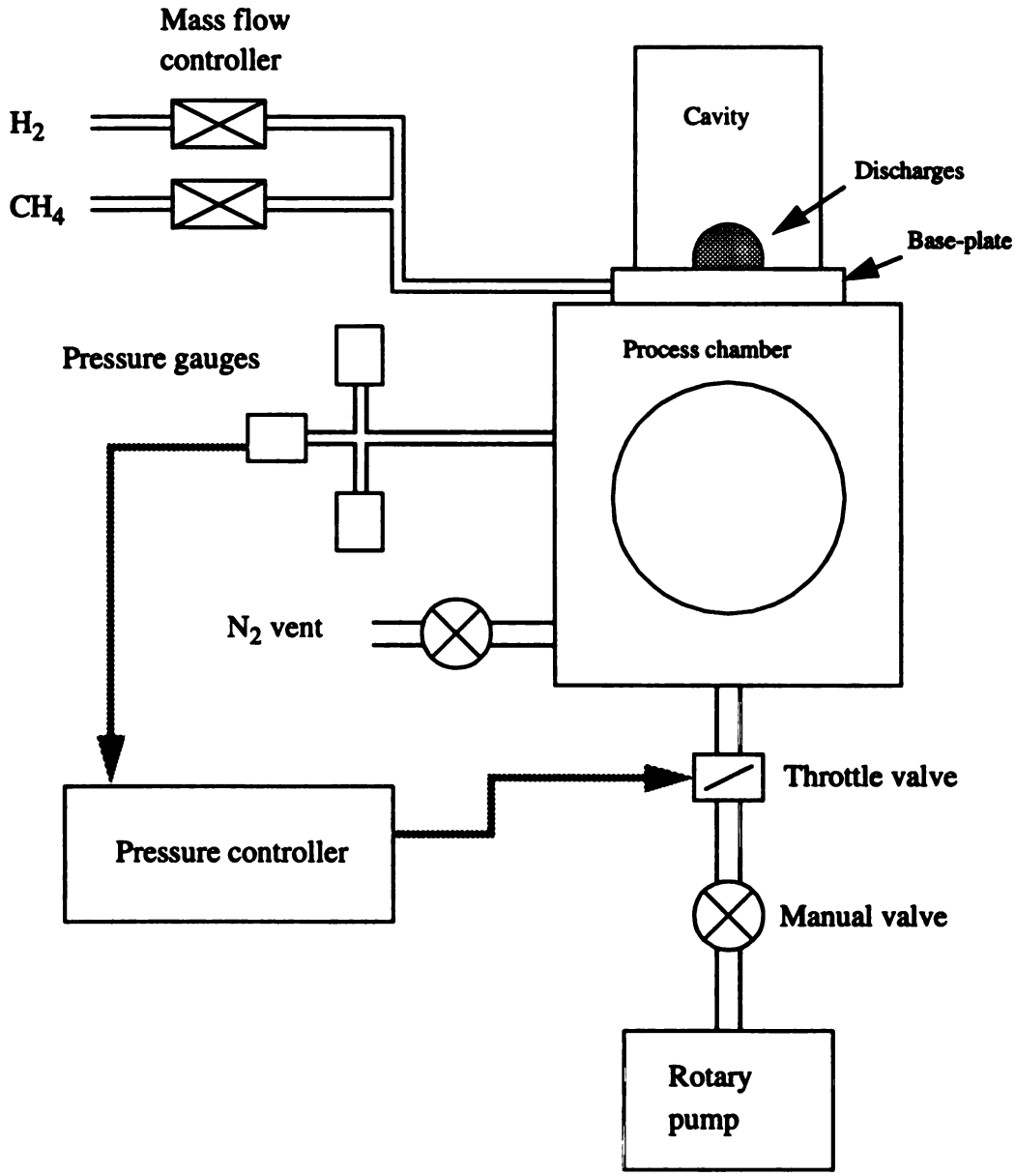

Figure 3.5 Schematic of MPCVD flow control and vacuum system.

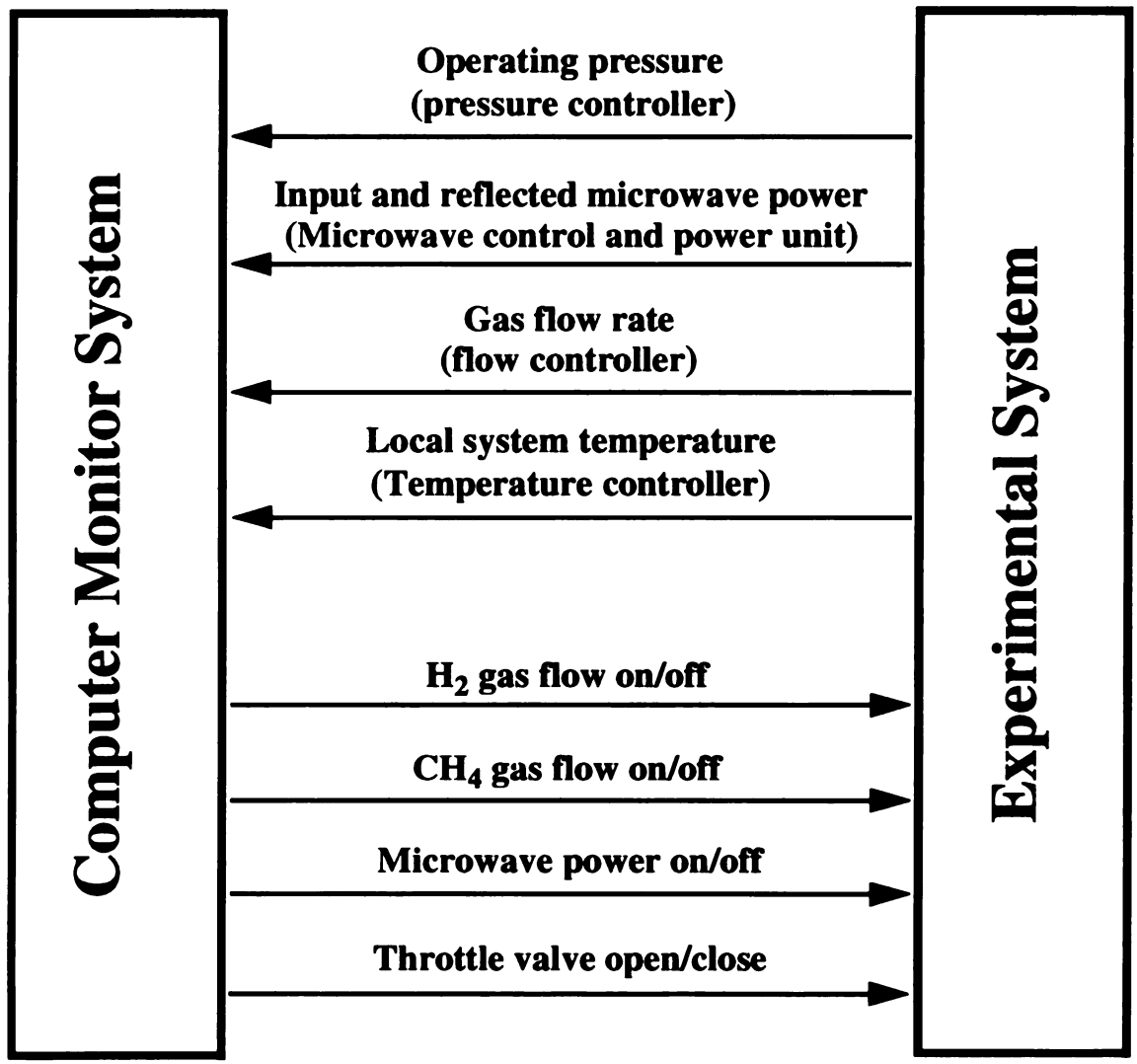

Figure 3.6 Block diagram of the computer monitor system.

limitation of seeding and patterning techniques used today, such as poor selectivity, ill reproducibility, and restriction to two dimensional structures. In this section, a development of ultrahigh density seeding technique, which enhances the nucleation up to 1.1 x 10^{11} cm^{-2}, is first described. The effect of nucleation density on the surface roughness and growth rate of CVD diamond is also evaluated at different deposition stages.

3.3.1 Diamond Powder Loaded Fluids (DPLF) Method

Diamond Powder Loaded Fluids (DPLF) with different carrier fluids, mean powder sizes and densities are coated on substrates to enhance the nucleation density. The idea of this method is to spread diamond crystals, suspended in carrier fluids, on the substrate surface. During the diamond deposition process, the carrier fluids are evaporated at initial stages leaving behind the diamond particles which act as seeds for diamond growth. DPLFs are applied to substrates through direct writing, spinning, spraying or brush-painting. The technical details of different DPLFs are summarized in Table 3.1. The DPLF1 and DPLF2 are commercially available diamond powder suspensions, 1/40 SQG and N-6, from Du Pont Chemicals-Repauno Plant, NJ. The DPLF3 is prepared by suspending diamond powders into photoresist [19,61]. In contrast to other nucleation procedures, DPLF method does not cause any damage to the substrate surface. This method is highly compatible with standard integrated circuit (IC) processes and amenable to patterning, doping, and coating of 3-D samples.

3.3.2 Ultrahigh Nucleation Density

Silicon wafers, cleaned by either the standard RCA or piranha solution (H_2SO_4 : H_2O_2

TABLE 3.1 Technical details of DPLF seeding processes.

	DPLF1	DPLF2	DPLF3
Carrier Fluid	Water	Water	Photoresist
Mean Powder Size	0.038 μm	0.101μm	0.101μm
Density	40 carats/liter	100 carats/liter	12 carats/liter
Nucleation Density	~10^{11} cm^{-2}	~10^{10} cm^{-2}	~10^{8} cm^{-2}
Application Methods	Spray, brushing, or direct-write	Spray, brushing, or direct-write	Spray or spain
Patterning	Photolithography or direct-write	Photolithography or direct-write	Photolithography

= 60% : 40%), were coated with different DPLFs to study the primary nucleation densities. Before the primary nucleation densities were measured, samples were treated in hydrogen environment at 900 °C for 10 minutes to evaporate the carrier materials, which were photoresist or pure water with a pH value of 7, and to etch any non-diamond carbon impurities. The nucleation densities were determined both by counting the number of particles appearing on atomic force microscopy (AFM) [118] micrographs and by the cross-section analysis function associated with AFM.

An extremely high primary nucleation density of 1.1 X 10^{11} cm^{-2} was achieved on Si substrates by coating with the 0.038 micrometer powder (DPLF1). By assuming that the diamond particles are closely and uniformly spread on the substrate surface and that each particle occupies a square or an equilateral triangle area with a diagonal or a side of 0.038

μm, the computed particle densities are 1.385 X 10^{11} cm^{-2} or 1.599 X 10^{11} cm^{-2}, respectively, which are consistent with our measurements. Moreover, this density is substantially higher than those found in previous reports [50-56,72]. The primary nucleation densities of DPLF2 and DPLF3 are in the ranges of 1.36 - 1.5 X 10^{10} cm^{-2} and 1.321 - 3.40 X 10^{8} cm^{-2}, respectively.

3.3.3 Effects of Nucleation Density

Samples coated with DPLF1, DPLF2, and DPLF3 are used to study the effect of nucleation density on diamond film deposition. The diamond films are synthesized by either HFCVD or MPCVD under temperature range of 470 - 900 °C for various periods of time. The detail sample preparation parameters are summarized in Table 3.2. The diamond film quality is monitored by SEM, AFM, and Raman spectroscopy. The grain size, nucleation density, and surface roughness were characterized directly by AFM. The film thickness was measured by either Dektak surface profilometery for patterned samples or SEM for un-patterned samples. In the case of DPLF3 films prepared by MPCVD at 850 °C for 5 and 15 minutes while the films were not yet continuous, the thickness is determined by averaging the thickness of those areas where most of grains were coalescent.

- **Deposition Time for Continuous Film**

The ultrahigh nucleation density tremendously reduces the deposition time needed for obtaining continuous films. Samples in group G-1, coated by DPLF1 (G-1a & b) and DPLF3 (G-1c & d), are deposited by both MPCVD and HFCVD at 470 °C and 900 °C, respectively, to study the deposition time needed for continuous films. In contrast to the

TABLE 3.2 Sample preparation parameters.

Group I. D.	Seeding Fluid	Deposition Parameters	Deposition Time	For study ...
G-1				
G-1a	DPLF1	MPCVD, 470 °C [1]	6 hours	deposition time for
G-1b		HFCVD, 900 °C	2 - 6 hours	continuous film.
G-1c	DPLF3	MPCVD, 470 °C [1]	6 hours	
G-1d		HFCVD, 900 °C	2 - 6 hours	
G-2				
G-2a	DPLF1	HFCVD, 900 °C	vary, to maintain	surface roughness
G-2b	DPLF3	HFCVD, 900 °C	film thickness within 0.95 - 1.1 μm	comparison.
G-3				
G-3a	DPLF1	MPCVD, 850 °C	5 - 60 min.	film characteriza-
G-3b	DPLF2	MPCVD, 850 °C	5 - 60 min.	tion at different
G-3c	DPLF3	MPCVD, 850 °C	5 - 60 min.	deposition stages
G-4	DPLF1	HFCVD, 900 °C	2.5 - 10 hours	as above

1. The 470 °C MPCVD films were grown by Prof. Reinhard using machine developed in M. J. Ulczynski's dissertation research.

DPLF3 seeded samples (G-1c & d), the high seeding density samples (G-1a & b) formed continuous films of sub-micron thickness after the deposition time of 6 hours for MPCVD and 2.5 hours for HFCVD even under a low growth rate of ~ 0.05 μm per hour and ~ 0.1 - 0.15 μm per hour. Figure 3.7 shows AFM micrographs of representative samples. Various colors in film appearance were observed due to light interference effect.

- **Surface Roughness Comparison**

The surface morphology are strongly influenced by the process parameters [67] which can affect the surface roughness through twining, growth competition, and texture evolution. To focus on the effect of nucleation density on surface roughness for different growth rates and temperatures, the deposition parameters are maintained in a comparable range for both HFCVD and MPCVD reactors.

Samples in group G-2 are prepared to compare the surface roughness of continuous films with the same thickness. The deposition was carried out by HFCVD under the deposition conditions listed in Table 3.3. The deposition time is varied to maintain the film thickness within the range of 0.95 - 1.1 μm. The average surface roughness of G-2a and G-2b samples, with a scan area of 3 μm square, are 29.311 and 124 nm, respectively. Figure 3.8 shows the surface profiles taken by AFM. The results indicate that in spite of the similarities in thickness and deposition conditions, films with smaller grain sizes and higher nucleation density are smoother than the other set of samples at early deposition stage.

- **Film characterization at different deposition stages**

To study the effect of nucleation density on film quality, surface roughness, and growth rate, samples in group G-3 pre-treated by three different seeding fluids were deposited by MPCVD at 850 ^{o}C at the same batch to minimize the influences of film

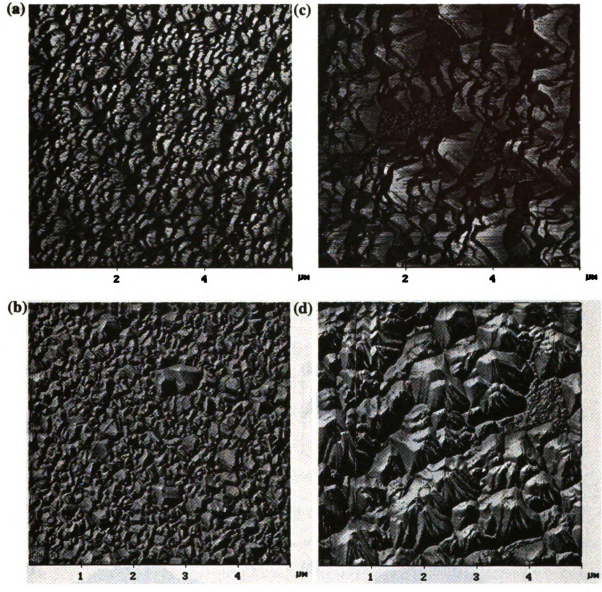

Figure 3.7 **Comparison of (a), (b) DPLF1 and (c), (d) DPLF3 samples. Samples (a) & (c) are deposited by MPCVD at 470 °C for 6 hours. Samples (b) & (d) are deposited by HFCVD at 900 °C for 4 hours. The DPLF1 samples are continuous.**

TABLE 3.3 Deposition parameters of HFCVD and MPCVD reactors.

Reactor	Operating pressure	Substrate temperature	Gas mixture	Note
HFCVD	50 torr	850 - 950 °C	H_2: 200 sccm	Filament Temperature
			CH_4: 1 sccm	2000 - 2200 °C
MPCVD	90 torr	850 °C	H_2: 500 sccm	Microwave power
			CH_4: 15 sccm	2 KW

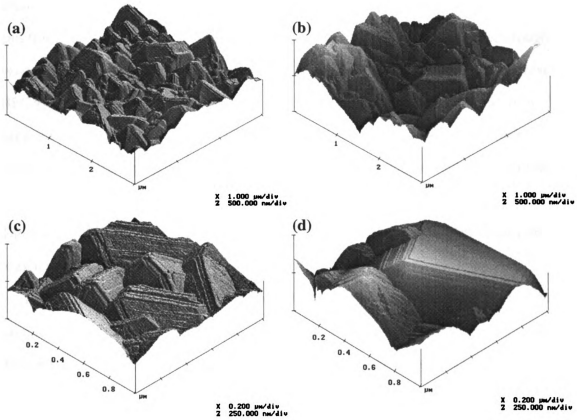

Figure 3.8 Surface roughness comparison of 1 µm thickness film; (a) DPLF1, (b) DPLF3, (c) closer view of DPLF1, (d) closer view of DPLF3.

morphology by different deposition conditions. Samples were characterized at several deposition stages by AFM, and Raman spectroscopy. The representative AFM surface profiles of films after 15, 25, and 60 minutes deposition are shown in Figure 3.9.

As observed in Figure 3.9, all films have similar surface texture and morphology in every characterization stages as a result of identical deposition condition which simplify the study of surface roughness. In the meantime, samples of G-3a with the highest primary nucleation density have the most smooth film surfaces as compared with those of G-3b and G-3c in all deposition stages. The well-faceted crystal structures became more pronounced after a longer deposition time for all three sets of samples. Similar results were observed in the case of samples in group G-4 prepared by HFCVD reactor, as shown in Figure 3.10. It is noteworthy that the samples (G-4) prepared by HFCVD have smoother surface than those by MPCVD regardless of the similarity in seeding density and film thickness, as indicated in Figure 3.11, which plots the average surface roughness versus film thickness for samples in both G-3 and G-4. More twinning was observed in HFCVD samples directly resulting in smaller surface grain sizes and smoother films. This suggests that growth conditions of different reactors play an important role on the exhibition of film morphology. Differences in the HFCVD samples and MPCVD samples include the operating pressure, temperature, and ratio of gas mixture, as summarized in Table 3.3, all of which may provide major contributions to the differences in film roughness [67,119].

Figure 3.11 shows the plot of average surface roughness versus film thickness for all samples prepared by both MPCVD and HFCVD (groups G3 and G4). It is clearly demonstrated that the surfaces of DPLF1 and DPLF2 samples become rougher gradually as the films become thicker. Because of the discontinuity of the lowest seeding density films (DPLF3) in early stage of deposition, the surface roughness does not show any major increase. However, the surface roughness of DPLF3 samples is expected to increase

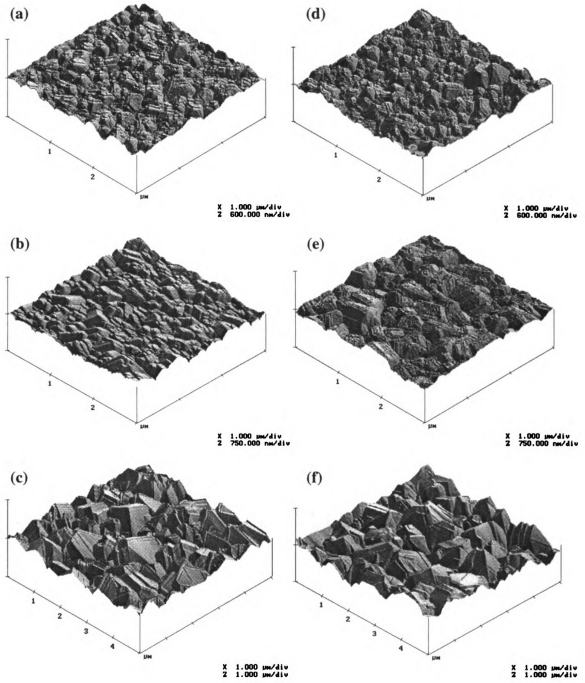

Figure 3.9 Different growth stages of diamond films deposited by MPCVD at 850 ^{o}C for 15, 25 and 60 minutes using DPLF1 (a, b, c), DPLF2 (d, e, f) and DPLF3 (g, h, i), respectively.

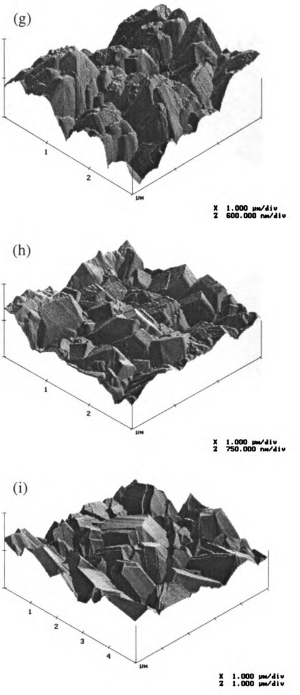

Figure 3.9 (cont'd)

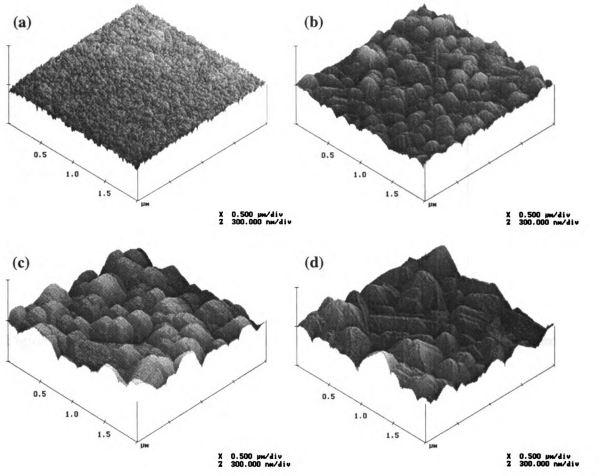

Figure 3.10 Different growth stages of DPLF1 films deposited by HFCVD at 900 ^{o}C for (a) 2.5, (b) 5, (c) 7.5 and (d) 10 hours.

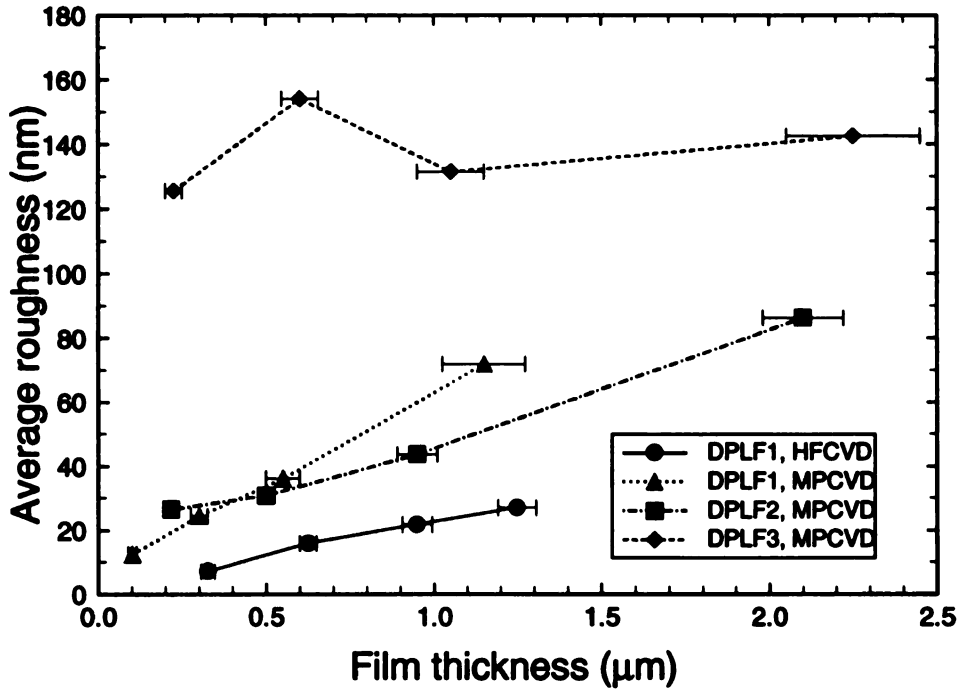

Figure 3.11 Average surface roughness versus film thickness for samples prepared by both HFCVD and MPCVD.

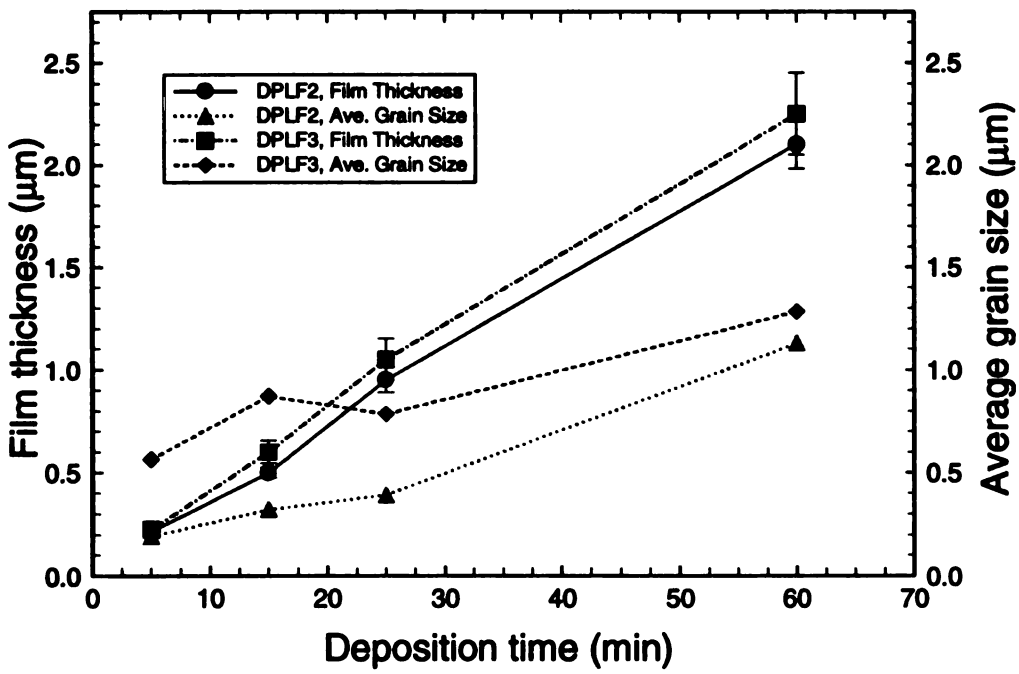

Figure 3.12 Film thickness and grain size versus deposition time for DPLF2 and DPLF3 samples prepared by MPCVD at 850 °C

after longer deposition times.

In Figure 3.12, the surface grain size and film thickness of DPLF2 (G-3b) and DPLF3 (G-3c) seeded diamond films prepared by MPCVD at 850 °C are plotted as a function of deposition time. Note that the DPLF2 and DPLF3 have the same powder size, but different nucleation densities. A large difference in surface grain sizes of two seeding samples at early deposition stages is observed and is mainly due to the discontinuity of DPLF3 films. In the case of DPLF2, the grains merged together after only five minutes of deposition time leading to continuous films which limit the increase in grain sizes. In the case of DPLF3, the films were not continuous until after 25 minutes of deposition. This allows individual crystals to grow out three dimensionally to a larger size. A reduced difference in grain sizes is observed for longer deposition times when both films are continuous. The results also suggest that there is no appreciable effect of nucleation density on growth rate (in terms of film thickness). The thicknesses of both samples are increased almost linearly with respect to deposition time. The small difference in thickness between two samples may be caused by the difference of initial seeding thickness or non-uniformity in growth of diamond films.

The surface roughness is plotted as a function of surface grain density for all samples in Figure 3.13. It is found that the surface roughness is strongly dependent on the surface grain density as well as primary nucleation density for all samples. Despite the differences in deposition time, reactors, and film thickness, films with higher surface grain density (or smaller grain size) show smoother surfaces. For the same surface grain density, the surface roughness tend to be larger for DPLF3 films which have a far lower primary nucleation density than the other two groups of samples.

The Raman spectra of group G-3 films after one hour of deposition are shown in Figure 3.14. The Raman spectra were excited from a HeNe laser with a wavelength of 633 nm and power of 25 mW. A large spot size of 250 μm was used to ensure a coverage of

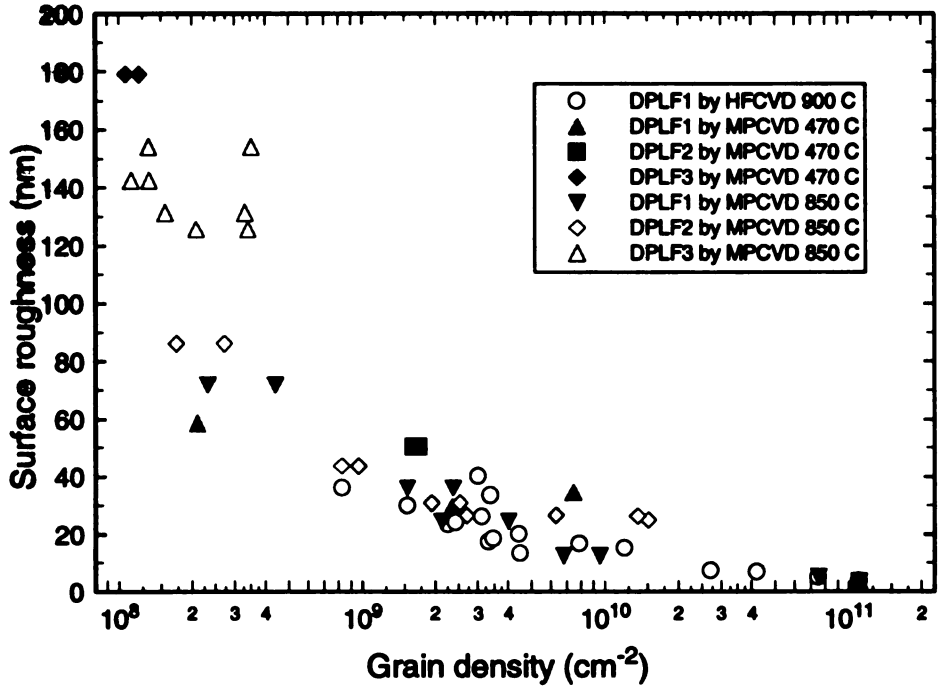

Figure 3.13 Surface roughness versus grain density for all samples.

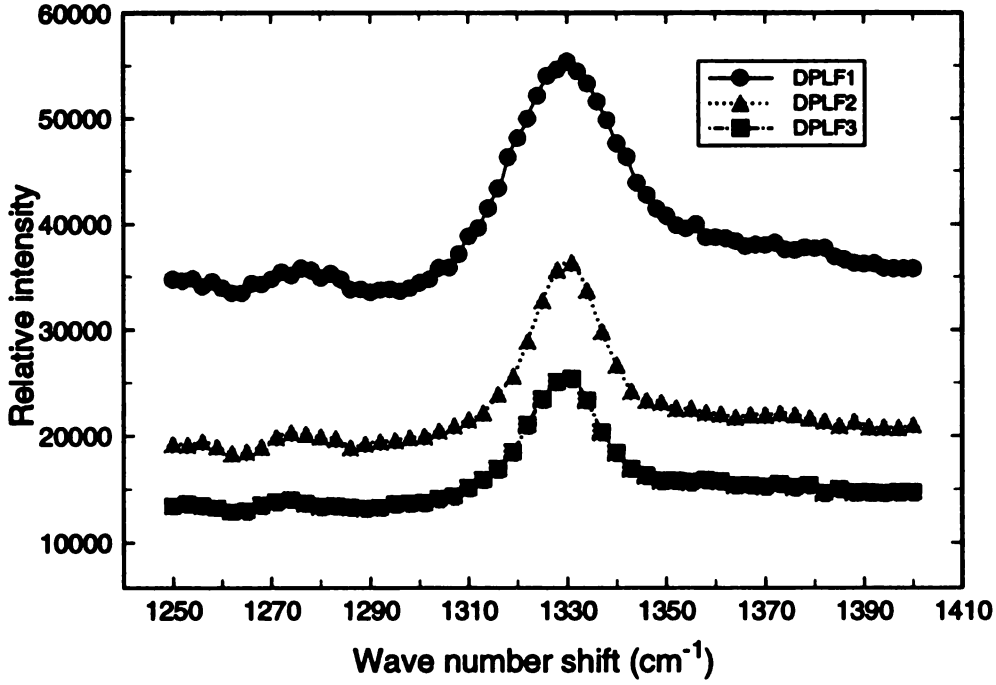

Figure 3.14 Raman spectra of three different seeding samples after 1 hour deposition by MPCVD at 850 °C.

fairly large number of grains. The full width at half maximum (FWHM) of Raman signal is usually an indication of the quality of the film. The broader Raman peak (~25 cm^{-1}) of DPLF1 sample may be due to a higher density of grain boundaries which contain a larger density of impurities and structure defects.

3.4 Diamond Device Fabrication Technologies

3.4.1 Patterning of Diamond Films

For many of the potential microelectronics and microsensor applications, the patterned polycrystalline diamond films are required. Various patterning techniques, as described in previous chapter (2.5.4), have been developed to fulfil the need of desirable structures in those applications. However, most of those techniques, which involve selective etching or selective deposition, either cause damages on substrate surfaces or have poor reproducibility. Recently, a novel patterning process, diamond power loaded photoresist (DPR) patterning technique, has been developed at Michigan State University to selectively deposit high quality polycrystalline diamond films through standard photolithographic processes [61]. This technique not only achieves excellent selectivity without surface damages, but is also compatible with the existing integrated circuit fabrication technology. This technique is adopted in the present research to pattern CVD diamond films. This section deals with the modification of DPR technique to incorporate patterning of ultrahigh nucleation density samples. In addition, problems, difficulties and proposed solution are also included in this section.

3.4.1.1 Photolithographic Methods

The DPR patterning technique is used in this research to prepare samples coated with DPLF3. In this technique, DPLF3 is spin-coated on substrates, Si or oxidized Si wafer in most cases, and is patterned by standard photolithography. The spin rate was in the range of 2000 - 4000 rpm. An enhanced diamond nucleation density was observed at lower spin rate, however, the seeding uniformity seems inferior. An optimal spin speed of 3000 rpm was found to possess a nucleation density on the order of 10^8 cm^{-2} with good uniformity. The ratio of nucleation density in the undesired area and that in the desired area is in the range of 7.57×10^{-3} - 3.38×10^{-4}. In the case of DPLF1 and DPLF2, a combination of seeding fluids and photoresist are used for seeding/patterning. As shown in Figure 3.15, first, a sacrificial layer of photoresist is uniformly spin-coated on the substrate with a high spin rate of 4500 rpm. The seeding fluid then is manually brushed over. The second layer photoresist is spin-coated at a speed of 4000 - 4500 rpm to prevent the seeding material from being removed during the developing process. Due to the poor transparency of DPLF1 and DPLF2, a full exposure of the first photoresist layer prior to the coating of seeding fluid is helpful to improve the selectivity. However, it may cause the problem of over developing resulting a poorly defined pattern edge. The schematic of DPLFs patterning procedure by standard photolithography is shown in Figure 3.15. SEM pictures of diamond structures[1] prepared by both patterning procedures are shown in Figure 3.16 for comparison. The wavy edge observed on DPLF1 pattern is mainly caused by the over developing of the first layer photoresist and the non-uniformity of DPLF1 seeding fluid coated by hand brushing. A uniform and well controlled application technique is essential to improve the pattern quality of DPLF1 and DPLF2 seeded samples.

---

1. The 1st mask of second generation testchip by Izzat Taher is used to define the diamond patterns.

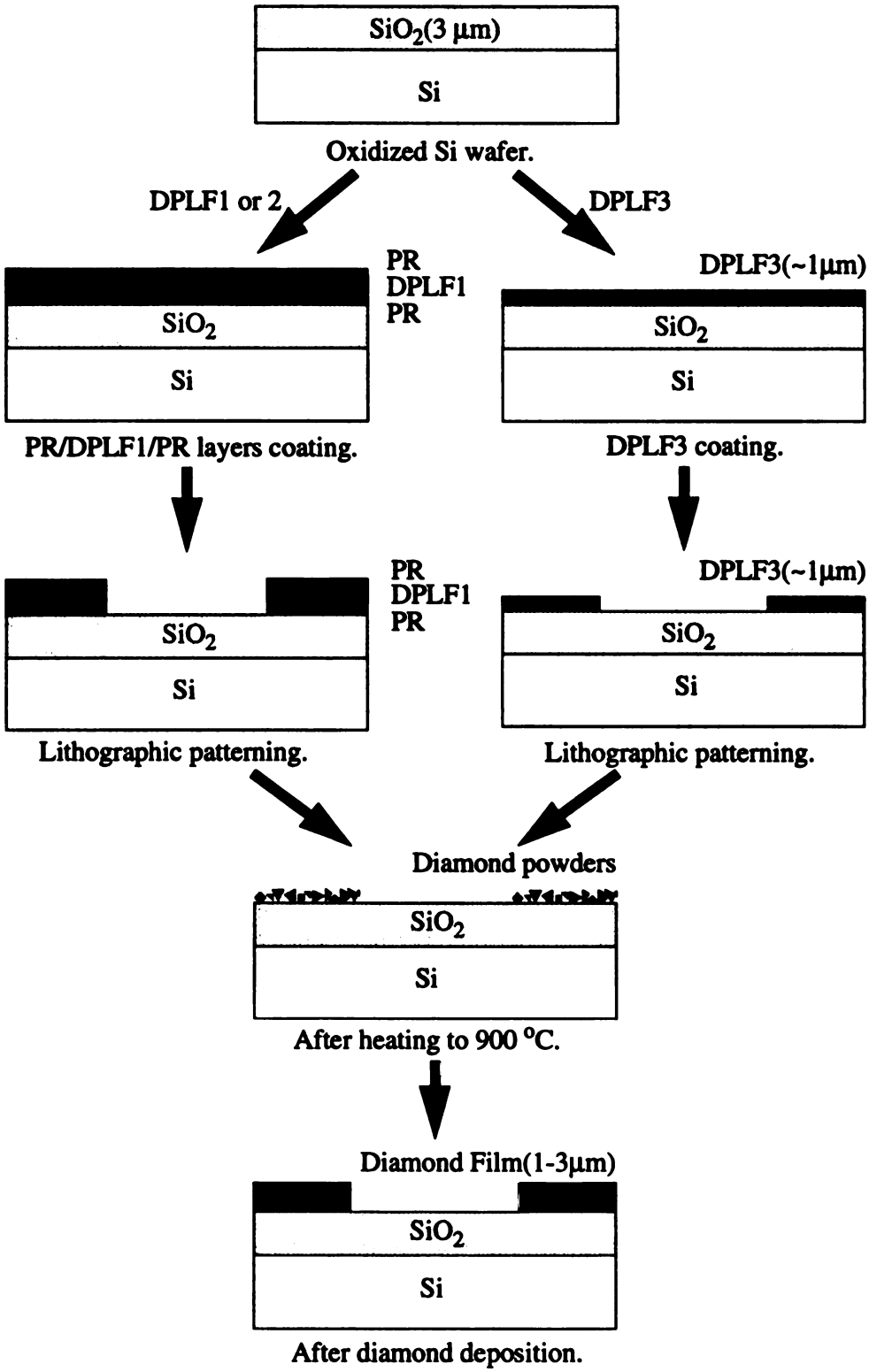

Figure 3.15 Patterning of diamond film by DPLFs method (not to scale).

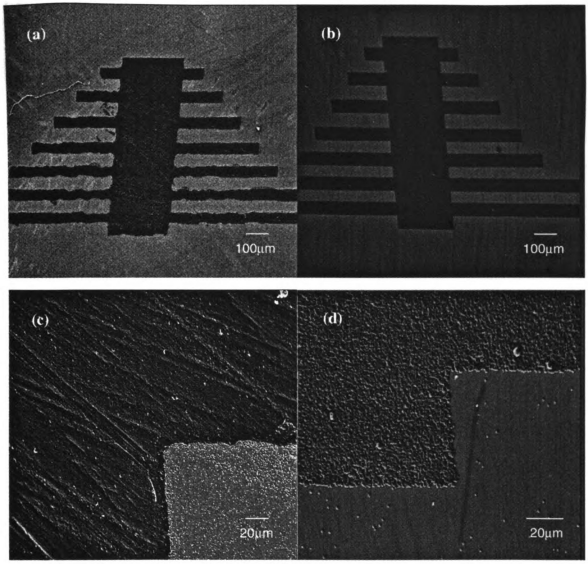

Figure 3.16 Patterning results of (a) & (c) DPLF1 and (b) & (d) DPLF3 samples by photolithography.

3.4.1.2 Direct-write Patterning Method

The nucleation enhancement and patterning techniques used today are mostly restricted to flat samples. In the case of real world micro-sensor or -heater applications, the objects are most likely to have arbitrary shapes. In order to take full advantages of CVD diamond devices, which can be deposited directly on the objects to minimize the uncertainties of measurements associated with the heat dissipation and the placement of sensing elements, there is a need to develop a seeding and patterning technique which is compatible with standard IC fabrication processes, amenable to ultrahigh nucleation density, capable to enhance the selectivity, and adaptable to three dimensional patterning.

In direct-write patterning technique, DPLFs are used as seeding materials and are applied to substrate surfaces via a fine spray nozzle. The minimum pattern size can be varied by selecting the opening sizes of nozzles. In initial experiments, a capillary of wire bonder, with an opening of ~40 μm (1.5 mils) was fixed in front of syringe needle and was used as a spray nozzle. The width of lines manually created on Si or oxidized Si wafers are in the range of 125 - 600 μm. In the case of DPLF1 and DPLF2, a substrate temperature of 65 - 75 ^{o}C is found optimal to dry the seeding fluids before it spreads out. Figure 3.17 shows a picture of diamond lines and patterns created in preliminary experiments.

3.4.1.3 Construction of Direct-write Seeding/Patterning System

A computer controlled direct-write system is therefore designed and constructed to optimize the performance of direct-write pattern technique. The simplified schematic diagram of this system is shown in Figure 3.18. This system consists of three major sub-systems, namely, a three dimensional linear position stage, a air pressure controlled spray nozzle, and a temperature controlled sample holder. The major assemblies sit inside a 24 inch I.D., 10 inch high stainless steel base chamber with a 20 inch high, 24 inch O.D.,

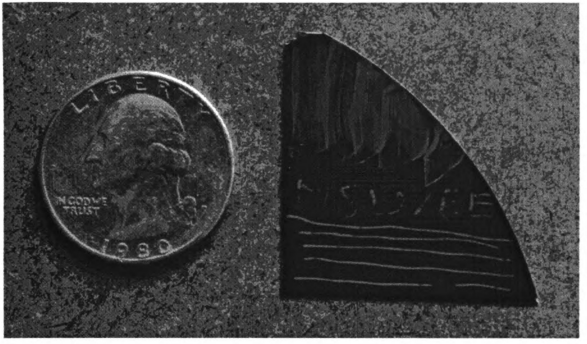

Figure 3.17 Diamond patterns by direct write method.

stainless steel bell jar cover. A Varian SD-200 rotary pump is used to evacuate the chamber.

• **3-D Position Stage**

Three AEROTECH model ATS-100 positional stages with a fine linear resolution of 1 μm along with a model U12R 4-channel motor controller are used to control the movement of the sample holder in X-Y axes and the nozzle in Z axis. In order to adopt 4 inch wafer technology, the linear movements of X, Y, and Z axes are 100, 100, and 50 mm, respectively. The 3 linear positional stages are prepared to be vacuum compatible to minimize the outgasing and contamination. The control unit of positional stages is interfaced with a personal computer via IEEE-488 interface.

• **Spray Nozzle**

A EFD[1] pressure controlled dispense valve system is used to spray the seeding material of DPLFs. The system consists of a model 740V-SS ultra precise needle valve, a 2.5 oz. cartridge reservoir, two air pressure regulators, and associated assembly. The amount of dispense fluid through the 740V-SS is determined by the valve open time, fluid pressure, flow control adjustment, dispense tip output size, and fluid viscosity. The operation of 740V-SS is triggered by a input gas, N_2, with a optimal operation pressure of 70 - 90 psi in a rated cycle frequency greater than 400 per minute. A solenoid valve, which is interfaced with a personal computer via an electrical relay, is chosen to control the on/ off of N_2 gas, thus determine the open time of 740V-SS. Figure 3.19 shows the circuit diagram of dispense valve system and the picture of 740V-SS needle valve.

• **Temperature Controlled Sample Holder**

1. EFD Dispense Valve Systems Group, East Providence, RI, U. S. A.

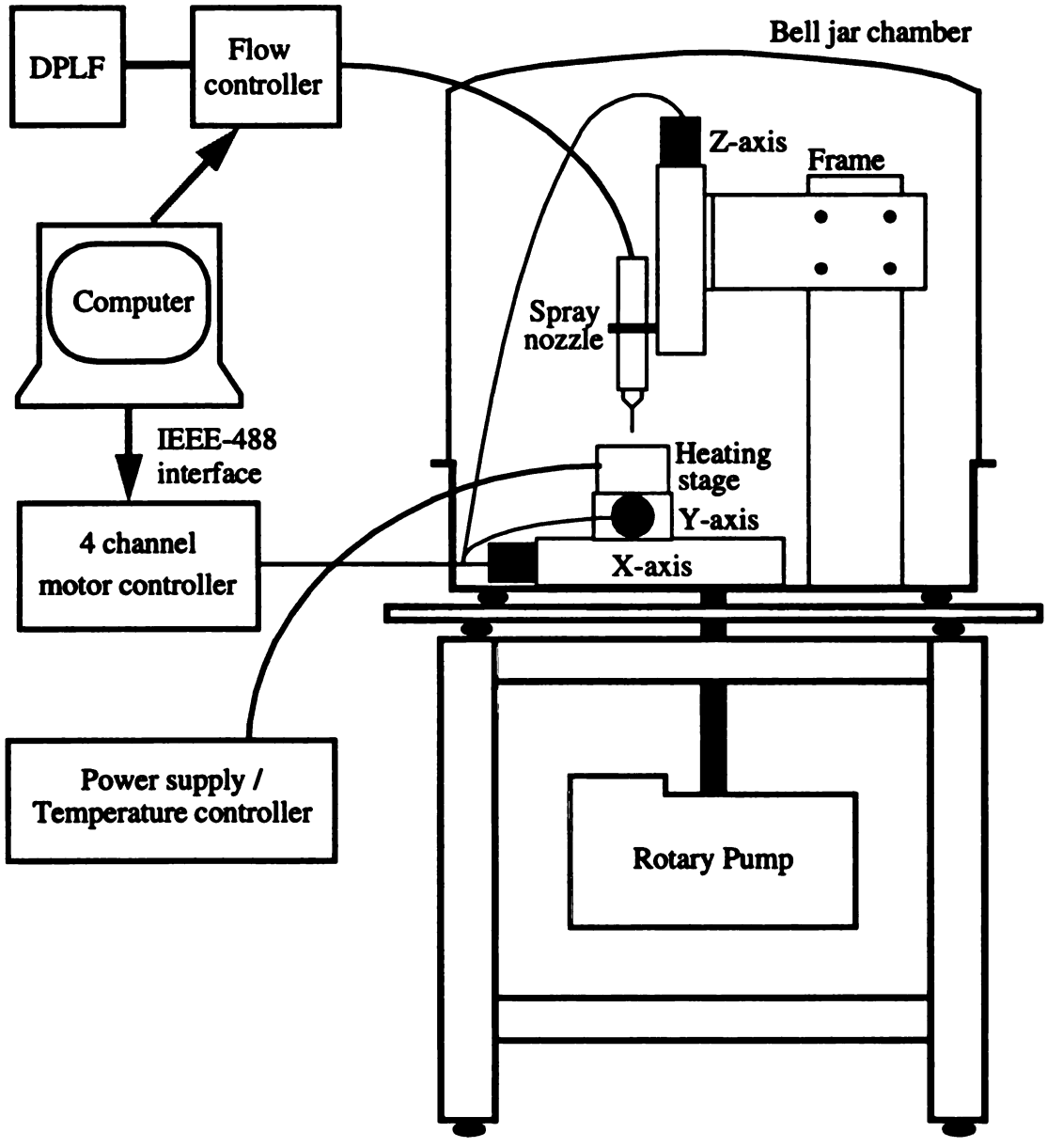

Figure 3.18 The schematic diagram of computer controlled direct-write system.

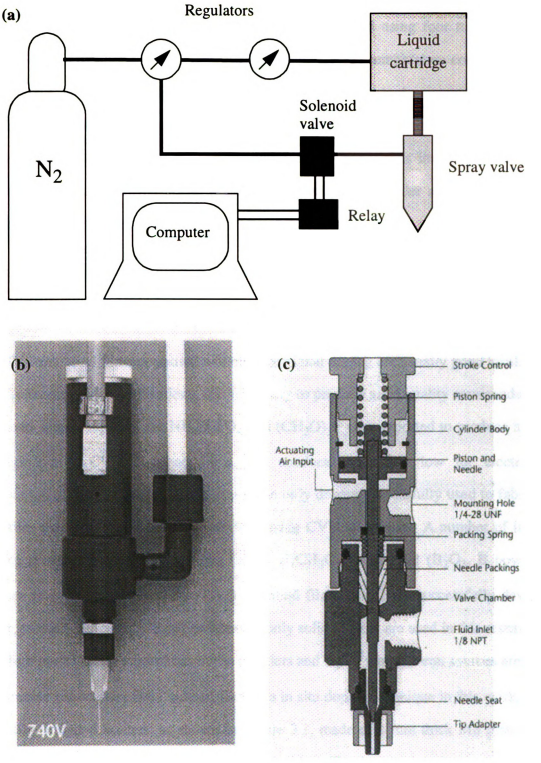

Figure 3.19 The circuit diagram of pressure controlled spray nozzle (a) and assemblies of dispense valve (b), & (c).

A circular stainless steel sample holder is built to hold samples up to 4 inch diameter. A uniform heating over the whole sample area is achieved using four tubular heaters connected in a parallel configuration. An Omegalux CN371 temperature controller along with a type K thermocouple are utilized to maintain a constant substrate temperature during seeding process. In order to avoid any damage of linear positional stage caused by excess heat, a 0.5 inch thick thermal insulating epoxy material is inserted between the heating plate and the linear stage. A drawing of the sample holder and a schematic of heating circuit are given in Figure 3.20.

3.4.2 Doping

CVD diamond films deposited without intentional doping are usually good insulators. For electronic device applications, it is necessary to produce good quality semiconductive diamond films. Although the $NH_4H_2PO_4$ and $(CH_3O)_3P$ were reported to produce n-type semiconductive CVD diamond films, the conductivity is too low for electronics application [120,121]. At present, boron is the only dopant successfully used to fabricate thin film diamond based electronic devices using CVD techniques. A number of in situ doping techniques involving gaseous (B_2H_6, $B(CH_3O)_3$) and solid (B_2O_3, B powders) sources to incorporate boron into CVD diamond films have been successfully devised. Since gaseous sources are highly poisonous, only solid sources are used in this research.

High purity (5N8) amorphous boron powders and B_2O_3[1] plana boron sources are used to fabricate semiconductive diamond films via in situ doping technique in this work. Two specially designed holders, as shown in Figure 3.1, made of 1 mm thick Mo plate were used to introduce boron powder into process chamber. The doping sources were placed on substrate holder during the deposition. In the earlier work, a uniform doping profile was

1. The boron doping source is available from Techneglas Co., Perrysburg, OH.

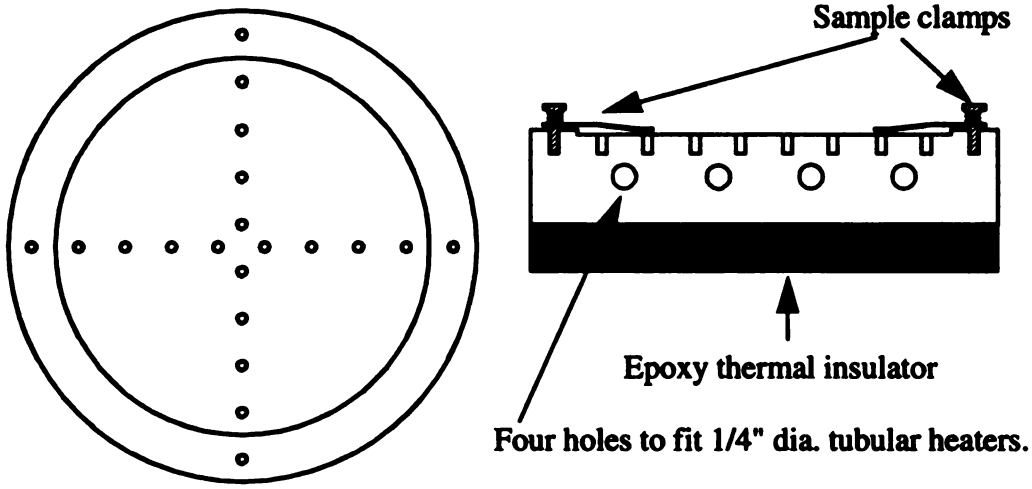

(a) Top view

(b) Side view

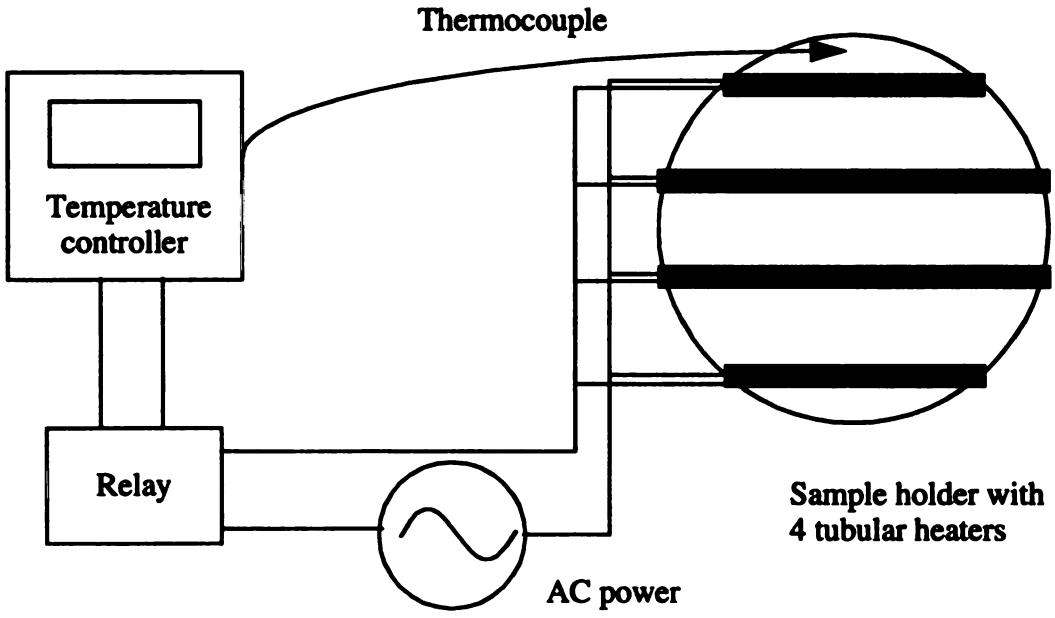

(c) Circuit diagram

Figure 3.20 Temperature controlled sample holder.

confirmed by secondary ion mass spectroscopy (SIMS) measurement [19]. A layer of undoped diamond under the p-type layer was found to enhance the quality of p-type diamond films, measured in terms of sp^3/sp^2 ratio by Raman spectroscopy, even for very high doping levels [19,122].

3.4.3 Metallization

Metallization is an important process in the fabrication of electronic devices. Ti/Au, Ti/Pt, and Ti/Mo/Au were reported by several workers to provide good contacts with both single crystal and polycrystalline diamonds. For the diamond sensor/heater application, the choice of contact metal was based on (i) ohmic contacts, (ii) good adhesion to both diamond and silicon dioxide and (iii) resistance to high temperatures.

Due to the limitation of single target metal evaporation facility, Al and Cr were tested on the samples which diamond films were synthesized on SiO_2 substrates. Both Al and Cr with a thickness in the range of 0.6 - 1 μm were thermally evaporated under a pressure less than 10^{-6} torr. Different patterns, used in the present research, were defined either by stainless steel shadow masks[1] or by photolithographic processes and wet etching. Due to the small sizes of single crystal samples and large grain polycrystalline diamond substrates, double layers of Pt/Ti (5000 A/500 A) contacts were thermally deposited through copper shadow masks[2].

After the metallization, samples with contact metals of Al, Cr, and Pt/Ti were thermally annealed at 500, 500, and 800 °C for 20, 20, and 5 minutes, respectively, in N_2 by tubular furnace or rapid thermal processor (RTP). Both Al and Pt/Ti contact layers

1. The masks were fabricated at the Ford photographic facility.
2. The Pt/Ti double layer was deposited using the two targets thermal evaporator in Department of Chemistry. The maximum sample size is limited to 1 inch diameter.

show good adhesion on diamond and SiO_2 (if any). The Cr contacts, especially on diamond area, peel off after heat treatment. It is believe that Cr oxidizes immediately in atmosphere ambient which results poor adhesion on diamond and SiO_2. A non-oxidized protective layer, such as Au, is suggested to form a reliable contact. Figure 3.21 shows SEM pictures of three metal contacts on single crystal and polycrystalline diamond samples after annealing. The ohmic contacts of Al with polycrystalline diamond films and Pt/Ti with both polycrystalline and single crystal diamond substrates are confirmed by I-V measurements at room temperature, as shown in Figure 3.22. A Keithley 224 programmable current source along with a Fluke 8840A multimeter are used for I-V characterization. The voltage reading was taken right after current was applied to minimize the self-heating effect especially at current > 10^{-4} A.

3.5 Summary

In this chapter, the development, modification and implementation of diamond infrastructure techniques are described in terms of thin film deposition, enhancement of nucleation density, and device fabrication.

In addition to the design and construction of a MPCVD reactor, the HFCVD deposition technique used for preparing CVD diamond samples in the present work is described in 3.2. In 3.3, an improved seeding technique for diamond thin film deposition is demonstrated. An extremely high nucleation density on the order of 1.1 x 10^{11} cm^{-2} was achieved by coating 0.038 μm diamond powders on Si substrates. One micrometer thick films with the mean surface roughness of 30 nm, as measured by AFM, were obtained [73,117]. The effects of nucleation density on growth rate, surface roughness and grain size are studied in the deposition temperature range of 470 - 950 °C using both HFCVD and MPCVD. It is found that the surface roughness is strongly dependent on nucleation

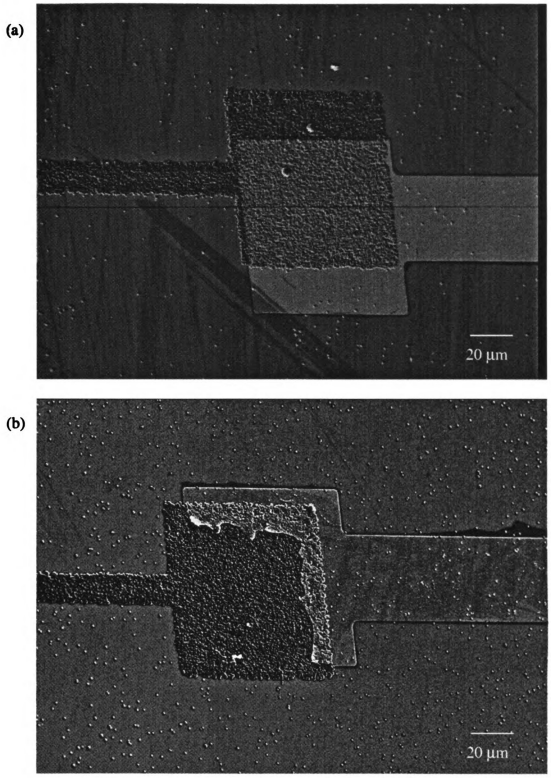

Figure 3.21 SEM pictures of metal contacts after annealing. (a) Al, (b) Cr on poly-diamond and SiO_2 substrates.

(c)

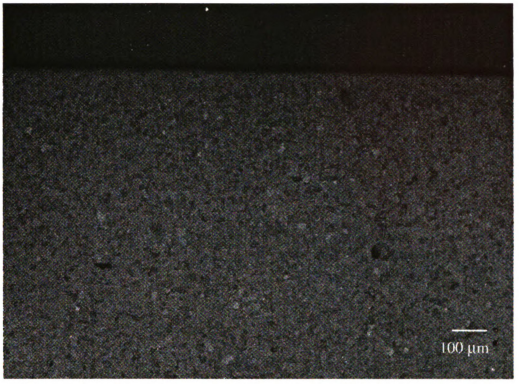

(d)

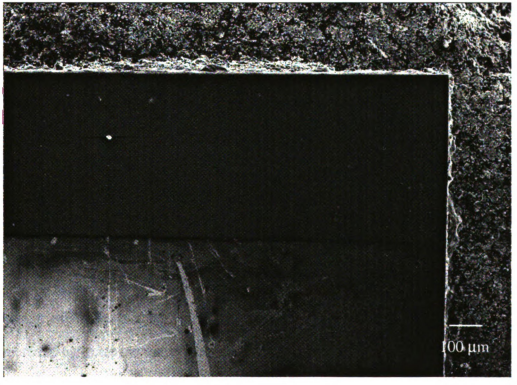

Figure 3.21 (Cont'd)

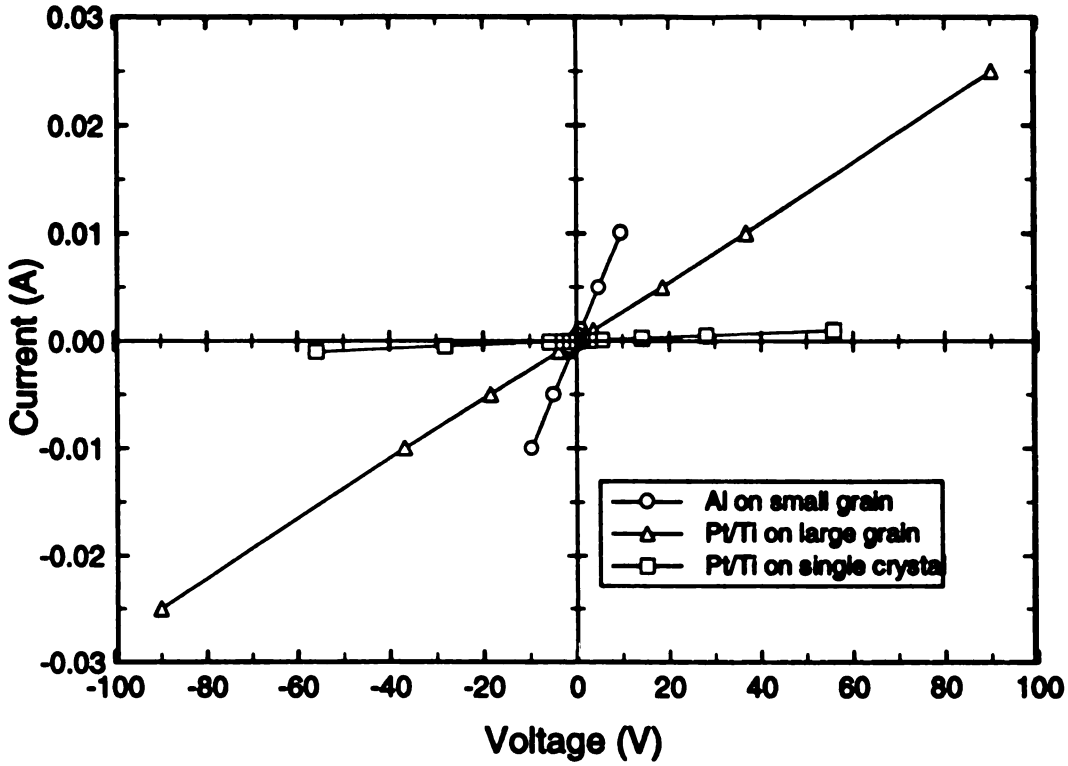

Figure 3.22 The I-V characterization of diamond testchips with different grain sizes and contact metals.

density at the early stage of deposition. This enhanced nucleation density is helpful to obtain continuous and smooth thin films for short deposition periods, especially at low temperatures. The techniques of diamond electronic device fabrication, such as patterning, doping, and metallization, are presented at 3.4. A direct-write technique is proposed in this chapter to enhance the selectivity of patterned polycrystalline diamond films. The preliminary experiments show encouraging results. A computer controlled system is constructed to optimize the performance.

CHAPTER 4

SINGLE ELEMENT DIAMOND SENSOR/HEATER STRUCTURE

4.1 Introduction

Heat generation and temperature sensing are required for controlled heating applications and for liquid level sensors, mass flow meters, and vacuum and pressure gauges, which operate based on the variations of heat dissipation [3]. As the materials commonly used as heating elements lack high sensitivity to the temperature change, different materials are utilized for heating and temperature sensing. In such a configuration, thermal and chemical properties of materials involved, if not carefully considered, may cause problems. It is also important to minimize the response time and uncertainties of measurements associated with heat dissipation and placement of sensing and heating elements. The use of a single element as a heater and a temperature sensor may help eliminate such problems.

Due to its large band gap, high thermal conductivity, high sensitivity to temperature change, micro-machining capability, the ability to be used as an electrical conductor and insulator, and chemical and mechanical stability, diamond is an excellent material for high temperature sensing and heating applications, especially under harsh environments. This chapter describes the temperature sensing and heating properties of single-element-

diamond sensor/heater structures.

4.2 Experimental

4.2.1 Sample Descriptions

P-type boron doped diamond resistors with different dimensions and structures are synthesized on oxidized Si wafers, polycrystalline and single crystal (100) type II-a diamond substrates by HFCVD. High purity boron powder or B_2O_3 planar boron wafer are used as sources for in-situ doping. The fabrication processes are described in previous chapters in detail. Figure 4.1 presents the schematic designs or photograph of all seven test structures. Table 4.1 summarizes some important parameters of samples of all test structures. The metal contacts, both Al and Pt/Ti double layer, are thermally deposited on p-type diamond as electrical connections. In the case of test structure #7 samples (group S7), the thermal annealing is done inside a thermal furnace with N_2 flow. For the rest of the samples, the annealing is performed by using a rapid thermal processor (RTP) in nitrogen environment. With the exception of test structures #3, #4, and #7 (groups S3, S4, and S7), samples are annealed before the metallization. Al contact then is annealed at 400 - 450 ^{o}C for 5 - 10 minutes in N_2.

The sample notation in the form of *"SX-Y"* are used through out this chapter to describe a single sample. The *"X"* specifies the group number as well as the test structure of the sample. The *"Y"* denotes sample number with the same structure. In the case of test structure #1 and #7 (groups S1 and S7), which contain more than one resistor per test chip, the form *"SX-RZ"* is used to indicate a certain resistor by number *"Z"*. For example, the S3-1 denotes the sample No. 1 with #3 test structure and S1-R3 refers to the number three resistor of test structure #1 sample.

TABLE 4.1 List of important process parameters of test structures

Test structure	Sample group	Grain size (μm)	Doping source	Metal contact	Annealing
#1	S1	1-2	Boron powder	Al	650 °C, 10 min
#2	S2	1-2	Boron powder	Al	750 °C, 10 min
#3	S3-1	15-50	Boron powder	Pt/Ti	800 °C, 5 min
	S3-2	15-50	B_2O_3		
	S3-3	150-350	B_2O_3		
#4	S4-1	None	Boron powder	Pt/Ti	800 °C, 5 min
	S4-2		B_2O_3		
#5	S5-1	1-2	Boron powder	Al	800 °C, 5 min
	S5-2		B_2O_3		
#6	S6-1	0.3-0.5	Boron powder	Al	700 °C, 10 min
	S6-2	1-2			
#7	S7	1-2	Boron powder	Al	500 °C, 20 min

Note : 1. Group S1, S2, S5, S6-2, and S7 samples are prepared by DPLF3 nucleation method.

2. S6-1 sample is prepared using DPLF1 nucleation method.

3. Group S3 substrates with large grain sizes are commercially available from Diamonex Incorporated, Allentown, PA.

4. Group S4 substrates are single crystal (100) type IIa diamond supplied by Dubbeldee Harris Diamond Corp.,Mount Arlinton, NJ.

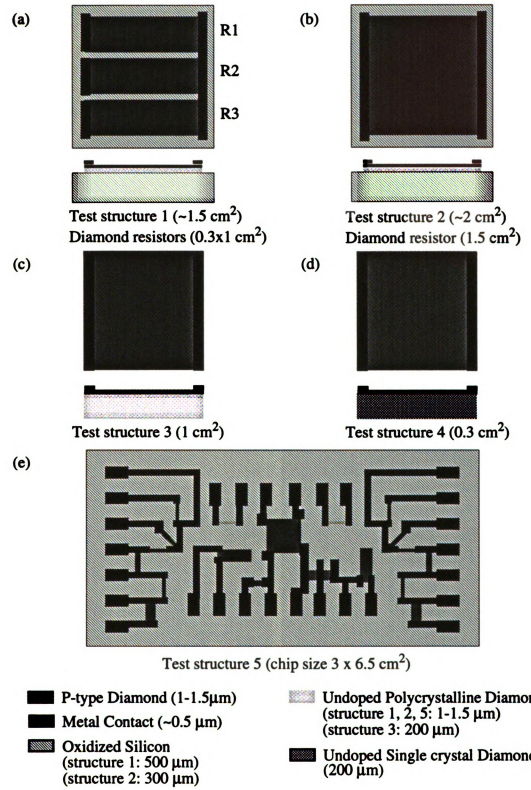

Figure 4.1 The schematic diagrams of diamond test structures.

(f)

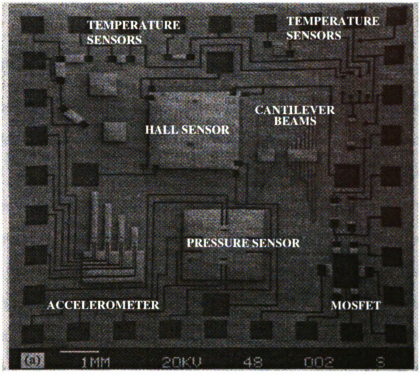

Test structure 6 (chip size 1 cm^2)

(g)

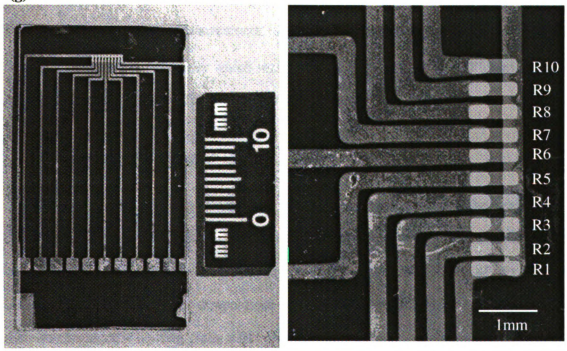

Test structure 7

(on the right shows the close view of diamond thermistors array)

Figure 4.1 (Cont'd)

4.2.2 Measurement Setups

A development in the characterization methods is important for new materials. Initially, performance of fundamental property characterizations is essential to understand the material and to identify applications. Once a prototype is developed, the characterization can then focus more on device performance to optimize device configuration and structure. The characterization of single element diamond sensor/heater structures in this research consists of temperature response characterization, heating properties characterization, and temperature profile characterization. In addition, the effects of grain size on electrical properties and resistivity stability are studied by Hall and R vs. Time measurements, respectively. This section describes the experimental measurement setups used in these characterizations in detail. With the exception of the Hall and infrared camera measurements, all measurements are performed inside a 18 inch stainless steel vacuum chamber which maintains a vacuum of 10^{-3} to 10^{-7} torr or a static atmosphere ambient to stabilize the temperature reading.

- **Temperature Response Characterization**

It is mainly an I-V measurement under different temperatures. The resistivity of diamond films is determined as a function of temperature by applying a constant current of 1 μA. Temperature is measured by type K thermocouples. The details of this setup can be found in Table 4.2. Since temperature of samples is varied via an external 1.75 inch diameter boralectric heating plate, a BN probe station, based on the considerations of high temperature stability and high thermal conductivity, is custom made for R vs. Temp. measurement. The electrical connection with remote equipment is provided through tungsten (W) probes along with stainless steel clamping bases. Oxidized Si wafer with the

TABLE 4.2 Details of measurement setups

Characterization	Equipment list	Sample placement
Temperature response	a. Keithley 224 programmable current source b. HP 3457A multimeter and/or Fluke 8840A multimeter c. Omega Digicator and/or CN9000 temperature read-out with type-K thermocouples	a. BN holder (5.08cm x 3.81cm x 0.635cm) b. Oxidized Si wafer (2.54cm x 2.54cm x 500μm)
Heating properties	a. HP 712B high voltage DC power supply b. HP 3457A multimeter and/or Fluke 8840A multimeter c. Omega Digicator and/or CN9000 temperature read-out with type-K thermocouples d. Boralectric heating plate	a. Al holder (5.08cm x 3.81cm x 0.635cm) b. Al clamp (0.9525cm x 3.81 cm x 0.3175cm) c. Mica glass holder (5.08cm x 3.81cm x 0.635cm)
Temperature profile	a. Variac AC power supply b. Fluke 77 portable multimeters c. Inframetrics Model 600L infrared imaging radiometer d. Thermoteknix ThermoGram image processing card e. FOR.A VTG33 video timer f. Video cassette recorder	Hanging in the air via two copper clamps.
Hall measurement	MMR technology Low temperature Hall system: a. H-50 Hall, Van Der Pauw controller b. R2500-2 LTHS refrigerator, c. K-20 programmable temperature controller	Substrate holder of LTHS.

thickness of 500 μm is also used as an alternation for measurements with maximum temperature higher than 900 K. A schematic diagram of measurement setup and different configurations of sample holders are shown in Figure 4.2.

• **Heating Properties Characterization**

Supplying a DC voltage up to 287 V, the temperature, applied voltage and current of diamond sensor/heater test structures are recorded. The applied power density and resistivity are then calculated from the collected data as functions of temperature for power density vs. heating temperature and simultaneous heating/sensing characterizations, respectively. Diamond samples were tested under different configurations using Al holder, mica glass holder, and Al clamp. Al holder, with high thermal conductivity, is used as a heating load for diamond thin film heater in a temperature range of 300 ~ 500 K. Al clamp is used to construct a cantilever configuration. Based on the consideration of high temperature capability and thermal insulation, a mica glass holder is chosen to reduce the amount of heat generated by diamond thin film heaters loss through conduction. Therefore, a high heating temperature of 950 K can be reached. A saw-toothed shape mica glass structure, placed under the sample, was found to further improve the thermal isolation. The temperatures are determined by type K thermocouples. Tungsten (W) probes along with stainless steel clamping bases are used to provide electrical contacts with the remote equipment. The details of equipment used in this setup are listed in Table 4.2. Figure 4.3 shows a schematic diagram of measurement setup and different sample holder configurations.

This setup is also adopted for resistivity stability evaluation.

• **Temperature Profile Characterization**

The temperature profile characterization of diamond thin film heaters were achieved

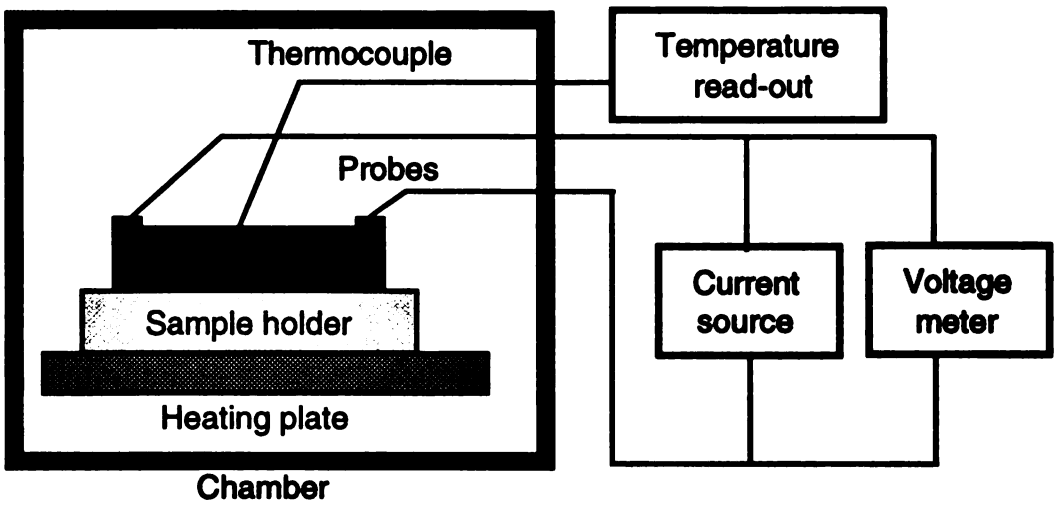

(a) Temperature response characterization

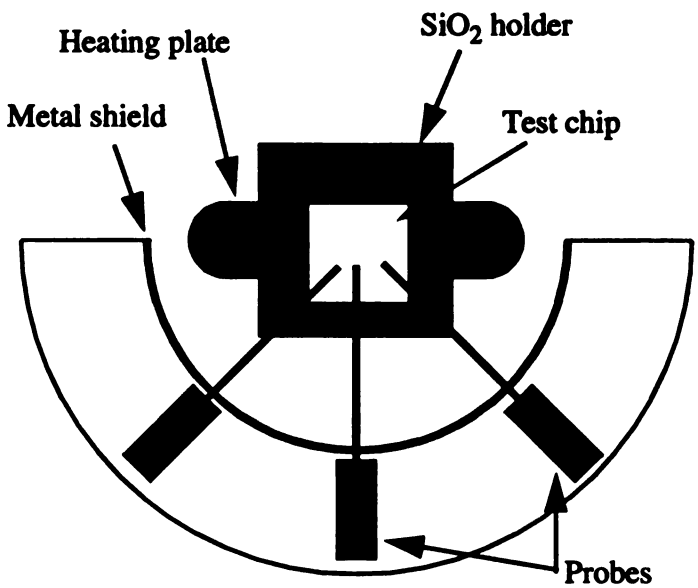

(b) Top view of SiO_2 holder configuration

Figure 4.2 The experimental setup configurations of temperature response characterization.

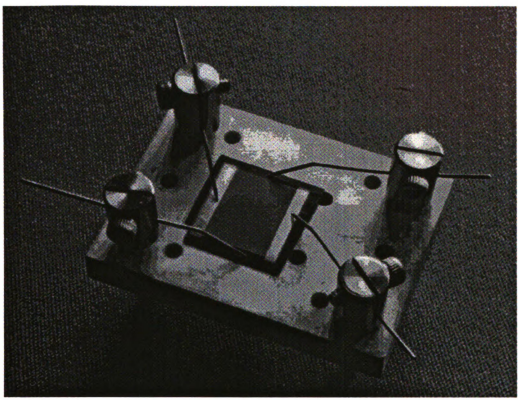

(c) BN holder

Figure 4.2 (Cont'd)

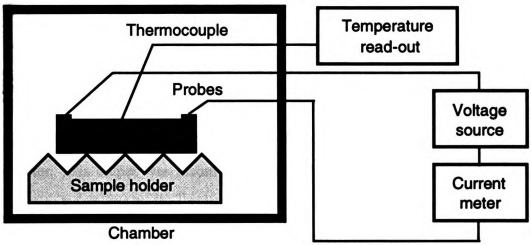

(a) Sensing/heating characterization

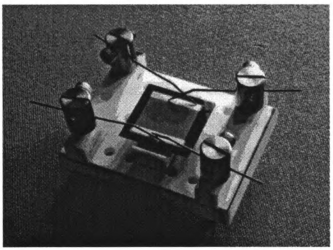

(b) Mica holder

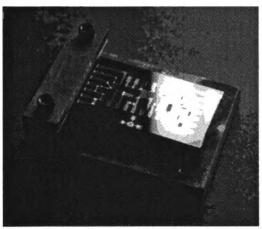

(c) Al holder/clamp

Figure 4.3 The experimental setup for heating/sensing characterization.

utilizing an infrared camera system, consisting of (i) Inframetrics Model 600L infrared imaging radiometer, (ii) thermal image processing system, (iii) FOR.A VTG33 video timer, and (iv) a video cassette recorder. The first two components, the infrared radiometer and the image processor are used for temperature measurement. The video timer was used to superimpose digital indications of time and date onto the transient output from radiometer. This output was recorded in standard RS-170 format on a video cassette recorder. A diagram of the data acquisition system is displayed in Figure 4.4.

Transient temperature measurements were made utilizing the Inframetrics 600L infrared radiometer in conjunction with the Thermoteknix ThermoGRAM image processing card. The system allows real-time thermal imaging of static and dynamic events with variable image averaging, temperature ranges, emissivity settings, and fields of view. Individual thermal images, consisting of 365x280 individual pixels can be acquired and saved. Temperatures are calculated from the radiant intensity of each pixel using calibration curves unique to the spectral response of the system. Over 102,000 surface temperature measurements are accessible in each thermal image.

The 8 bit infrared system can operate in a variety of temperature span settings. In its smallest setting of 5 ^{o}C, a maximum thermal sensitivity of 0.02 ^{o}C can be obtained. The special external optics used, consisting of a 6" close - up lens attached to the end of a 3X telescopic lens, allows a spatial resolution of better than 1 pixel/10 μm in the smallest field of view. The smallest area that can be fully imaged is approximately 4 mm x 3 mm.

- **Hall Measurement**

A MMR Technology low temperature Hall Van der Pauw system is used to measured the Hall concentration and mobility at 300 K.

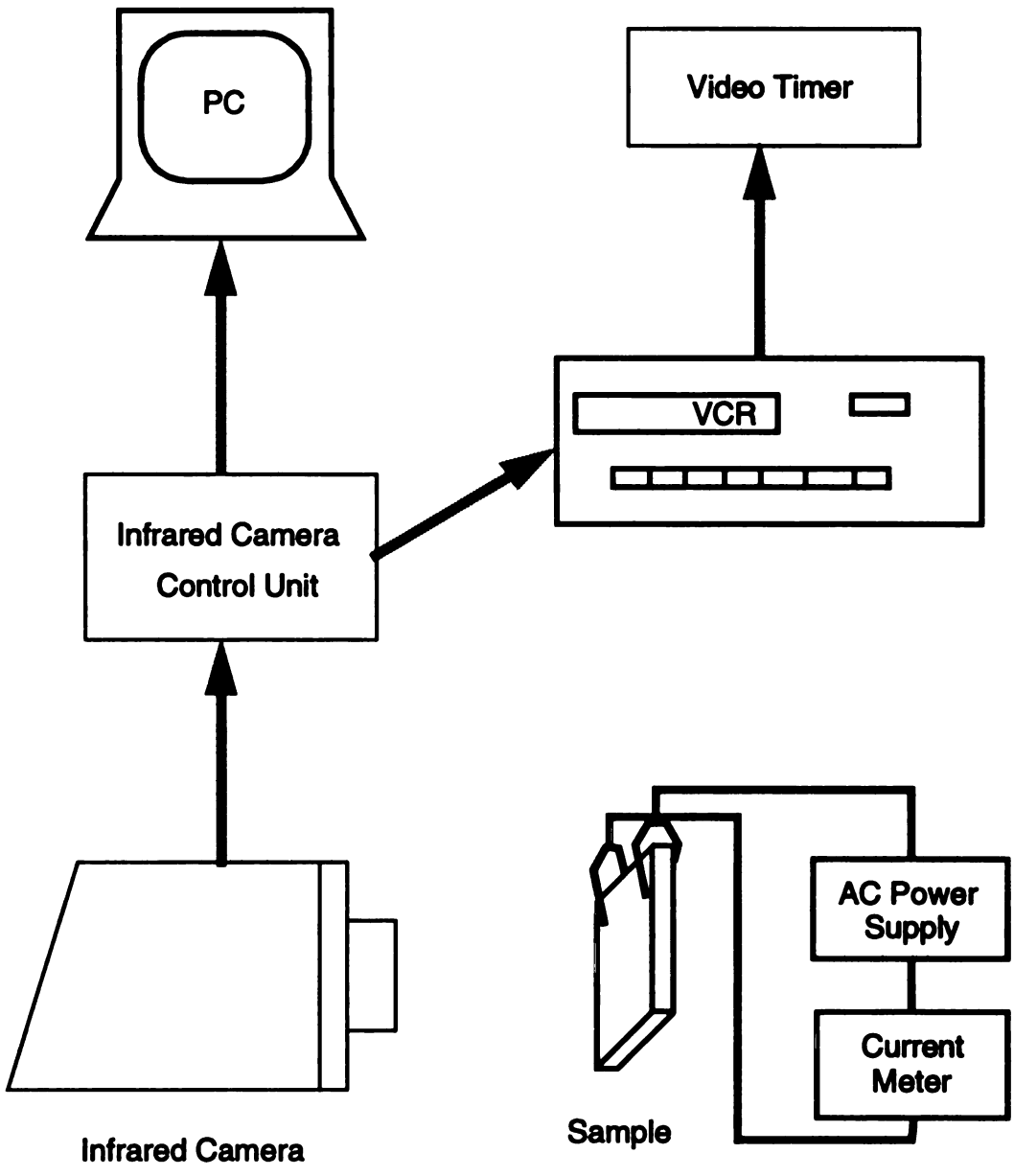

Figure 4.4 Schematic of temperature profile characterization.

4.3 Temperature Sensors

Due to its negative temperature coefficient of resistivity, diamond can be used as a temperature sensor [18]. In this section, the temperature response of diamond is studied over a wide variety of sample structures (homoepitaxial and polycrystalline), grain sizes, doping levels, and annealing temperatures. A qualitative description of results is provided at the end of this section.

4.3.1 Contact Resistance

With the exception of the study of annealing effect on resistivity, the electrical contacts were provided by thermally evaporated Al (on small grain films) or Pt/Ti (on both large grain and homoepitaxial diamonds). Annealing prior to electrical measurements was performed to enhance the contact quality. The representative I-V curves of three different metal-diamond interface structures, shown in Figure 4.5, indicate an ohmic behavior over a large applied current range after annealing. Plot (a) and (b) present the applied currents in both forward and reverse directions. Low contact resistivity on the order of 10^{-6} Ωcm^2 was reported using carbide forming metal (Ti) on both single crystal and polycrystalline diamond [88,89,90]. A small applied current of 1 μA was used for the resistivity measurements in the present study. As the contact resistance is negligible, two point-contact configuration was used unless noticed otherwise. The electrical contacts used in annealing effect study will be discussed in next section.

4.3.2 Effect of High Temperature Annealing on Resistivity

In order to produce reliable diamond temperature sensors, the effect of high

(a)

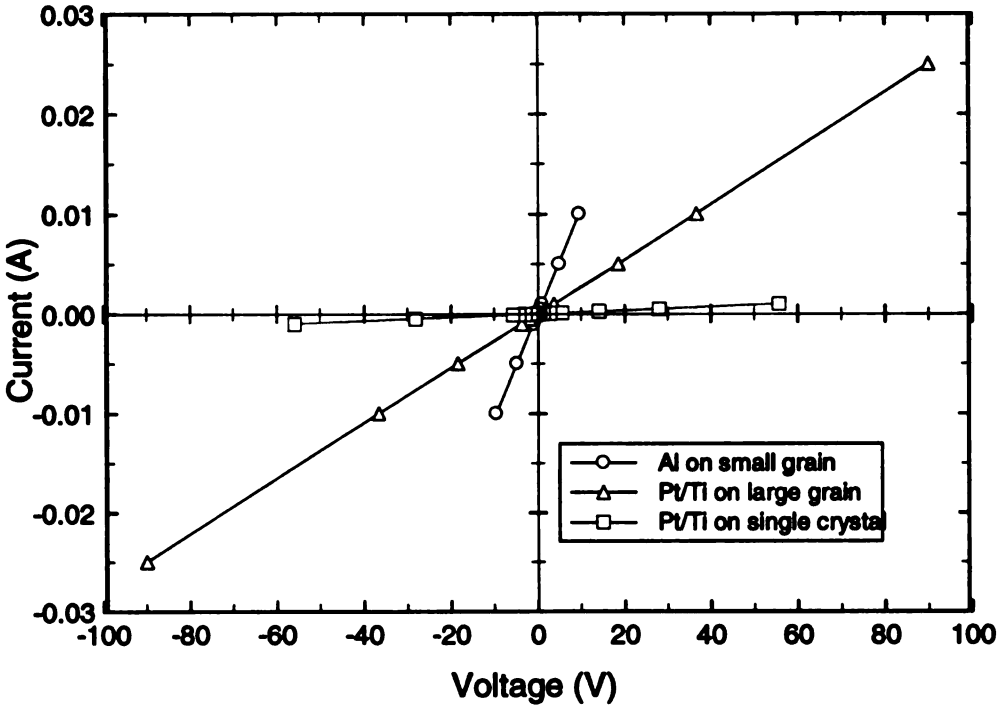

(b)

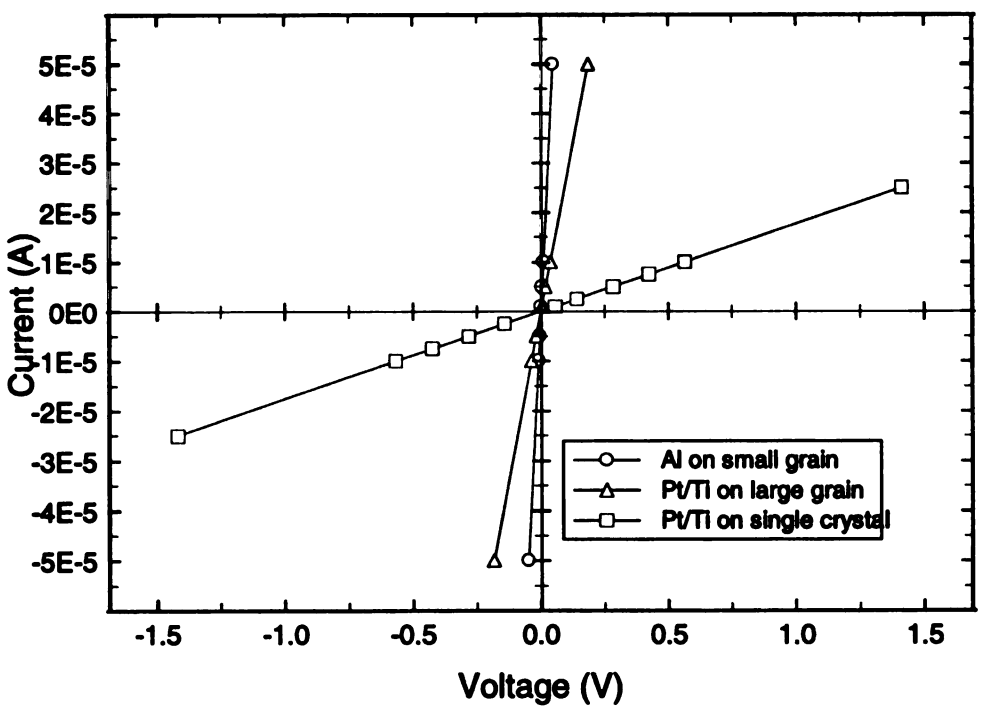

Figure 4.5 The I-V characterization of three different metal contact structures.

temperature annealing on resistivity of diamond films was monitored before and after a heat treatment using RTP (for both groups S3 and S4 samples) or tubular furnace (for group S7 samples). A 4-point probe station was utilized to measure the resistivity of large grain samples in group S3. Due to the small size of single crystal samples in group S4 (0.3 cm^2), only two inner probes of the 4-point probe station could form press contacts on the surface of tested films. In the case of small grain samples (group S7), evaporated Al was used in 2-point contact configuration. The details of sample description can be found in Table 4.1 and Figure 4.1. Table 4.3 summarizes the change in resistivity of these samples after a thermal annealing, where ρ_1 and ρ_2 represent the resistivity before- and after-annealing, respectively. A 460 - 985% increase in resistivity was observed for homoepitaxial diamond samples in group S4. No appreciable change in resistivity was observed in the case of large grain sizes polycrystalline diamond samples (group S3). The ratio of resistivity after and before annealing of S3 samples was in the range of 0.963 - 1.415. The resistivity of small grain samples (group S7) showed a 50 - 80% decrease after thermal annealing at 500 ^{o}C. Figure 4.6 plots the ratio of ρ_2/ρ_1 versus grain sizes. The present results show that the overall increase in resistivity after thermal annealing is more prominent for single crystal diamonds. The thermal annealing was found helpful to stabilize the resistivity-temperature characteristics of diamond films within the maximum annealing temperature.

4.3.3 Effects of Crystal Structure and Grain Size on Resistivity

Using single crystal substrates and polycrystalline films with grain sizes in the range of 0.2 - 300 μm, the effects of crystal structure and grain size on resistivity were studied to control the doping of CVD diamond. Table 4.4 summarizes the representative results. Several observations can be made based on the data in Table 4.4:

TABLE 4.3 The effect of thermal annealing on resistance

Sample No.	ρ_1 (Ωcm)	ρ_2/ρ_1	Grain size (μm)	Annealing	Contact method
S3-1	0.40675	1.185	15-50	800 °C, 5 min	4 point probe
S3-2	2.78530	1.415	15-50	800 °C, 5 min	4 point probe
S3-3	0.46898	0.919	150-350	800 °C, 5 min	4 point probe
S4-1	0.36939	10.849	Single crystal	800 °C, 5 min	2 point probe
S4-2	1.81588	5.605	Single crystal	800 °C, 5 min	2 point probe
S7-R1	61.7801	0.202	1-2	500 °C, 20 min	Evaporated Al
S7-R3	52.7231	0.222	1-2	500 °C, 20 min	Evaporated Al
S7-R6	110.568	0.480	1-2	500 °C, 20 min	Evaporated Al
S7-R9	174.904	0.394	1-2	500 °C, 20 min	Evaporated Al
S7-R10	167.075	0.392	1-2	500 °C, 20 min	Evaporated Al

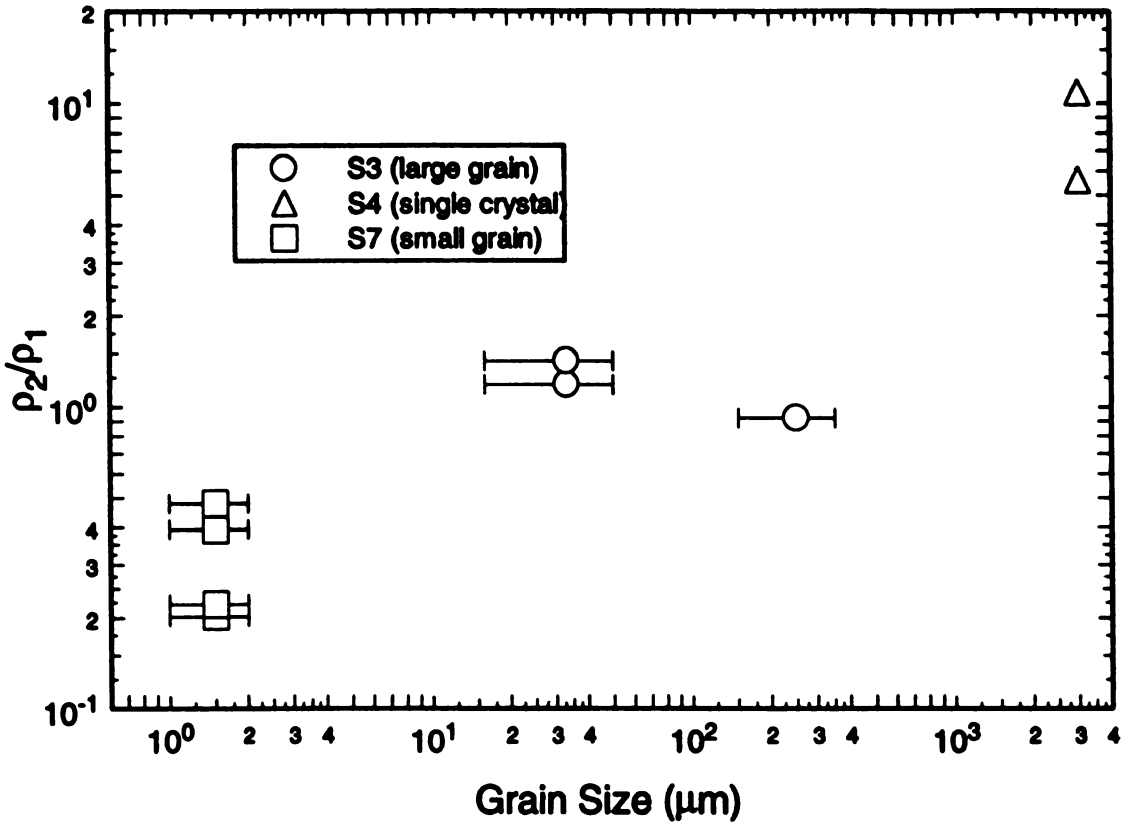

Figure 4.6 The grain size effect on resistivity before and after thermal annealing.

(1) The resistivity strongly depends on the relative position of samples with respect to the doping source during the deposition. In deposition batch #4, samples in group S2 with the same test structure and grain size were placed along the same direction but different distances from the boron source. The resistivity of these samples were found to increase as the distance from the doping source increased. The non-uniform doping is due mainly to the concentration gradient of boron atom in gas phase during deposition process.

TABLE 4.4 Comparison of resistivity for samples deposited at the same batch.

Batch No.	Sample No.	Grain Size (μm)	Distance from doping source	Resistivity (Ωcm)
#1	S6-1	0.3 - 0.5	2 cm	6.9461
	S6-2	1 - 2	2 cm	27.0538
#2	S3-1	15 - 50	1.5 cm	0.4823
	S4-1	Single crystal	1.5 cm	4.0075
	S5-1	1 -2	1.5 cm on the 90° direction	3.0619
#3	S5-2	1 -2	2.5 cm	1.5691
	S3-2	15 - 50	2.5 cm	3.9412
	S3-3	150 - 350	1 cm	0.4312
	S4-2	Single crystal	1 cm	10.1780
#4	S2-7	1 - 2	1 cm	0.25395
	S2-1	1 - 2	3 cm	1.1339
	S2-5	1 - 2	5 cm	3.83849

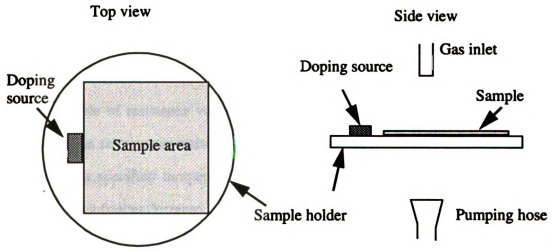

Figure 4.7 Schematic of typical placement of samples and doping source.

(2) The resistivity is also affected by the crystal structure and grain size of diamond films. Maintaining the same relative position to boron source in the same deposition batch, polycrystalline diamond samples with small grain sizes tend to have lower resistivity and higher Hall concentration[1] than those of samples with large grain sizes, as evidenced in deposition batch #1 (S6-1 vs. S6-2) and in batch #3 (S5-2 vs. S3-2). Similar results were obtained in the comparison of polycrystalline films versus homoepitaxial films. In the case of both batch #2 (S3-1 vs. S4-1) and batch #3 (S3-3 vs. S4-2), the polycrystalline samples have lower resistivity than the single crystal diamonds do.

(3) In batch #2, the small grain sample S5-1 possesses higher resistivity than that of large grain S3-1, although the distances between each sample and boron source are the same. This may be attributed to the inhomogenerous boron distribution in the gas phase due to the directional gas flow inside the deposition chamber.

4.3.4 Temperature Dependence of Resistivity

In the practical temperature sensing application, the zero-power resistance of a thermistor is measured to determine the temperature using a given characteristic equation or a listed table of resistance versus temperature values associated with this particular thermistor. The zero-power resistance is defined as a DC resistance value of a thermistor measured at a specified temperature with a power dissipation by the thermistor low enough that any further decrease in power will result in not more than 0.1% (or 1/10 of the specified measurement tolerance, whichever is smaller) change in resistance [123].

1.Due to the pattern of metal contacts, room temperature Hall measurement is only performed for group S6 samples.

In the present study, the resistivity not considering the effect of resistor dimensions on resistance is used to compare diamond resistors having different dimensions and structures. The zero-power resistivity, determined from the applied voltage, constant current of 1 μA and the resistor dimensions, is calibrated as a function of temperature in the temperature range of 300 - 1000 K for samples in groups S1, S2, S3, S4, and S7. The important parameters and schematic diagrams of samples used in this study are described in Table 4.1 and Figure 4.1, respectively. It is found that the R versus T characteristic of the diamond thermistor is reproducible after a thermal annealing of temperature higher than the maximum characterization temperature. Representative curves of resistivity versus reciprocal of temperature for samples with different substrate structures are presented in Figure 4.8. The plot (a) shows that the initial measurement results of small grain samples from groups S2 and S7 over a resistivity range of 0.156 - 65.493 Ωcm. The initial measurement data of samples from groups S3 (large grain) and S4 (single crystal) are presented in the plot (b). A significant reduction in resistivity ranged from 50% to two orders of magnitude was observed over the temperature range of 300 K to 673 K. It suggests that boron doped CVD diamond films are an excellent material for temperature sensing.

Non-linear relations of the log(ρ) versus 1000/T were observed for both single crystal and polycrystalline diamonds. For the small grain polycrystalline samples in groups S2 and S7, the linearity of log(ρ) vs. 1000/T relation seems to decrease with increasing resistivity, as shown in the Figure 4.8 (a). A merge of log(ρ) versus 1000/T curves of samples S2-4 and S7-R1 at temperature higher than 670 K suggests a slightly different temperature dependence between two sample groups. Due to the different doping sources (boron powder vs. B_2O_3 wafer) were used to prepare the p-type diamond films in the case of single crystal and large grain samples, different temperature behaviors were observed for these samples, as indicated in Figure 4.8 (b). The log(ρ) versus 1000/T curves were

(a)

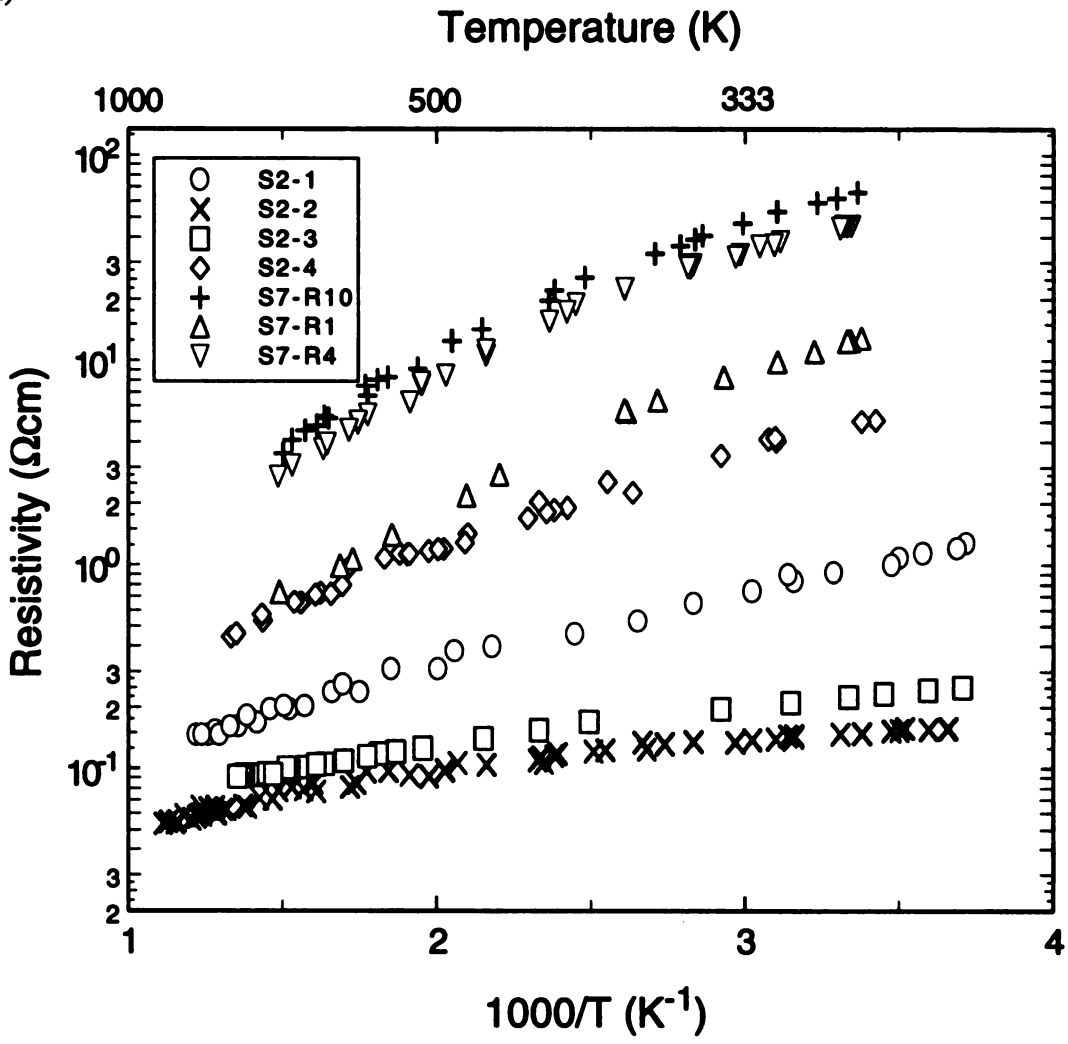

Figure 4.8 **The representative measured data of (a) small grain polycrystalline diamond (S2 & S7), (b) large grain polycrystalline (S3) and single crystal (S4) samples.**

(b)

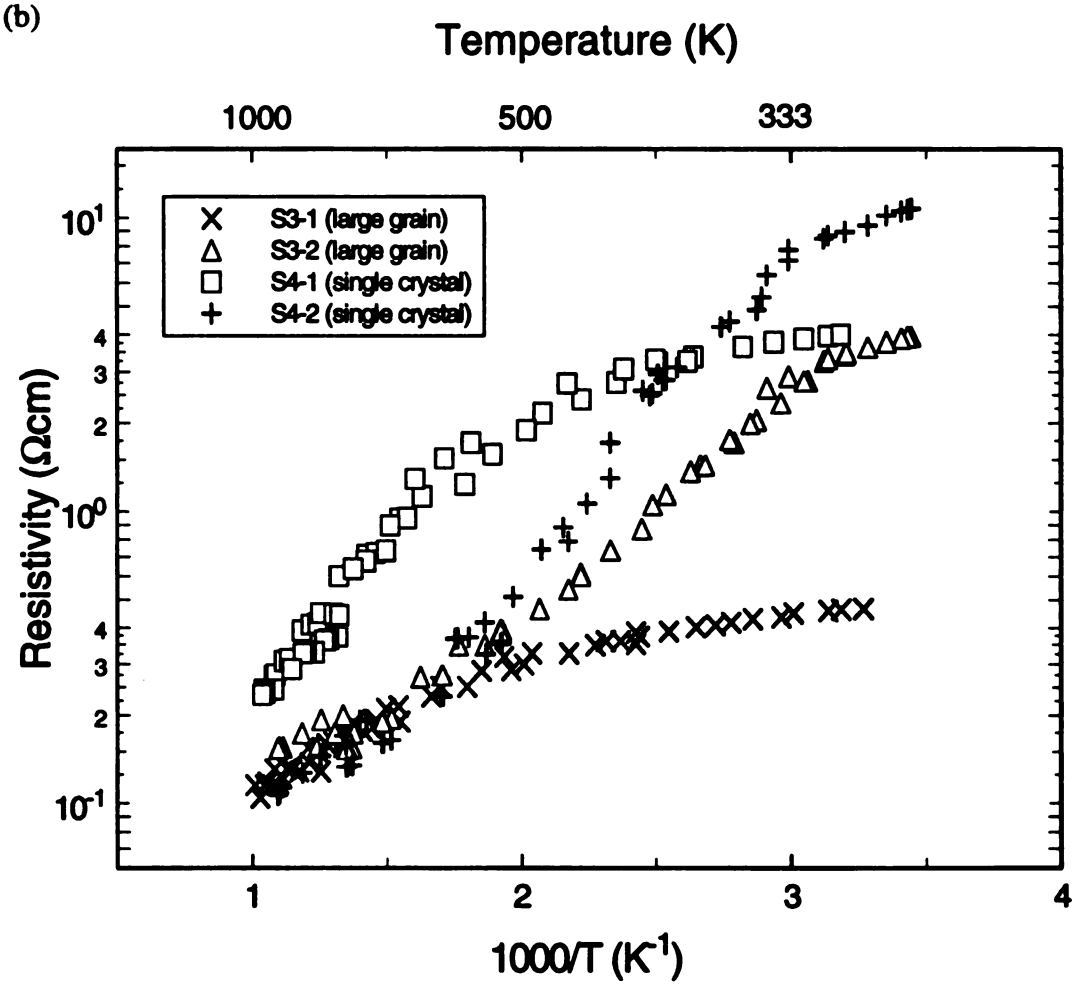

Figure 4.8 (Cont'd)

merged at 670 K for large grain samples (S3-1 and S3-2). In the case of single crystal samples (S4-1 and S4-2), the merge of log(ρ) versus 1000/T curves was occurred at 380 K.

A large variation in the room temperature resistivity was observed for small grain polycrystalline diamond thermistors in each sample groups of S2 and S7, despite the thermistors in each group were deposited in the same batches. The non-uniform resistivity distribution of resistors in the same deposition batch is discussed in 4.3.3. It is noteworthy that the percentage change of resistivity at different temperatures is found to be consistent for thermistors in group S7. However, no consistence of R-T behaviors was found for group S2 samples. Figure 4.9 (a) shows the resistivity versus temperature plots for selected resistors in the group S7. The corresponding temperature dependence of normalized resistivity (R_T/R_{To}), which represents a percentage change in resistivity due to temperature, is shown in Figure 4.9 (b). The R_T/R_{To} vs. T curves of thermistors on sample S7 were consistent. The R vs. T and R_T/R_{To} vs. T plots of samples in group S2 appear in Figure 4.10 (a) and (b) for comparison. In contrast to Figure 4.9 (b), no consistence behavior of normalized resistivity was found in Figure 4.10 (b).

4.3.5 Temperature Sensing

- **Characteristic equation**

Due to the non-linearity of log(ρ) and inverse temperature relation of diamond thermistors, the third order Steinhart-Hart equation [3,20], defined by

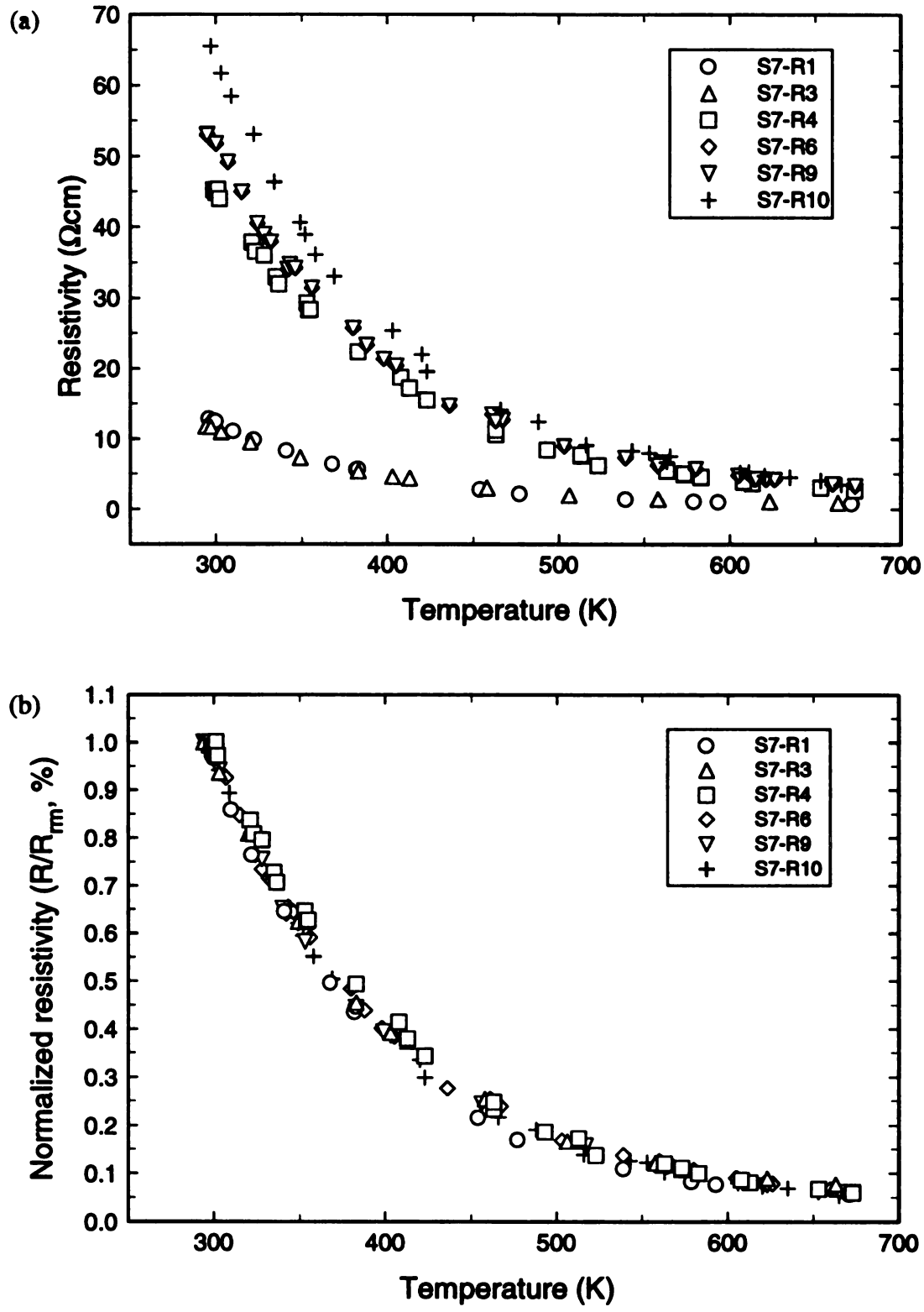

Figure 4.9 The resistivity (a) and normalized resistivity (b) versus temperature for selected diamond thermistors in sample S7.

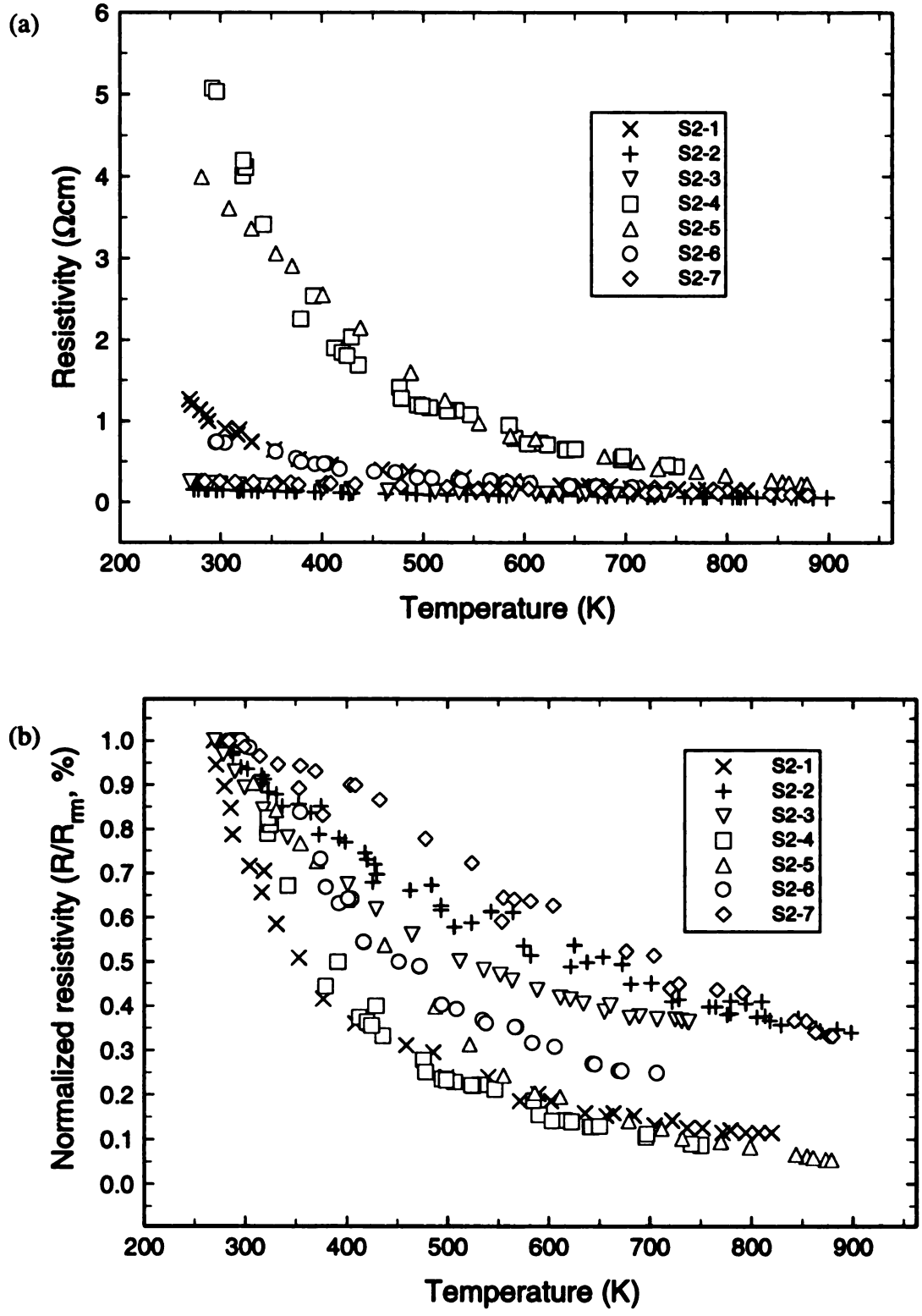

Figure 4.10 The resistivity (a) and normalized resistivity (b) versus temperature for selected diamond thermistors in sample S2.

$$\frac{1}{T} = a + b(\ln\rho) + c(\ln\rho)^2 + d(\ln\rho)^3,$$

is adopted to describe the resistivity-temperature relation for temperature sensing applications. The Steinhart-Hart equation is determined to be an excellent mathematical expression of thermistors with negative temperature coefficients of resistivity over a large temperature range [3,20]. The average percentage difference between temperatures computed from Steinhart-Hart equation and those measured directly by thermocouples is in the range of 0.3289% - 4.8759% (1.4270 K - 25.8909 K) over the entire characterization temperature range. Table 4.5 lists the calibration results of selected diamond thermistors. It is worth pointing out that the reference temperature measured by thermocouples has a certain degree of uncertainty. The limits of error for type K thermocouples are rated as 2.2 K in the range of 73 to 273 K or 0.75% above 273 K [21,23]. According to its specification, the average error of type K thermocouples over the present characterization temperature range is 4.875 K. Therefore, a precise temperature measurement and a tightly controlled calibration temperature, which are difficult to achieve using currently available equipment, are essential to fully characterize the accuracy of diamond thermistors.

- **Sensitivity of diamond temperature sensor**

The sensitivity of a semiconductor thermistor is usually characterized by the factor β [5] which is defined by

TABLE 4.5 The calibration results of selected diamond thermistors.

Sample No.	Resistivity @300K (Ωcm)	Grain size (μm)	ΔT (K)	$\Delta T/T_{mea}$ (%)	β (K)
S1-R1	0.4924	1 - 2	2.4806	0.5028	985.042
S1-R2	0.5887	1 - 2	3.8809	0.7338	1015.97
S1-R3	0.7925	1 - 2	1.8464	0.3747	977.467
S2-1	1.1339	1 - 2	11.4208	1.9979	963.570
S2-2	0.1478	1 - 2	15.2163	2.7111	384.808
S2-3	0.2243	1 - 2	5.7503	0.9396	457.117
S2-4	5.0337	1 - 2	8.0798	1.6527	1163.38
S3-1	0.4823	15 - 50	17.7358	2.5722	471.025
S3-2	3.9412	15 - 50	20.6596	3.0826	1591.50
S4-1	4.0075	Single crystal	19.3886	2.9830	846.442
S4-2	10.1780	Single crystal	17.1291	2.8256	2208.45
S7-R1	12.3600	1 - 2	1.4270	0.3289	1530.50
S7-R4	45.3008	1 - 2	3.0807	0.6433	1525.52
S7-R10	65.4931	1 - 2	4.0216	0.7974	1586.13

Note: 1. ΔT denotes the average difference of temperature calculated from S-H equation and temperature measured by thermocouple.

$$\beta = \frac{\ln\left(\frac{R_1}{R_2}\right)}{\left(\frac{1}{T_1} - \frac{1}{T_2}\right)},$$

where R_1 and R_2 are resistance at temperatures T_1 and T_2, respectively. Another commonly used indicator of sensitivity of temperature sensors is the temperature coefficient α which is defined as

$$\alpha = \frac{1}{R}\frac{dR}{dT} = -\beta T^{-2}$$

It is usually expressed in terms of the percentage change in resistance per degree. Since α is a strong function of temperature for semiconductor thermistors and it doesn't represent any more information than β factor, β is chosen in the present study to evaluate the sensitivity of diamond thermistors. Based on the definition of β factor, it is also a strong indicator of temperature behavior of diamond thermistor in a specified temperature range. The room temperature resistivity and β values calculated over 300 - 683 K of selected diamond thermistors are listed in Table 4.5. The results suggest that β, as well as temperature behavior, strongly depends on the resistivity and crystal structures. In the present study, β values of all thermistors range from 349.334 to 2208.452 K. The corresponding room temperature resistivity and resistance values are in the ranges of 0.1507 - 65.493 Ωcm and 0.977 - 509.5 KΩ, respectively. The reported β value of diamond thermistors is in the range of 940 - 5500 K [97,124] as compared to 2000 - 4000 K for conventional metal-oxide thermistors [3] for the temperature range of 300 - 673 K.

However, high sensitivity (β = 5500 K) is achieved at lower doping level, the corresponding resistance values are unacceptably high (> 1MΩ) for practical applications. The low resistivity is helpful to maximize applied power and heating temperature for heating application.

- **Long term stability**

Due to the difficulty of maintaining a constant environment temperature other than room temperature, the long term (48 hours) stability of resistivity are studied only under room temperature for selected samples in group S3 (large grain) and S4 (single crystal). The attempt to maintain a stable environmental temperature for calibration was achieved by performing the experiments inside a 18" stainless steel vacuum chamber under a pressure range of 10^{-6} torr. The sample holder was arranged to have the maximum thermal isolation in such a configuration that a mica glass holder was suspended by two ceramic bars to minimize the contact area with chamber body. An average resistivity variation in the range of 0.1367 - 0.4778% is observed which corresponds to an ambient temperature change of 1 - 2 ^{o}C. The substrate temperature monitored by thermocouples during each of the characterization periods also showed a small change in 1 - 2 ^{o}C with time. It is reasonable to believe that the resistivity of diamond thermistors maintains a constant value at a specified temperature close to room temperature. Figure 4.11 shows the representative results of long term stability characterization. Due to the potential possibility of property changes or failures in sensor material, electrical lead, and contact interface, a similar study at high temperature range is essential to ensure the long term reliability of diamond thermistors.

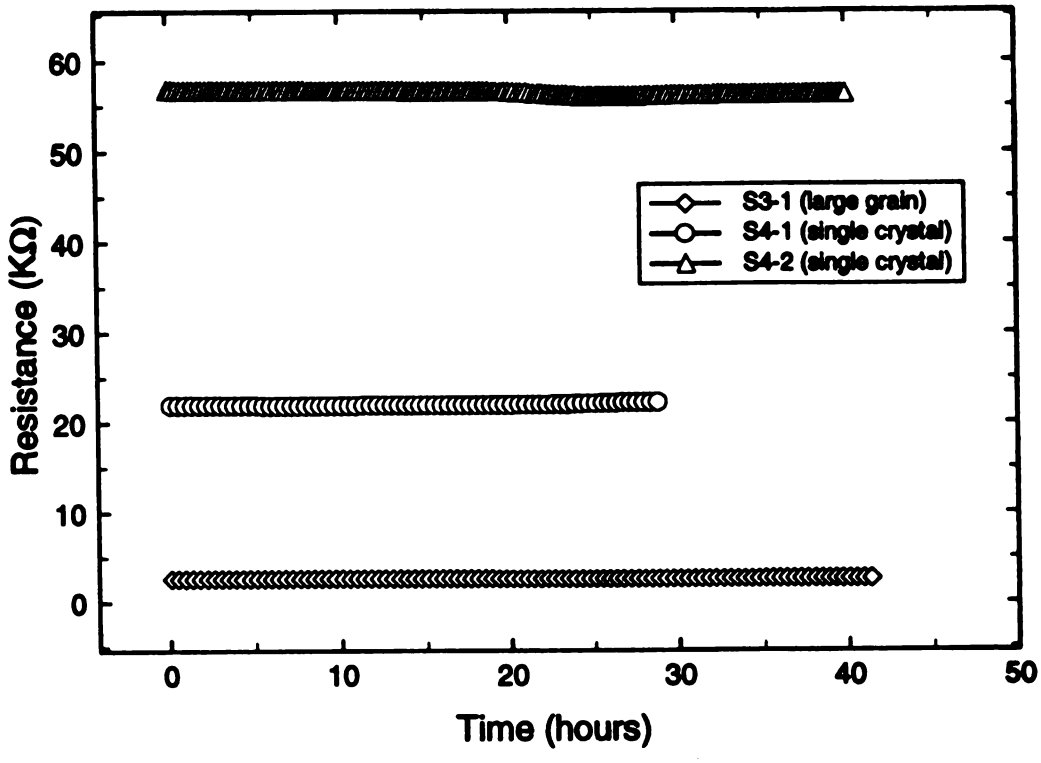

Figure 4.11 The long term stability of diamond resistivity.

4.3.6 Discussions

A better understanding of conduction mechanisms in CVD diamond is essential to properly interpret the temperature response of diamond films and to maximize the performance of diamond thermistors. Due to its large bandgap of 5.45 eV, the temperature ranges of semiconducting conductions in diamond are higher than those in Si. The existence of relatively high density of defects and impurities in CVD diamond results in increased charge carrier scattering and possibly the impurity/defect band conduction. This

makes the understanding of charge carrier transport mechanism in diamond difficult. In the case of polycrystalline diamond, the presence of grains and grain boundaries makes the conduction even more complicated.

For p-type semiconductive diamond, valence band conduction, impurity band conduction, and hoping conduction are reported [95,125]. The extrinsic conductivity, under the conditions of partial compensation and nondegeneracy, may be expressed as sum of three terms

$$\sigma = \sigma_1 \exp\left(-\frac{E_1}{kT}\right) + \sigma_2 \exp\left(-\frac{E_2}{kT}\right) + \sigma_3 \exp\left(-\frac{E_3}{kT}\right)$$

where σ_1, σ_2, and σ_3 are constants and E_1, E_2, and E_3 are the activation energies associated with the valence band conduction, the impurity band conduction, and the hopping conduction.

A comprehensive grain-boundary trapping theory, originated from the study of polycrystalline silicon [95,126], may be helpful for understanding the grain boundary conduction of CVD diamond. This theory states:

(1) For p-type semiconductor;

(i) Dopant (boron) is evenly distributed throughout the film but holes are trapped at the grain boundaries which contain high densities of traps.

(ii) Due to the presence of trapped holes, a region of width ω into the grain is depleted and the free carrier concentration in the films is reduced.

(iii) The buildup of charge at the grain boundaries leads to the formation of a potential barrier, which reduces the mobility of free carriers crossing the grain boundaries.

(2) In the case of n-type material, dopant atoms, such as P, segregate in the grain boundary region.

In the case of CVD polycrystalline diamond, non-diamond carbon present at the grain boundaries may have higher conduction than that of grains. Most studies tend to suggest that the charge transport in p-type CVD diamond results from valence band conduction, and impurity/defect band conduction at temperature above 300 K.

• **Effect of high temperature annealing on resistivity**

In our study, the thermal annealing is found helpful to stabilize the resistivity-temperature response of CVD diamond. A similar observation was also reported by several researchers and was attributed to dissociation of hydrogen from the diamond surface which cause anomalous or unstable conduction [127]. The hydrogen is also believed to exist in CVD diamond films and to passivate the deep traps [128]. The thermal annealing causes hydrogen to outdiffuse resulting in an increase of trapping density leading to increased capture of holes. An increase in resistivity of diamond films was observed for both undoped and B-doped polycrystalline diamonds after annealing [129]. This effect is reported to be more prominent for low doping level and high quality (in term of grain boundary density) diamonds [130].

In the present study, a tremendous increase in resistivity was found for single crystal diamonds (group S4) after annealing. The increase of resistivity is believed to be due mainly to the reduction in the concentration of free carriers due to traps vacated by the hydrogen outdiffusion after annealing. The small change of resistivity after annealing found in the large grain samples (group S3) suggests that the conduction of polycrystalline films may be dominated by the conduction through grain boundaries, which may not be affected by the outdiffusion of hydrogen [130]. In addition, the reduced annealing effects on the resistivity of highly doped samples (S3-1 and S3-3) were observed as compared to

that of lightly doped sample (S3-2). one may assume that the average density of traps generated by hydrogen outdiffusion is same for all doping levels [130]. Therefore, the annealing should affect the resistivity of highly doped samples to less extent. In the case of small grain samples (group S7), two thermally evaporated Al strips were used as electrical contacts. Therefore, the observation of decreased resistivity after annealing may be attributed to the reduction of contact resistance of Al pads after annealing. In order to quantitatively explain the observations in the current research, it is important to know the conduction mechanism at grain boundary and its contribution.

- **Effects of crystal structure and grain size on resistivity**

As described in section 4.3.3, the resistivity of diamond resistors prepared within the same deposition batch strongly depends on the grain size and crystal structure. The resistivity of boron doped diamond films is determined by both carrier concentration and mobility. The Hall mobility of homoexpitaxial diamond is reported to be an order of magnitude higher than that of polycrystalline diamond (~1000 vs. >100 $cm^2V^{-1}s^{-1}$) [42,95,129]. Therefore, the relative low resistivity of polycrystalline samples found in the present research may be explained by the higher activated carrier concentration due to the dominant impurity/defect band conduction.

The impurity/defect band conduction mechanism was evident for both boron doped polycrystalline and homoepitaxial films with doping levels of 1.5×10^{20} cm^{-3} and 4×10^{19} cm^{-3}, as measured by SIMS, respectively [95]. It is more prominent in polycrystalline films due to the high incorporated boron concentration. It has been reported that the polycrystalline films incorporated 2 - 4 times more boron than homoepitaxial films within the same growth batch [95]. The corresponding room temperature resistivity and Hall concentration for polycrystalline and homoepitaxial films were reported to be ~0.2 Ωcm and 3.7×10^{19} cm^{-3}, and ~60 Ωcm and 6.8×10^{15} cm^{-3}, respectively. The room

temperature resistivity of both polycrystalline and homoepitaxial films used in the present study are in the comparable ranges with the reported values. It is likely that the impurity conduction actually takes place, especially for polycrystalline films. The extremely high activated carrier concentration of polycrystalline films caused by the reduction of activation energy due to impurity/defect band conduction is therefore expected resulting in low resistivity as compared to that of homoepitaxial films.

The boron incorporated rate for (111) growth planes has been reported to be higher than that of (100) growth planes [129]. The boron-doped homoepitaxial diamond films used in this research were grown on (100) oriented diamond crystals. The B-doped polycrystalline diamond films had dominant grain orientation of (111). Whether the lower resistivity of polycrystalline films can be attributed to the orientation effect is not clear and need further study. Enhanced boron concentration along the grain boundary may also be responsible for low resistivity. For p-type polycrystalline diamond films, the segregation of boron at crystal defects and grain boundaries was suggested resulting in high local concentration [95].

Non-diamond carbon presented at the polycrystalline diamond grain boundary may be electrically conducting [131,132]. Therefore, depending upon the level of intra-grain conduction versus grain boundary conduction, the conduction of polycrystalline diamond films can be dominated at grain boundary region. The results of even lower resistivity for smaller grain size polycrystalline samples, which consist of larger proportion of grain boundaries, than that of large grain samples further support the above conclusion.

- **Temperature dependence of resistivity**

The non-linear log(ρ) vs. 1000/T relation observed in the present study also suggests the existence of multiple conduction processes in CVD diamond films. For boron-doped CVD diamonds, the valence band conduction mechanism has been identified for

homoepitaxial films in the temperature range of 300 - 600 K with an activation energy of ~0.37 eV [95]. The impurity band conduction has been suggested to dominate the conduction in polycrystalline diamonds at the boron concentration higher than 2×10^{20} cm^{-3}, as measured by SIMS [95,125]. The hopping mechanism became evident at temperature below 280 K [95]. In addition, the presence of defects, impurities, dislocations, and grain boundaries, in the case of polycrystalline films, can introduce different scattering mechanisms which may strongly alter the conduction process. With the exception of hopping conduction which becomes more prominent at temperature range lower than the current characterization temperature range, all other conduction processes may play a role in our samples.

In the mono- and poly- crystalline films, different temperature behaviors were observed in Figure 4.8 which may be attributed to the presence of both valence band conduction and impurity band conduction. In order to further illustrate the differences in resistivity-temperature behaviors of single crystal and polycrystalline samples, selected R vs. T curves of both mono- and poly-crystalline samples in Figure 4.8 with comparable room temperature resistivity values of ~4.5 and ~10.5 Ωcm are re-plotted in Figure 4.12. With comparable grain size, polycrystalline samples with low resistivity values possess smaller slopes of log(ρ) vs. 1000/T curves as compared to those of high resistivity samples in the low temperature ranges. For the small grain samples, the slope of low resistivity sample (S2-4) is smaller than that of high resistivity sample (S7-R3), as shown in Figure 4.12. The similar result was also found in the case of large grain samples of S3-1 and S3-2 at temperature less than 625 K. This suggests that the impurity band conduction, whose activation energy is less than that of valence band conduction, plays a more important role in the conduction of sample with lower resistivity (thus higher dopant concentration). The change of slope of S3-1 sample at temperature higher than 625 K may be due to the increased valence band conduction at high temperature. In the case of single

crystal diamonds, similar result was observed for samples S4-1 and S4-2. The transition occurred for sample S4-1 at ~570 K may be due to the increased contribution of valence band conduction at high temperature range. With the exception of samples S4-1, the activation energies, as indicated by the slope of log(ρ) vs. 1000/T curves, of all samples in Figure 4.12 follow the order of single crystal, large grain, then small grain films. It seems to agree with the conclusion that impurity/defect band conduction is more prominent in polycrystalline films due to the high incorporated boron concentration. In spite of the nonlinear relation of log(ρ) vs. inverse temperature, a better linearity is observed for polycrystalline samples (S2-4, S3-2, & S7-R3) as compared to single crystal diamonds (S4-1 & S4-2) in Figure 4.12. The superior linearity of R-T dependence suggests that polycrystalline diamond is preferable to single crystal samples for thermistor application.

The different R vs. T behaviors found for the small grain polycrystalline samples in groups S2 and S7, as shown in Figure 4.9 and 4.10, suggest that the films quality of diamond films alter the R-T behaviors of diamond thermistors. Due to the natural sag of 4.5 x 5 $inch^2$ horizontally mounted filament array equipped in HFCVD reactor, a non-uniform temperature distribution of substrate holder was resulted which introduced a perturbation of deposition condition. This caused differences in surface morphology and crystal structure of films deposited in the same batch. In the case of group S7 samples, the thermistor array, which contains 10 resistors, is occupied within a relatively small spread area of ~1 x 3.5 mm^2 on each test chip (see Figure 4.1 for details). Only a small variation of deposition condition in this case is expected thus the similar diamond quality is resulted for every thermistors on the S7 test chip. In contrast, each thermistor on group S2 samples occupied an area of 1.5 x 1.5 cm^2. The wide spread deposition position of nine samples in the same batch may introduce difference in film quality for each thermistor. Different resistivity-temperature behaviors observed for each samples in group S2 may then be

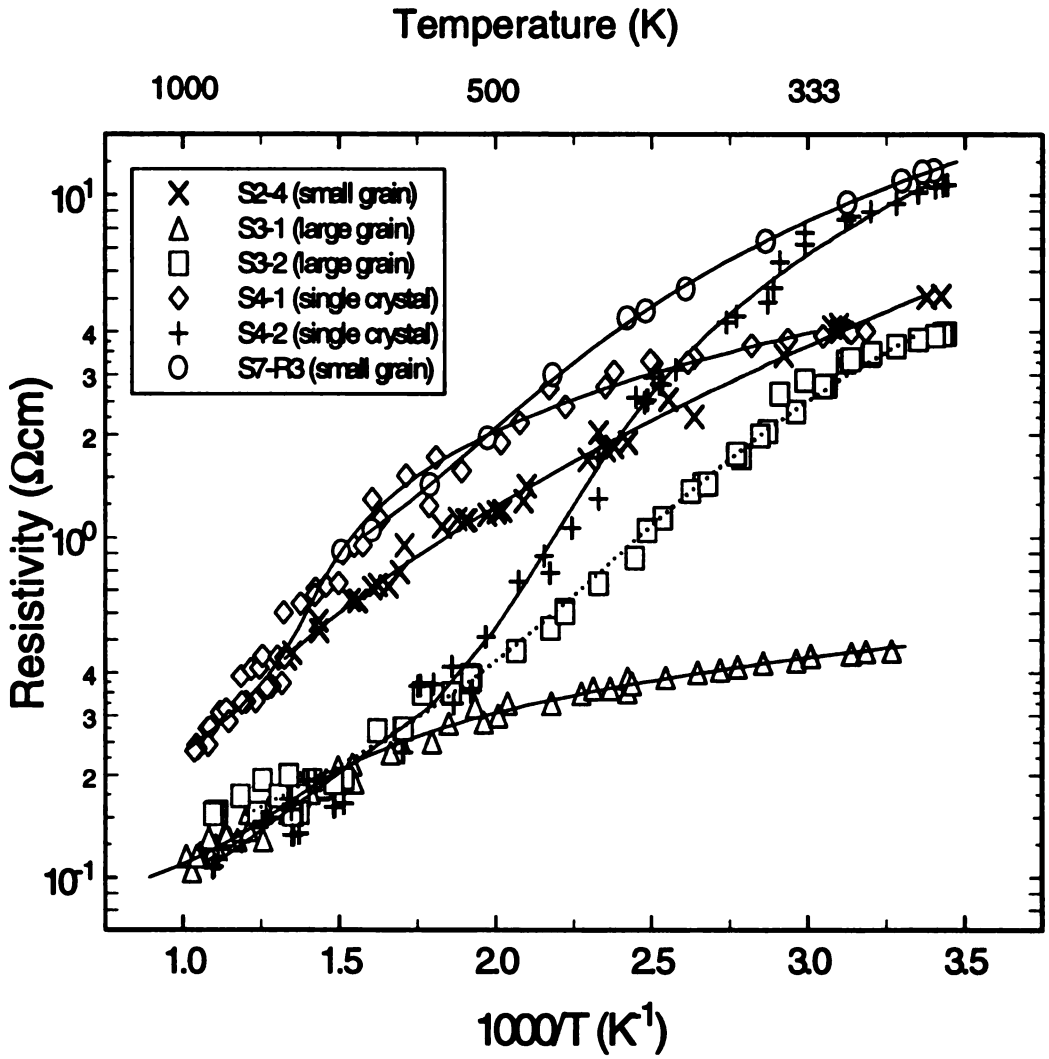

Figure 4.12 The comparison of temperature response of single crystal and polycrystalline diamond samples with compatible room temperature resistivity values.

attributed to the difference in film quality. The important parameters of film quality include crystal structure, surface morphology, grain size, grain boundary volume, defects, and impurity concentration. However, further study is necessary to identify the parameters of film quality that dominate the temperature behavior of diamond thermistors. By tightly controlling the deposition conditions and thus diamond film quality, a universal equation can be used to describe the R_T/R_{To} vs. T relation of thermistors fabricated in the same batch despite the difference in room temperature resistivity. It is helpful in the practical applications, as no individual characterization is needed for every thermistors. It is noteworthy that the difference in the annealing temperature and procedure of sample groups S2 and S7 may also have an impact on the R-T behavior. In the case of S2 samples, a 10 minutes annealing at 750 ^oC in N_2 was performed prior to the metallization. The Al contacts were then annealed at 400 - 450 ^oC for 10 minutes in N_2. Only a 20 minutes 500 ^oC annealing was performed for S7 samples with Al contacts deposited. However, the effect of annealing temperature and procedure is not clear at this point.

The β values of thermistors in groups S1, S2, S3, S4 and S7 are plotted as function of resistivity in Figure 4.13. Basically the β value indicates the sensitivity of thermistor to temperature change. It is also a indication of activation energy. With the exception of groups S1 and S7, the β values increase with the room temperature resistivity of thermistors for groups S2, S3, and S4, as indicated in Figure 4.13. For heavily doped samples, the low β value which relates to low activation energy seems to indicate that the impurity/defect band conduction may be dominant. In addition, the degree of β value increment seems increasing with grain size, i.e., the effect of doping level on the thermistor sensitivity is less pronounced for polycrystalline films than for single crystal diamonds. The result suggests that with a specific sensitivity requirement, the resistivity of polycrystalline diamond thermistors can be varied in a large range to fulfil the requirement of a particular application. The similar β values of S1 and S7 samples

represent the similarity in temperature behavior as described previously.

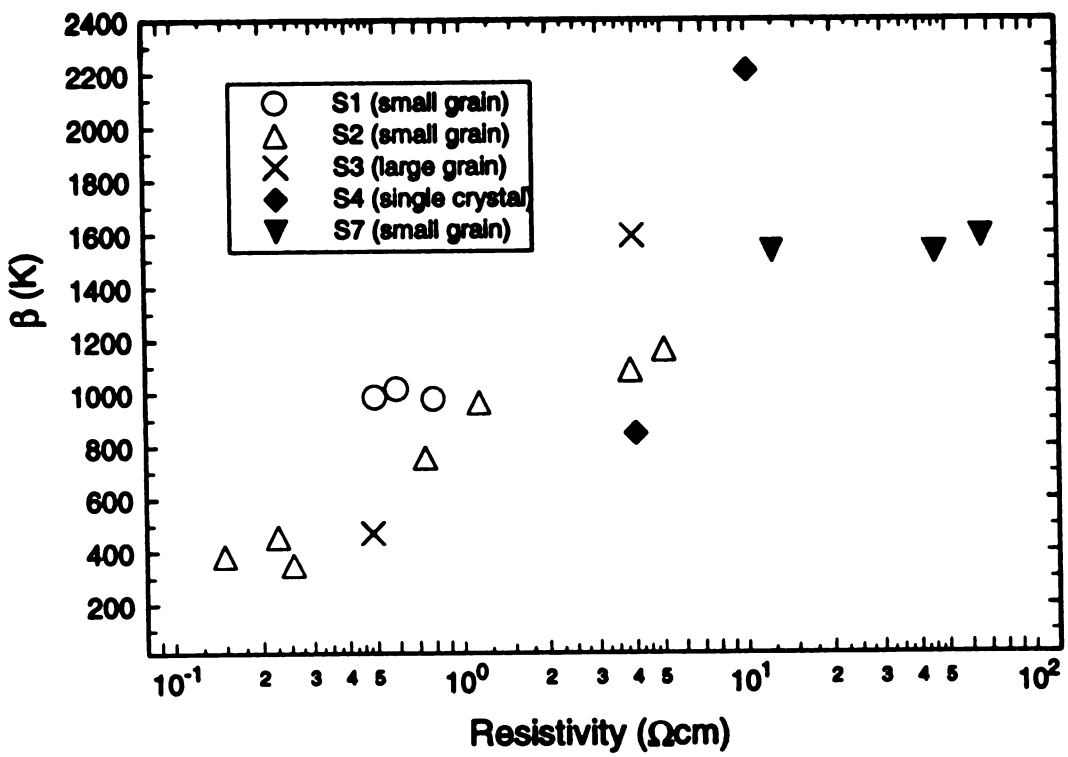

Figure 4.13 The β versus resistivity

4.4 Thin Film Heaters

The characterization of diamond thin film heater includes heating temperature, power density and heating uniformity. Group S1, S2, and S3 samples are used for heating study in this section.

4.4.1 Heating Temperature and Power Density

Supplying DC voltage up to 287 V, the temperature of the samples, subjected to Joule heating, was measured as a function of applied power density by thermocouples at different points of resistors. Representative curves of data collected for temperature measured at the center of each resistor are shown in Figure 4.14 for three test structures under different configurations. The details of sample structure and measurement configuration can be found in Table 4.1, Figure 4.1, and Figure 4.3, respectively. Several observations and explanations can be made based on the heating temperature data of these diamond heater structures:

(1) The heating temperature shows a linear increase with applied power density up to 550 K in all data sets. A non-linear relationship between power density and resulting temperature was observed at high heating temperature range. Based on the Stefan-Boltzmann law, the energy emitted from an emitting surface is proportion to 4th power of object temperature as described by [133],

$$W = \varepsilon\sigma T^4$$

Where W is the rate of energy emission per unit area, T is the absolute temperature of the body, ε is a universal physical constant, and σ is the emissivity of the material. Therefore, the inferior heating efficiency at high temperature range can be explained by an increased amount of heat loss through radiation.

(2) The heating efficiency mainly depends on the size of heat capacity and the amount of heat loss through conduction. Sample S3-1 shows the best heating

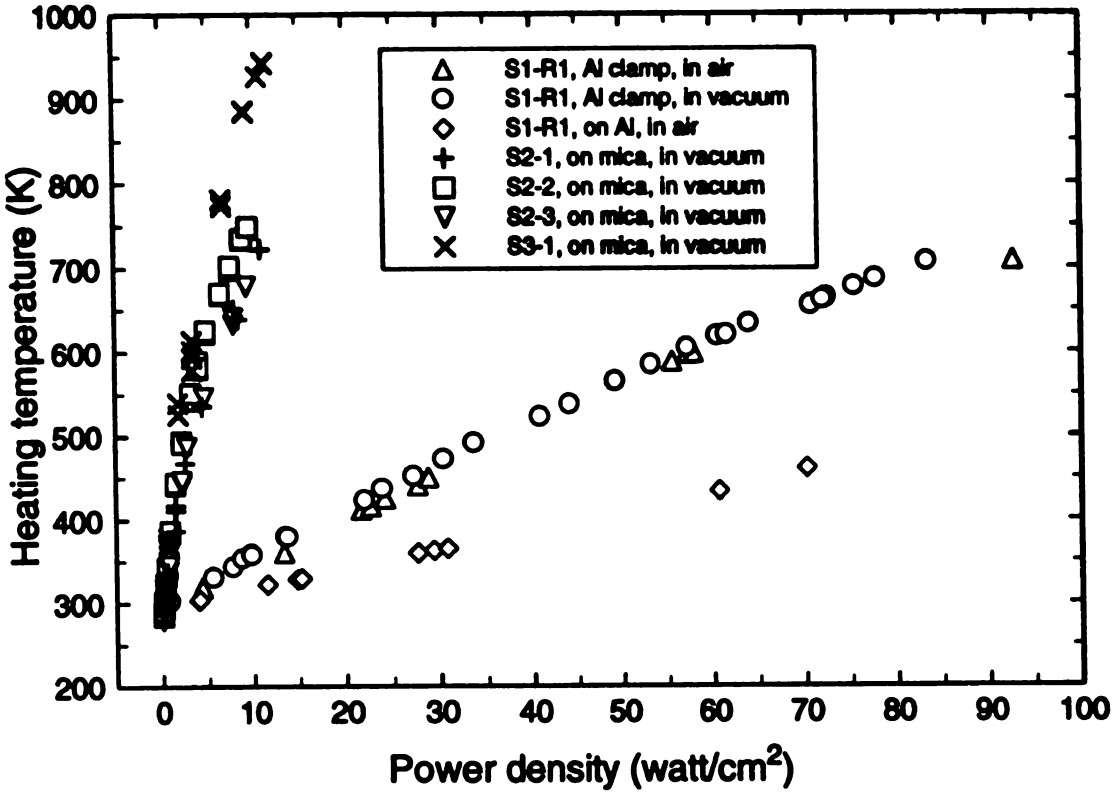

Figure 4.14 Temperature versus power density under different measurement configurations.

efficiency due to the smallest heat capacity of the sample substrate and the least conduction and convection losses of mica glass holder and vacuum environment, respectively. Under the same experiment configuration as sample S3-1, a relatively good heating efficiency of test structure #2 samples (S2-1, -2 & -3) was also observed. The slight different results of S2-1, -2, and -3 samples are believed due mainly to the small variation of Si substrate dimensions. In the case of test structure #1 sample (S1), since heat is generated by one of the three resistors (R1) only, the relatively large Si substrate and both Al clamp and Al holder represent large heat capacity to the diamond heater. The poor heating efficiency then is

resulted. Due to the smaller contact area with Al clamp in the cantilever configuration than that of on Al holder configuration, higher heating efficiency of Al clamp configuration is also observed.

(3) A slightly less effective heating is observed when the measurements of S1 sample is performed in the air as compared to that under vacuum in the temperature range of 300 - 700 K. This result suggests that the heat loss during the characterization is dominated by the conduction through the Al clamp and the heat loss via the natural convection of the static air inside the chamber is relatively small. The convection heat loss into the air can be simply described by the Newton's law of cooling [133]:

$$q = hA\Delta t \qquad \text{(Btu/hr)}$$

Where q, A, and Δt denote the rate of heat flow, contact area, and temperature difference of heated object and surrounding air, respectively. The h in the above equation is known as the heat transfer coefficient, film coefficient, or film conductance. In the case of horizontal plates with heated upper surface, the h of free convection for air can be approximated by [133]

$$h = 0.27\left(\frac{\Delta t}{L}\right)^{\frac{1}{4}} \qquad \text{(Btu/hr-ft}^2\text{-F)}$$

The rate of heat flow by conduction across an area of A is given by Fourier's law as [134]

$$q = kA\frac{\Delta t}{\Delta L} \qquad \text{(Btu/hr)}$$

The constant k is the thermal conductivity of material through which the heat transmits. By a simple calculation, the convection and conduction heat losses of S1 sample fixed on the Al clamp at 673 K are 7.96 and 4382.4 Btu/hr, respectively, which agree well with the experimental observation.

By varying the doping level and resistivity, the applied voltage required to reach certain heating temperature can be optimized for a particular application. Table 4.6 summarizes the resistivity at room temperature and applied voltage and power needed to reach 480 and 680 K of all samples for comparison. In the case of samples from test structure #2 group (S2-1, -2, & -3), relatively low voltage is required to drive the sample with low resistivity to a certain temperature, in spite of the applied powers are in the compatible range. The "~" sign denotes the approximated value computed from the experimental data.

A heating temperature in excess of 950 K was measured at the center of the test structure #3 sample while a power of 8.6 watts was supplied under vacuum environment ($<10^{-5}$ torr). The maximum heating temperature of test structure #1 and #2 is limited by the diamond oxidation temperature of ~ 873 K and the Al melting point of 933 K. If diamond is heated to temperatures above 873 - 973 K in oxygen, it oxidizes [34] and the film may be completely etched in a few minutes. An Al contact failure was observed for heating over 850 K even under vacuum. Thus, a higher maximum heating temperature is possible if (1) a high melting point metal contact, such as: Pt/Ti or Au/Ti, is used, and (2) a passivation layer, such as SiO_2 is present or if the heater is operated under non-oxidizing

TABLE 4.6 List of applied voltage and power at 480 and 680 K for diamond heaters with different resistivity.

Sample No.	Resistivity @300 K (Ωcm)	Heating temperature			
		480 K		680 K	
		Voltage (V)	Power (W)	Voltage (V)	Power (W)
S1-R1	0.4924	~275	~8	~287	~21
S2-1	1.1339	103.5	4.59	~140	~17
S2-2	0.1478	46.55	3.31	73.05	11.65
S2-3	0.2243	59.45	4.16	93.3	16.99
S3-1	0.4823	~47	~2.27	~66	~6

environment. A relatively high power density of 93 watt/cm^2 was used in the case of test structure #1 sample due to a large thickness of Si substrate (500 μm) as compared to that of diamond film (2 - 3 μm). The maximum power and operating temperature of commercially available thick film heaters (nickel, Al, or carbon steel alloy) [8,11] are in the ranges of 0.775 - 38.75 watt/cm^2 and 573 - 1473 K, respectively. The high breakdown voltage of diamond heater allows a high voltage and a large power density to be applied for fast heating speed even under a large load.

4.4.2 Temperature Profile of Diamond Thin Film Heaters

It is of advantage to characterize the temperature profile of whole heater substrate in

stead of only single point temperature, especially when uniform heating and precisely controlled temperature are required. In this section, the temperature profile of diamond heater substrates is studied by using an infrared camera[1] system. The information of experimental setup is described in 4.2.2. The samples were suspended vertically using two copper clamps for support as well as electrical contacts. With this arrangement, heat was dissipated by conduction through the electrical contacts and by natural convection. While applying a AC voltage of 100 V, the substrate transient temperature profiles of samples S2-6 and S3-1 are recorded.

The thermal imaging radiometer responds to the sum of the emitted, reflected, and transmitted energies emanating from the object of interest. This combination of energies is called the target radiosity. To obtain the target temperature, the emitted energy must be determined from the total energy of the incoming radiosity. The result is then scaled up by an emissivity correction factor to obtain a blackbody equivalent value. This value is then converted to a temperature using the calibration curves within the imaging software. Therefore, before accurate thermal images can be acquired, the emissivity of the diamond samples must be determined.

For the sample S3-1, the surface of the diamond substrate was such that uniform emissivity could be assumed. The emissivity was determined by comparing the energy of two radiating bodies transmitted through and reflected by the surface. Using this method the emissivity of sample S3-1 was found to be 0.64. The maximum heating temperatures in excess of 673 K was reached after 65 second of heating with a applied current value of 75 mA. The one dimensional temperature profiles taken at the center of substrates perpendicular to the direction of the current flow are plotted in Figure 4.15 (a) for every 10 to 15 second of heating period. Plot (b) shows two dimensional temperature distribution of S3-1 sample after 65 seconds of heating. Due to the high thermal conductivity of diamond

1. The infrared system is available in Dept. of ME. All the measurements are performed by Matt White under the supervision of Dr. John McGrath.

substrate, the substrate was relatively isothermal. The low temperature region appeared at the lower portion of the infrared image was due to the presence of one copper clamps.

In the case of sample S2-6, the diamond pattern of 15 x 15 x 0.003 mm was deposited on 300 μm thick Si wafer with a 3 μm layer of SiO_2 in between. Two Al contact regions, deposited directly on the substrate, created non-uniformity in the surface emissivity. The initial experiment shows a relatively low temperature reading on the metal contact areas as displayed in Figure 4.16 (a) and (b). Plot (a) shows the substrate temperature profile along the current flow direction. The images of two Al contact areas and copper clamps are clearly illustrated in 2-D surface temperature profile of plot (b). These artificial results are introduced by the difference in the emissivity of diamond and Al contacts.

A thin coat of flat black paint was then applied on the sample surface to reduce this non-uniform surface emissivity. The emissivity of this black paint was assumed to be 0.95. Figure 4.17 (a) and (b) show the one dimensional time varying substrate temperature perpendicular to the current flow direction and two dimensional temperature plot, respectively. As we can see in Figure 4.17 (b), with the exception of the presence of two copper clamps, the surface temperature was relatively uniformly distributed. The heating temperatures saturated at 440 K after about 65 second of heating and the corresponding current values were in the range of 49 to 52.2 mA.

4.5 Heater/Sensor Structures

Samples with test structure #1, #2, and #3 are used in this section to study the simultaneous sensing performance of diamond heater structures.

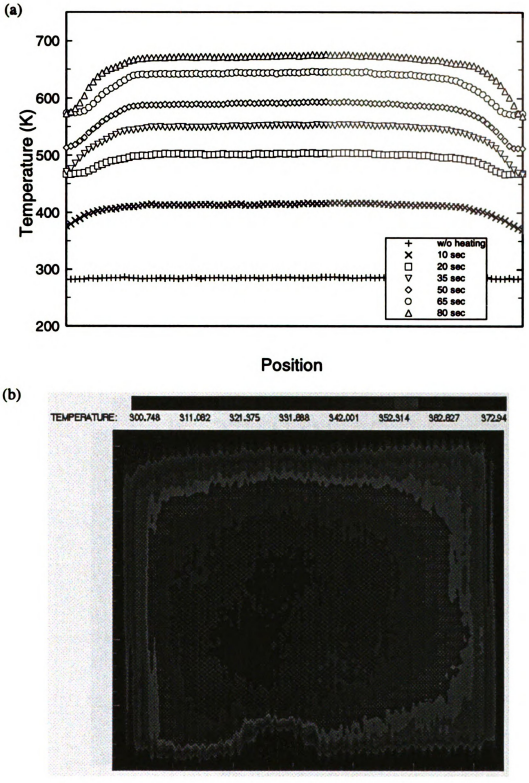

Figure 4.15 The temperature profiles of sample S3-1.

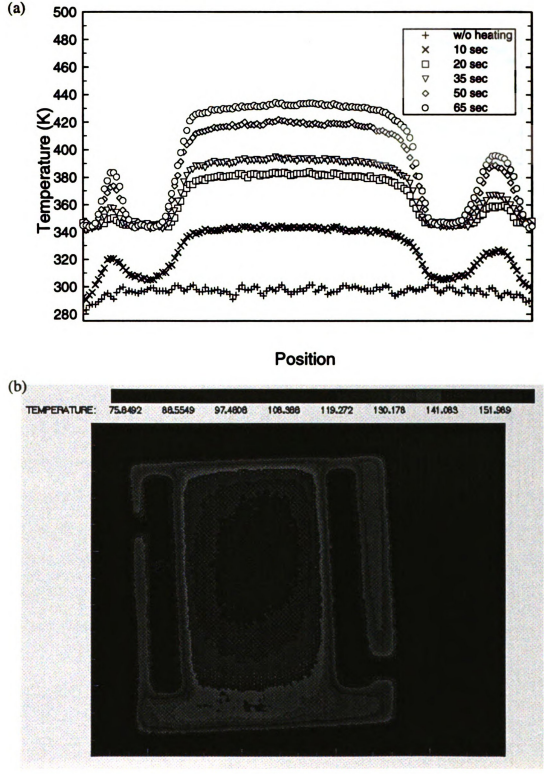

Figure 4.16 The temperature profiles of sample S2-6 before the black paint coating.

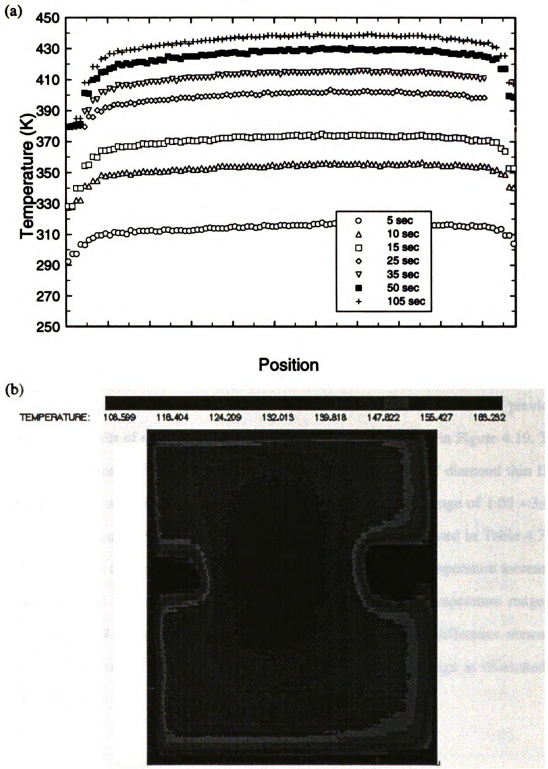

Figure 4.17 The temperature profiles of sample S2-6 with black paint coating.

4.5.1 Diamond Resistors for Temperature Sensing

The resistivity-temperature relation of every sensor/heater test structures used in this section is first calibrated followed by the procedures described in section 4.3.4 and 4.3.5. Figure 4.18 shows both experimental data and the fitted curves of resistivity-temperature characteristics for all samples. The fitting results will be used to determine the temperate during the heating application. The evaluated coefficients (***a***, ***b***, ***c***, ***d***) of 3rd order Steinhart-Hart equations are listed in Table 4.7.

4.5.2 Self-sensing diamond heater

During a heating process, the resistivity, determined from resistor dimensions and applied voltage and current, is computed to determine the heating temperature via Steinhart-Hart equation with pre-determined coefficients (as described in the previous section). The results of such a heating/sensing experiment are shown in Figure 4.19. The average differences of the temperature determined by self-sensing of diamond thin film heaters and the temperature measured by thermocouple are in the range of 1.05 - 3.6% over the entire characterization temperature range. The details are listed in Table 4.7. It may be noted that the sensitivity of diamond sensors decreases as temperature increases. This results in an increase in the temperature difference at high temperature range as shown in Figure 4.20 (a). However, the percentage of temperature difference seems to remain in a comparable range over the entire heating temperature range as illustrated in Figure 4.20 (b).

4.6 Summary

A single CVD diamond resistor is used as a thin film heater and a temperature sensor

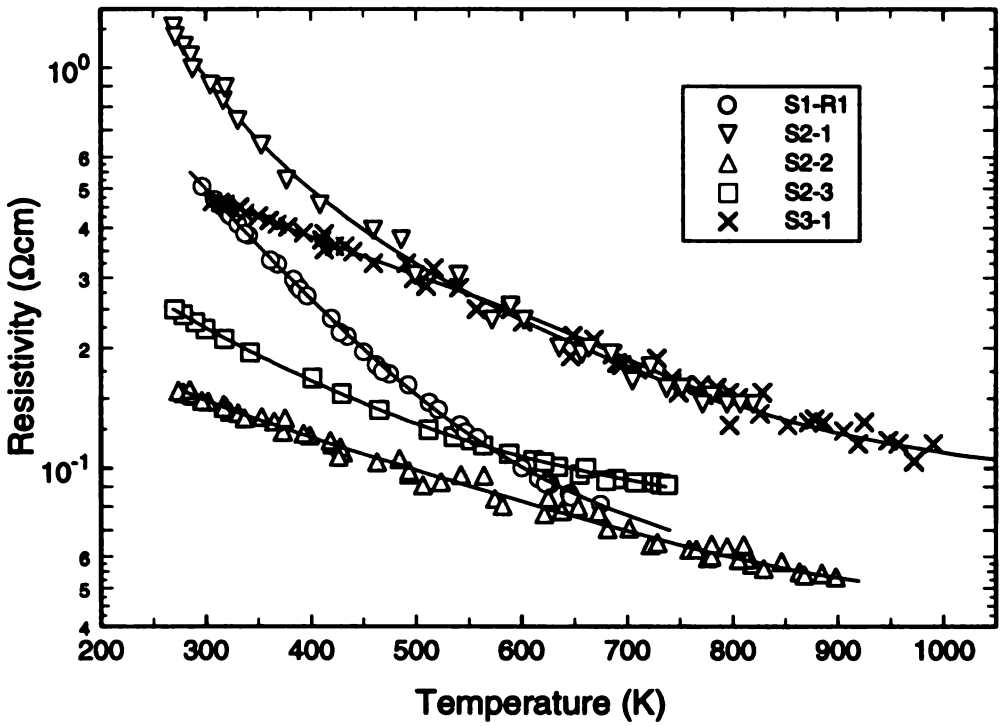

Figure 4.18 The temperature sensing characterization of all sensor/heater samples. The solid lines represent fitting curves by Steinhart-Hart equation.

TABLE 4.7 The results of heating/sensing study.

Sample No.	*a* ($x10^3$)	*b* ($x10^3$)	*c* ($x10^5$)	*d* ($x10^5$)	ΔT (K)	$\Delta T/T_{mea}$ (%)
S1-R1	4.84816	2.75084	94.0121	15.047	5.4007	1.0530
S2-1	3.41489	1.35979	4.27009	-4.37662	4.7714	1.1136
S2-2	37.2139	36.2285	1253.31	149.24	5.4537	1.4044
S2-3	16.9735	17.2692	703.979	106.368	17.5895	3.5756
S3-1	8.37893	10.2236	522.01	95.2057	19.0476	2.7982

Note: 1. [a, b, c, d] are the coefficients of Steinhart-Hart fitting equation.

2. ΔT denotes the average difference between the heating temperature determined by self-sensing and that by thermocouple.

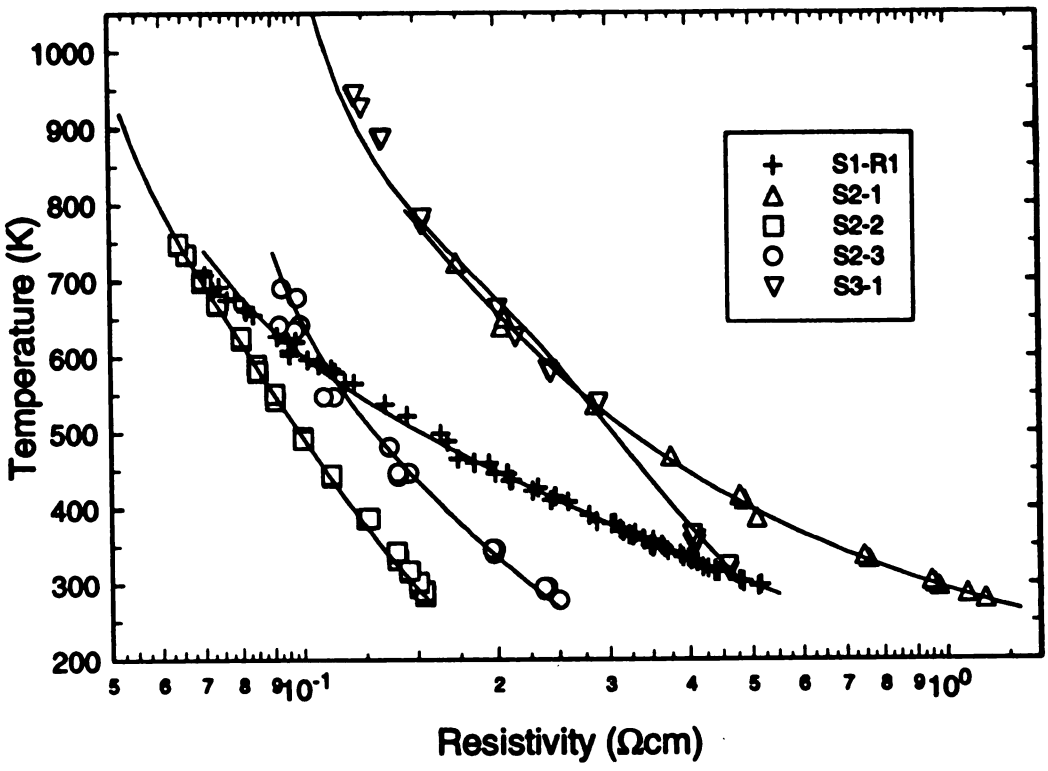

Figure 4.19 Results of self-sensing diamond heaters.

in the present study. The temperature sensing properties of diamond are studied over a variety of sample substrates and configurations in the temperature range of 300 - 1000 K. An excellent sensitivity is observed under 673 K. Due to its resistivity-temperature characteristics, diamond thermistors are less sensitive at high temperature range. The average error of sensing temperature as compared to that measured by thermocouple is found in the range of 0.3289 - 4.8759%.

Due to its high thermal conductivity, diamond thin film heater promises a uniformly

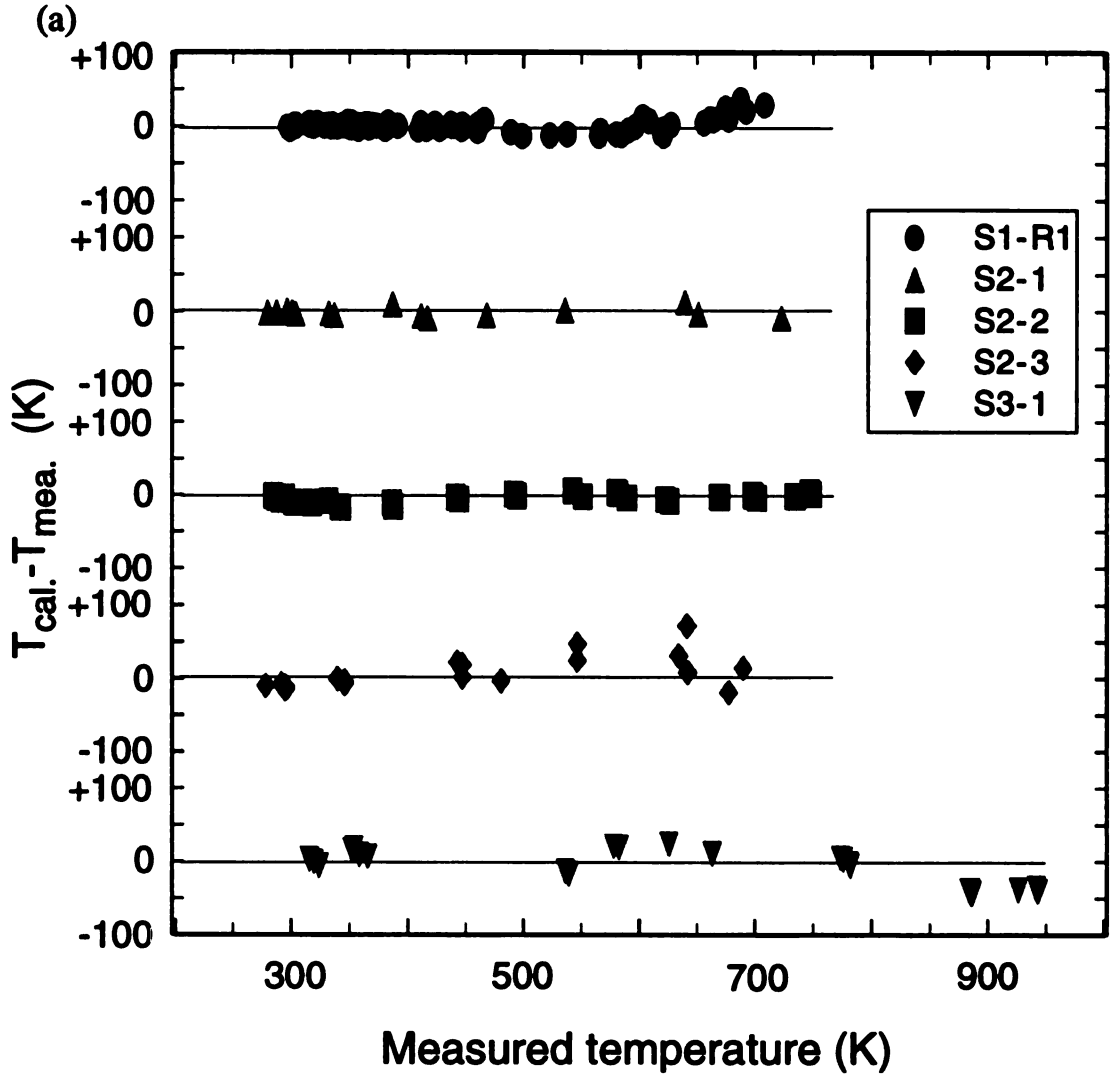

Figure 4.20 The difference of heating temperature determined by self-sensing ($T_{cal.}$) and that by thermocouple ($T_{mea.}$).

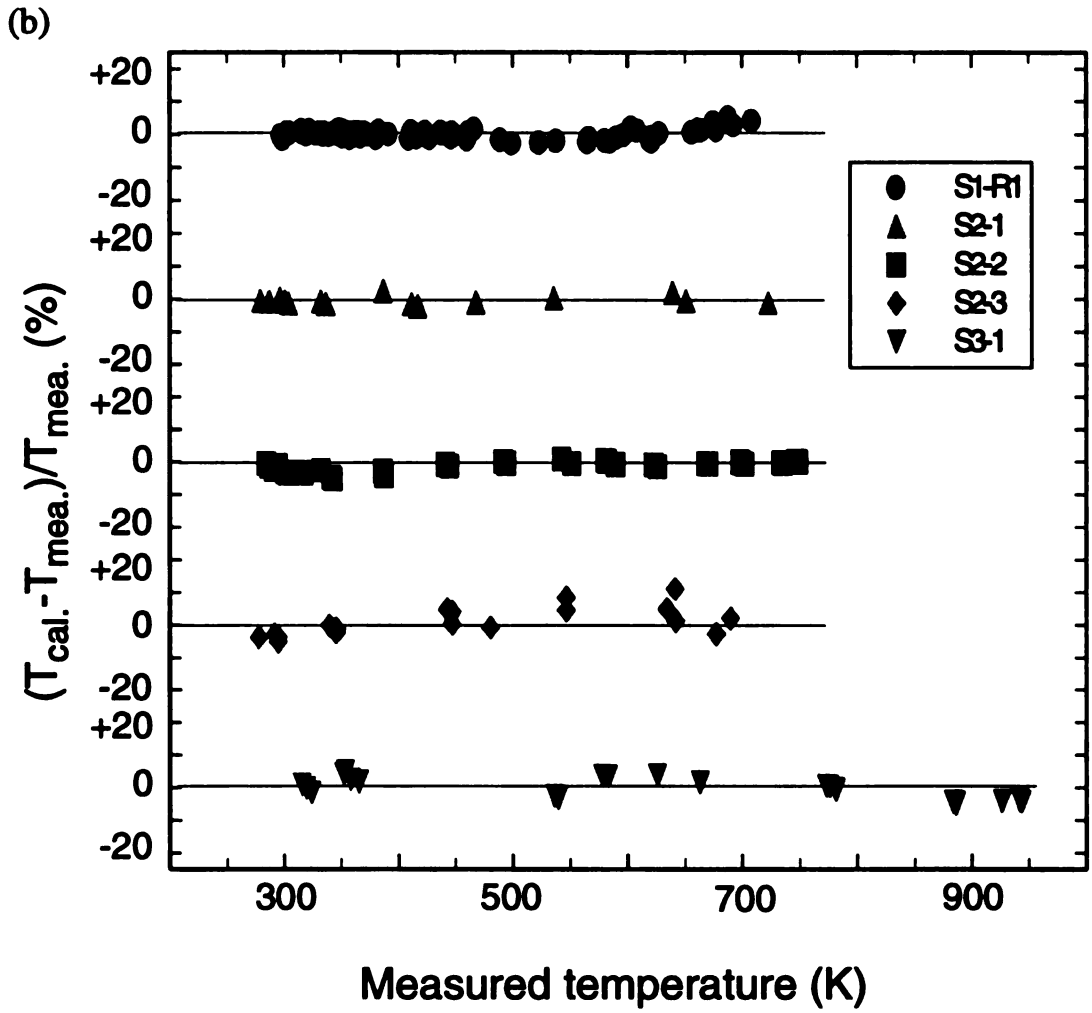

Figure 4.20 (Cont'd)

distributed temperature profile under ideal boundary conditions. The power density and heating temperature are in the ranges of 0 - 93 watt/cm^2 and 300 - 950 K, respectively. Because of the negative temperature coefficient of resistance, diamond heater possesses a high heating efficiency in the high temperature range. The average error of self-temperature-sensing during heating application is in the range of 1.0530 - 3.5756%. By varying the doping level, these parameters can be optimized for various applications, particularly in harsh environments. In addition, the diamond resistors could be directly deposited on the object to be heated and/or sensed with an exact and accurate custom designed pattern.

CHAPTER 5

CONCLUSIONS AND FUTURE RESEARCH

5.1 Introduction

The primary objective of this research is to realize the usage of CVD diamond thin films for temperature sensing and heating applications. In order to achieve this goal, first, the development of diamond device infrastructure technologies were addressed to successfully fabricate the diamond sensor and/or heater test structures. The temperature sensing and heating properties of diamond were then individually characterized on a variety of test structures. Finally, the performance of a single element diamond temperature sensor and heater structure was evaluated. The current research is excepted to extend the applications of CVD diamond on a variety of sensing areas, including gas sensor, liquid level sensors, mass flow meters, and vacuum and pressure gauges, and to help commercialize the diamond temperature sensors and thin film heaters in the near term.

5.2 Summary of Contributions

- **Ultrahigh nucleation density**

An improved nucleation technique for diamond thin film deposition was demonstrated. An ultrahigh nucleation density on the order of 10^{11} cm^{-2}, achieved using diamond powders with an average particle size of 0.038 μm, is the highest reported value. Using this technique, a mean surface roughness of 30 nm, as measured by AFM, was achieved for 1 μm thick films. The ultrahigh nucleation density technique can provide submicron continuous films in a short deposition period.

- **Temperature Sensing**

The annealing effect was studied using single crystal diamonds and polycrystalline films with different grain sizes. The increase in resistivity after annealing was found more prominent for single crystal diamonds. The third order Steinhart-Hart equation was used to calculate the temperature from measured resistivity with an average difference in the range of 0.3289% - 4.8759% (1.4270 - 25.8909 K) as compared to reference temperature measured by thermocouples. The sensitivity measurement of β factor in the range of 349.334 - 2208.452 K was found to increase with the room temperature resistivity.

- **Heating**

The heating properties of CVD diamond thin film heaters were studied for the first time. The applied power density and maximum heating temperature were in the range of 0 - 93 watt/cm^2 and 950 K, respectively. Due to the high thermal conductivity of diamond, the heater substrates were found relatively isothermal.

- **Self-sensing diamond heater**

A single element diamond resistor was used as heater as well as a temperature sensor simultaneously. The heating temperature determined from the R-T characterization of the

diamond resistor was found to possess an average difference in the range of 1.0530% - 3.5756% (4.7714 - 17.5895 K) as compared to that directly measured by thermocouple. By varying the doping level, the performance of such a sensor/heater element can be optimized for particular application.

5.3 Future Research

Although in the present research, a diamond sensor/heater structure is characterized for the first time, there is a need in the following areas for realization of the diamond sensor/heater applications.

(i) The understanding of electrical transport mechanisms of semiconducting CVD diamonds is important to optimize the performance of diamond sensor/heater structures.

(ii) Different filament configuration should be tested to improve the consistency of film quality over a large deposition area.

(iii) The uniformity of doping need to be enhanced by gaseous boron source in HFCVD reactor.

(iv) A passivation material should be carefully chosen to overcome the oxidation of diamond for high temperature operation.

(v) The potential applications of the diamond sensor/heat structure, include gas sensors, liquid level sensors, mass flow meters, and vacuum and pressure gauges, need to be developed.

BIBLIOGRAPHY

BIBLIOGRAPHY

1. Ed. N. Eror et al., *Expanding the Vision of Sensor Materials*, National Academy Press, Washington, D. C., 1995.

2. G. Harsanyi, *Polymer Films in Sensors Applications*, Technomic Publishing Company, Lancaster, PA, 1995.

3. H. B. Sachse, *Semiconducting Temperature Sensors and their Applications*, John Wiley & Sons, New York, 1975.

4. J. A. Hall, *The Measurement of Temperature*, Chapman and Hall, London, 1966.

5. T. D. McGee, *Principles and Methods of Temperature Measurements*, John Wiley & Sons, New York, 1988.

6. R. P. Benedict, *Fundamentals of Temperature, Pressure, and Flow Measurements*, John Wiley & Sons, New York, 1984.

7. R. B. Tait, R. Humphries, and J. Lorenz, "Thick Film Heater Elements and Temperature Sensors in Modern Domestic Appliances," *IEEE Transactions on Industry Applications*, vol. 30, no. 3, pp. 573-577, 1994.

8. A. Sale, R. Tait, J. Whitmarsh, and M. A. Stein, "Thick Film Heater Elements and Heat Sensors," *Hybrid Circuit Technology*, pp. 37-43, 1991.

9. *Flexible Heating Elements*, a product catalogue of The Ohmwave Company, Inc., Niantic, CT.

10. *Product Bulletin of The Electro-Flex Heat*, Inc., Bloomfield, CT, 1995.

11. *The Electric Heaters Handbook*, vol. 28, Omega Engineering, Inc., Stamford, CT.

12. I. M. Buckley-Golder, P. R. Chalker, C. Johnston, S. Romani, and M. Werner, "High Temperature Electronic Applications of Diamond," *Advances in New Diamond*

Science and Technology, Ed. S. Saito, N. Fujimori, O. Fukunaga, M. Kamo, K. Kobashi and M. Yoshikawa, MYU, Tokyo, pp. 669-678, 1994.

13. D. G. Bhat, "Diamond-coated Cutting Tools: a Status Report," *Mat. Tech.*, vol. 9, no. 11/12, pp. 253-261, 1994.

14. R. Hay, "A Hard Tool is Good to Find," *Cutting Tool Engineering*, vol. 45, no. 1, 1993.

15. T. J. Moravec and A. Partha, "Diamond Takes the Heat," *Advanced Packaging*, October, pp. 8-11, 1993.

16. M. W. Geis, N. N. Efremow, J. D. Woodhouse, M. D. Aleese, M. Marchywka, D. G. Socker, and J. F. Hochedez, "Diamond Cold Cathode," *IEEE Elec. Dev. Lett.*, vol. 12, pp. 456-459, 1991.

17. D. Hong, and M. Aslam, "Field Emission from P-type Polycrystalline Diamond Films," *J. Vac. Sci. Technol. B*, vol. 13, no. 2, pp. 427-430, 1995.

18. M. Aslam, G. S. Yang, and A. Masood, "Boron-doped Vapor-deposited Diamond Temperature Microsensors," *Sensors and Actuators: A.*, vol. 45, no. 2, pp. 131-137, 1994.

19. A. Masood, "Technology and Electronic Properties of Diamond Film Microsensors for Thermal Signals," *Ph. D. dissertation*, Michigan State University, 1991.

20. R. Pallas-Areny and J. G. Webster, *Sensors and Signal Conditioning*, John Wiley & Sons, Inc., New York, 1991.

21. D. I. Finch, *General Principles of Thermoelectric Thermometry*, Reinhold Publishing Corporation, Philadelphia, PA, 1962.

22. A. Boyer, E. Cisse, Y. Azzouz, and J. P. Ceron, "Narrow-bandgap Semiconductor Based Thermal Sensors," *Sensors and Actuators: A.*, vol. 25-27, pp. 637-640, 1991.

23. *The Temperature Handbook*, vol. 28, Omega Engineering, Inc., Stamford, CT.

24. S. Wessel, M. Parameswaran, S. R. Morrison, and R. F. Frindt, "CMOS Thermally-isolated Heater Structure as a Substrate for Semiconductor Gas Sensors," *Microelectronics Journal*, vol. 23, no. 6, pp. 451-456, 1992.

25. M. Gottschalk, "Tungsten Heater Boosts Rocket Fuel Efficiency," *Design News*, vol.

49, no. 23, pp. 95-97, 1993.

26. M. N. Yoder, "The Vision of Diamond as an Engineered Material," *Synthetic Diamond: Emerging CVD Science and Technology*, Ed. K. E. Spear and J. P. Dismukes, pp. 3-17, John Wiley & Sons, New York, 1994.

27. E. M. Wilks and J. Wilks, "The Hardness and Wear of Diamond During Grinding and Polishing," *Physical Properties of Diamond*, Ed. R. Berman, pp. 221-250, Clarendon Press, Oxford, 1965.

28. F. P. Bowden and D. Tabor, "Deformation, Friction, and Wear of Diamond," *Physical Properties of Diamond*, Ed. R. Berman, pp. 184-220, Clarendon Press, Oxford, 1965.

29. T. H. Huang, C. T. Kuo, T. S. Lin, and C. S. Chang, "Wear Behaviour of Various Diamond-coated Cutting Tools under Different Deposition Conditions," *Diamond and Related Materials*, vol. 2, pp. 928-932, 1993.

30. S. Tolansky, "Optical Studies on Diamond," *Physical Properties of Diamond*, Ed. R. Berman, pp. 135-173, Clarendon Press, Oxford, 1965.

31. H. W. Ko, S. E. Hsu, S. J. Yang, M. S. Tsai, and Y. H. Lee, "Characterization of Diamond Films for Optical Coatings," *Diamond and Related Materials*, vol. 2, pp. 694-698, 1993.

32. J. E. Field, *The Properties of Diamonds*, Academic Press, London, 1979.

33. Ed. W. J. Choyke et al., *Materials for High-Temperature Semiconductor Devices*, National Academy Press, Washington, D. C., 1995.

34. W. Zhu, X. H. Wang, A. R. Badzian, and R. Messier, "An Investigation of the Oxidation Behavior of CVD Diamond Films," *New Diamond Sci. and Tech., MRS Int. Conf. Proc.*, pp. 821-826, 1991.

35. J. Wei and Y. Tzeng, "Reaction of CVD Diamond with Molten Iron Film," *2nd Int. Conf. on Appl. of Diamond Films and Related Materials*, Ed. Yoshikawa et al., vol. 2, pp. 609-612, Tokyo, Japan, 1993.

36. M. H. L. Pryce, "Electronic Structure of Diamond," *Physical Properties of Diamond*, Ed. R. Berman, pp. 251-273, Clarendon Press, Oxford, 1965.

37. F. C. Champion, *Electronic Properties of Diamonds*, Butterworths & Co. Ltd.,

London, 1963.

38. P. J. Kemmey and P. T. Wedepohl, "Semiconducting Diamond," *Physical Properties of Diamond*, Ed. R. Berman, pp. 325-355, Clarendon Press, Oxford, 1965.

39. R. Berman and M. Martinez, "Diamond Research," *Industrial Diamond Review*, 1976.

40. D. M. Malta, L. S. Plano, G. J. Tessmer, C. T. Kao, and B. A. Fox, "Improvements in the Electronic Properties of CVD Diamond Films for Device Applications," *Proceeding of 2nd International High Temperature Electronics Conference*, vol. 2, pp. P75-80, Charlotte, NC, 1994.

41. B. R. Stoner, C. T. Kao, D. M. Malta, and R. C. Glass, "Hall Effect Measurements on Boron-doped, Highly Oriented Diamond Films Grown on Silicon via Microwave Plasma Chemical Vapor Deposition," *Appl. Phys. Lett.*, vol. 62, pp. 2347-2349, 1993.

42. J. A. von Windheim, V. Venkatesan, D. M. Malta, and K. Das, "Comparison of the Electric Properties of Single-crystal and Polycrystalline Diamond by Hall Effect and Capacitance-voltage Measurements," *Diamond and Related Materials*, vol. 2, pp. 841-846, 1993.

43. A. Masood, M. Aslam, M. A. Tamor, and T. J. Potter, "Synthesis and Electrical Characterization of Boron-doped Thin Diamond Films," *Appl. Phys. Lett.*, vol. 61, pp. 1832-1834, 1992.

44. J. L. Davidson, "Diamond Electrical Properties and Electronic Device Behavior," *Synthetic Diamond: Emerging CVD Science and Technology*, Ed. K. E. Spear and J. P. Dismukes, pp. 355-399, John Wiley & Sons, New York, 1994.

45. T. Sugino, K. Karasutani, H. Kataoka, K. Kobashi, and J. Shirafuji, "Electrical Characterization of Boron-doped Polycrystalline Diamond Films Synthesized by Hot Filament CVD," *Advances in New Diamond Science and Technology*, Ed. S. Saito, N. Fujimori, O. Fukunaga, M. Kamo, K. Kobashi and M. Yoshikawa, MYU, Tokyo, pp. 705-708, 1994.

46. L. S. Pan, D. R. Kania, S. Han, J. W. Agerii, M. Landstrass, L. O. Landen, and P. Pianetta, "Electrical Transport Properties of Undoped CVD Diamond Films," *Science*, vol. 255, pp. 830-833, 1992.

47. M. A. Plano, M. I. Landstrass, L. S. Pan, S. Han, D. R. Kania, S. McWilliam, and J. W. Ager, "Polycrystalline CVD Diamond Films with High Electrical Mobility," *Science*, vol. 260, pp. 1310-1312, 1993.

48. L. S. Pan, S. Han, D. R. Kania, M. A. Plano, and M. I. Landstrass, "Electrial Properties of High Quality Diamond Films," *Diamond and Related Materials*, vol. 2, pp. 820-824, 1993.

49. N. Fujimori, T. Imai, and A. Doi, "Characterization of Conducting Diamond Films," *Vacuum*, vol. 36, pp. 99-102, 1986.

50. R. Erz, W. Dotter, K. Jung and H. Ehrhardt, "Preparation of Smooth and Nanocrystalline Diamond Films," *Diamond and Related Materials*, vol. 2, pp. 449-453, 1993.

51. Y. Hayashi, W. Drawl, R. W. Collins, and R. Messier, "In-process Ellipsometric Monitoring of Diamond Film Growth by Microwave Plasma Enhanced Chemical Vapor Deposition," *Appl. Phys. Lett.*, vol. 60, no. 23, pp. 2868-2870, 1992.

52. E. J. Bienk and S. S. Eskildsen, "The Effect of Surface Preparation on the Nucleation of Diamond on Silicon," *Diamond and Related Materials*, vol. 2, pp. 432-437, 1993.

53. J. S. Ma, H. Kawarada, T. Yonehara, J. I. Suzuki, J. Wei, Y. Yokota and A. Hiraki, "Selective Nucleation and Growth of Diamond Particles by Plasma-assisted Chemical Vapor Deposition," *Appl. Phys. Lett.*, vol. 55, no. 11, pp. 1071-1073, 1989.

54. M. P. Everson and M. A. Tamor, "Studies of Nucleation and Growth Morphology of Boron-doped Diamond Microcrystals by Scanning Tunnelling Microscopy," *J. Vac. Sci. Technol. B*, vol. 9, no. 3, pp. 1570-1575, 1991.

55. S. Iijima, Y. Aikawa, and K. Baba, "Early Formation of Chemical Vapor Deposition Diamond Films," *Appl. Phys. Lett.*, vol. 57, no. 25, pp. 2646-2648, 1990.

56. K. Hirabayashi, Y. Taniguchi, O. Takamatsu, T. Ikeda, K. Ikoma, and N. Iwasaki-Kurihara, "Selective Deposition of Diamond Crystals by Chemical Vapor Deposition Using a Tungsten-filament Method," *Appl. Phys. Lett.*, vol. 53, no. 19, pp. 1815-1817, 1988.

57. B. W. Sheldon, R. Csencsits, J. Rankin, and R. E. Boekenhauer, "Bias-enhanced Nucleation of Diamond During Microwave-assisted Chemical Vapor Deposition," *J. Appl. Phys.*, vol. 75, no. 10, pp. 5001-5008, 1994.

58. B.R. Stoner, G. H. Ma, S. D. Wolter, and J. T. Glass, "Characterization of Bias-enhanced Nucleation of Diamond on Silicon by in vacuo Surface Analysis and Transmission Electron Microscopy," *Phys. Rev. B*, vol. 45, pp. 11067-11084, 1992.

59. X. Jiang, C. P. Klages, R. Zachai, M. Hartweg, and H. J. Fusser, "Epitaial Diamond Thin Films on (001) Silicon Substrates," *Appl. Phys. Lett.*, vol. 62, pp. 3438-3440, 1993.

60. M. P. Everson and M. A. Tamor, "Investigation of Growth Rates and Morphology for Diamond Growth by Chemical Vapor Deposition," *J. Mater. Res.*, vol. 7, no. 6, pp. 1438-1443, 1992.

61. A. Masood, M. Aslam, M. A. Tamor and T. J. Potter, "Techniques for Patterning CVD Diamond Films on Non-diamond Substrates," *J. Electrochem. Soc.*, vol. 138, no. 11, pp. L67-L68, 1991.

62. J. C. Angus and C.C. Hayman, "Low-temperature, Metastable Growth of Diamond and Diamond-like Phases," *Science*, vol. 241, pp. 913-922, 1988.

63. F. P. Bundy, H. T. Hall, H. M. Storng and R. H. Wentroff, "Man-made Diamond," *Nature*, vol. 176, pp. 51-55, 1955.

64. S. Matsumoto, Y. Sato, M. Kamo and N. Setaka, "Vapor Deposition of Diamond Particles from Methane," *Jpn. J. Appl. Phys.*, vol. 21, pp. L183-L185, 1982.

65. S. Matsumoto, Y. Sato, M. Tsutsumi and N. Setaka, "Growth of Diamond Particles from Methane-hydrogen Gas," *J. Materials Science*, vol. 17, pp. 3106-3122, 1982.

66. J. C. Angus, Y. Wang, and M. Sunkara, "Metastable Growth of Diamond and Diamond-like Phases," *Annu. Rev. Mater. Sci.*, vol. 21, pp. 221-248, 1991.

67. T. D. Moustakas, "Growth of Diamond by CVD Methods and Effects of Process Parameters," *Synthetic Diamond: Emerging CVD Science and Technology*, Ed. K. E. Spear and J. P. Dismukes, pp. 145-192, John Wiley & Sons, New York, 1994.

68. K. Suzuki, A. Sawabe, H. Yasuda, and T. Inuzuka, "Growth of Diamond Thin Films by DC Plasma Chemical Vapor Deposition," *Appl. Phys. Lett.*, vol. 50, no. 12, pp. 728-729, 1987.

69. S. Matsumoto, "Chemical Vapour Deposition of Diamond in RF Glow Discharge," *J. Mater. Sci. Lett.*, vol. 4, pp. 600-602, 1985.

70. K. A. Snail, R. G. Vardiman, J. P. Estrera, J. W. Glesener, C. Merzbacher, C. J. Craigie, C. M. Marks, R. Glosser, and J. A. Freitas, Jr., "Diamond Growth in Turbulent Oxygen-acetylene Flames," *J. Appl. Phys.*, vol. 74, no. 12, pp. 7561-7571, 1993.

71. G. M. Ma, B. E. Williams, J. T. Glass, and J. T. Prater, "Analysis via Transmission Electron Microscopy of the Quality of Diamond Films Deposited from the Vapor Phase," *Diamond and Related Materials*, vol. 1, pp. 25-32, 1991.

72. J. J. Dubray, C. G. Pantano, M. Meloncelli, and E. Bertran, "Nucleation of Diamond on Silicon, SiAlON, and Graphite Substrates Coated with an a-C:H Layer," *J. Vac. Sci. Technol. A*, vol. 9, no. 6, pp. 3012-3018, 1991.

73. G. S. Yang and M. Aslam, "Ultrahigh Nucleation Density for Growth of Smooth Diamond Films," *Appl. Phys. Lett.*, vol. 66, no. 3, pp. 311-313, 1995.

74. Y. Namba, E. Heidrarpour, and M. Nakayama, "Size Effects Appearing in the Raman Spectra of Polycrystalline Diamond," *J. Appl. Phys.*, vol. 72, no. 5, pp. 1748-1751, 1992.

75. S. L. Flegler, J. W. Heckman, and K. L. Klomparens, *Scanning and Transmission Electron Microscopy*, W. H. Freeman and Company, New York, 1993.

76. J. B. Bindell, "Scanning Electron Microscopy," *Encyclopedia of Materials Characterization*, Ed. C. R. Brundle, C. A. Evans, Jr., and S. Wilson, pp. 70-84, Butterworth-Heinemann, Boston, 1992.

77. R. S. Howland and M. D. Kirk, "Scanning Tunnelling Microscopy and Scanning Force Microscopy," *Encyclopedia of Materials Characterization*, Ed. C. R. Brundle, C. A. Evans, Jr., and S. Wilson, pp. 85-98, Butterworth-Heinemann, Boston, 1992.

78. J. D. Hunn and C. P. Christensen, "Ion Beam and Laser-assisted Micromachining of Single-crystal Diamond," *Solid State Technology*, pp. 57-60, 1994.

79. M. W. Leksono and H. R. Shanks, "Patterning of Microwave Plasma Deposited Diamond Films," *Mat. Res. Soc. Symp. Proc.*, vol. 189, pp. 87-90, 1991.

80. T. Roppel, R. Ramesham, C. Ellis, and S. Y. Lee, "Thin Film Diamond Microstructures," *Thin Solid Films*, vol. 212, pp. 56-62, 1992.

81. P. R. de la Houssaye, C. M. Penchina, C. A. Hewett, J. R. Zeidler, and R. G. Wilson, "Hall Mobility and Carrier Concentration versus Temperature for Type IIa Natural

Insulating Diamond Doped with Boron by Ion Implantation," *J. Appl. Phys.*, vol. 71, no.7, pp. 3220-3224, 1992.

82. J. Bernholc, S. A. Kajihara, and A. Antonelli, "Theory of Doping of Diamond," *Mat. Res. Soc. Symp. Proc.*, vol. 242, pp. 323-333, 1992.

83. G. Z. Cao, F. A. J. M. Driessen, G. J. Bauhuis, L. J. Giling, and P. F. A. Alkemade, "Homoepitaxial Diamond Films Codoped with Phosphorus and Nitrogen by Chemical Vapor Deposition," *J. Appl. Phys.*, vol. 78, no. 5, pp. 3125-3131, 1995.

84. J. G. Ran, C. Q. Zheng, J. Ren, and S. M. Hong, "Properties and Texture of B-doped Diamond Films as Thermal Sensor," *Diamond and Related Materials*, vol. 2, pp. 793-796, 1993.

85. G. Kawaguchi, J. Nakanishi, A. Otsuki, T. Oku, and M. Murakami, "Dependence of Contact Resistance on Metal Electronegativity for B-doped Diamond Films," *J. Appl. Phys.*, vol. 75, no. 10, pp. 5165-5170, 1994.

86. C. F. Chen and S. H. Chen, "Effects of Annealing on the Electrical Properties of Boron-doped Diamond Films," *Advances in New Diamond Science and Technology*, Ed. S. Saito, N. Fujimori, O. Fukunaga, M. Kamo, K. Kobashi and M. Yoshikawa, MYU, Tokyo, pp. 709-712, 1994.

87. A. Otsuki, J. Nakanishi, G. Kawaguchi, T. Oku, and M. Murakami, "Formation of Carbide Ohmic Contacts for p-type Diamond," *Advances in New Diamond Science and Technology*, Ed. S. Saito, N. Fujimori, O. Fukunaga, M. Kamo, K. Kobashi, and M. Yoshikawa, MYU, Tokyo, pp. 713-716, 1994.

88. C. A. Hewett, M. J. Taylor, J. R. Zeidler, and M. W. Geis, "Spectfic Contact Resistance Measurements of Ohmic Contacts to Semiconducting Diamond," *J. Appl. Phys.*, vol. 77, no. 2, pp. 755-760, 1995.

89. J. Nakanishi, A. Otsuki, T. Oku, O. Ishiwata, and M. Murakami, "Formation of Ohmic Contacts to p-type Diamond Using Carbide Forming Metals," *J. Appl. Phys.*, vol. 76, no. 4, pp. 2293-2298, 1994.

90. Y. Nishibayashi, N. Toda, H. Shiomi, and S. Shikata, "Thermally Stable Ohmic Contact to Boron Doped Diamond Films," *Advances in New Diamond Science and Technology*, Ed. S. Saito, N. Fujimori, O. Fukunaga, M. Kamo, K. Kobashi, and M. Yoshikawa, MYU, Tokyo, pp. 717-720, 1994.

91. B. A. Fox, D. M. Malta, H. A. Wynands, S. R. Sahaida and J. A. von Windheim,

"High Temperature Electrical Measurements and Properties of Diamond," *Proceeding of 2nd International High Temperature Electronics Conference*, vol. 2, pp. VI3-8, Charlotte, NC, 1994.

92. P. R. Chalker, C. Johnson, J. A. A. Crossley, J. Ambrose, C. F. Ayres, R. E. Harper, I. M. Buckley-Golder, and K. Kobashi, "Degradation Mechanisms of Passivated and Unpassivated Diamond Thermistors," *Diamond and related Materials*, vol. 2, pp. 1100-1106, 1993.

93. A. D. Khazan, *Transducers and Their Elements*, PTR Prentice Hall, Englewood Cliffs, NJ, 1994.

94. L. J. Van der Pauw, "A Method of Measuring Specific Resistivity and Hall Effect of Discs of Arbitrary Shapes," *Phillips Res. Repts*, vol. 13, pp. 1-9, 1958.

95. D. M. Malta, J. A. von Windheim, H. A. Wynands, and B. A. Fox, "Comparison of the Electrical Properties of Simultaneously Deposited Homoepitaxial and Polycrystalline Diamond Films," *J. Appl. Phys.*, vol. 77, no. 4, pp.1536-1545, 1995.

96. L. S. Pan, D. R. Kania, P. Pianetta, J. W. Ager, M. I. Landstrass, and S. Han, "Temperature Dependent Mobility in Single-crystal and Chemical Vapor-deposited Diamond," *J. Appl. Phys.*, vol. 73, no. 6, pp. 2888-2894, 1993.

97. J. P. Bade, S. R. Sahaida, B. R. Stoner, J. A. von Windheim, J. T. Glass, K. Miyata, K. Nishimura, and K. Kobashi, "Fabrication of Diamond Thin-film Thermistors for High-temperature Applications," *Diamond and Related Materials*, vol. 2, pp. 816-819, 1993.

98. G. S. Yang and M. Aslam, "CVD Diamond Resistor as Heater and Temperature Sensor," *Applications of Diamond Films and Related Materials; Third International Conference*, Ed. A. Feldman, Y. Tzeng, W. A. Yarbrough, M. Yoshikawa, and M. Murakawa, NIST Special Publication, Washington D. C., pp. 125-128, 1995.

99. D. R. Kania, M. I. Landstrass, M. A. Plano, L. S. Pan, and S. Han, "Diamond radiation detectors," *Diamond and related Materials*, vol. 2, pp. 1012-1019, 1993.

100. V. V. Tokiy, V. I. Timchenko, V. A. Soroka, N. Tokiy, B. V. Spitsyn, and L. L. Bouilov, "Diamond Film Metal-Semiconductor-Metal Photodetector," *Applications of Diamond Films and Related Materials; Third International Conference*, Ed. A. Feldman, Y. Tzeng, W. A. Yarbrough, M. Yoshikawa, and M. Murakawa, NIST Special Publication, Washington D. C., pp. 145-148, 1995.

101. S. Han, R. S. Wagner, J. Joseph, M. A. Plano, and M. D. Moyer, "Chemical Vapor Deposited Diamond Radiation Detectors for Ultrahigh Radiation Dose-rate Measurements: Response to Subnanosecond, 16-MeV Electron Pulses," *Rev. Sci. Instrum.*, vol. 66, no. 12, pp. 5516-5521, 1995.

102. S. Han, S. G. Prussin, L. S. Pan, D. R. Kania, S. M. Lane, G. Dennis, R. S. Wagner, and K. Harris, "Temporally Resolved Response of a Natural Type IIA Diamond Detector to Single-Particle Excitation," *Diamond and Related Materials*, vol. 2, pp. 835-840, 1993.

103. V. F. Dvoryankin, A. A. Kudryashov, Yu. Sh. Temirov, L. L. Bouilov, G. A. Sokolina, and A. E. Alexenko, "CVD Diamond Films for X-ray Detectors," *Applications of Diamond Films and Related Materials; Third International Conference*, Ed. A. Feldman, Y. Tzeng, W. A. Yarbrough, M. Yoshikawa, and M. Murakawa, NIST Special Publication, Washington D. C., pp. 145-148, 1995.

104. S. H. Lin and L. H. Sverdrup, "Electron Beam Activated Diamond Devices," *Applications of Diamond Films and Related Materials; Third International Conference*, Ed. A. Feldman, Y. Tzeng, W. A. Yarbrough, M. Yoshikawa, and M. Murakawa, NIST Special Publication, Washington D. C., pp. 79-82, 1995.

105. M. Marchywka, J. Hochedez, M. W. Geis, D. G. Socker, D. Moses, and R. T. Goldberg, "Ultraviolet Photoresponse Characteristics of Diamond Diodes," *Appl. Optics*, vol. 30, no. 34, pp. 5011-5013, 1991.

106. M. Marchywka and D. Moses, "Optical Characterization of Diamond MIS Capacitors," *IEEE Trans. Elect. Devices*, vol. 41, no. 7, pp. 1265 - 1272, 1994.

107. V. I. Latsa and Y. M. Rotner, "Effect of Axial Pressure on Some Properties of Synthetic Semiconductor Diamonds (original in Russian)," *Vys. Davleniya Svoita Mater.*, pp. 55-59, 1980.

108. V. I. Latsa, I. N. Mikhailik, and G. V. Krishchuk, "Current-Voltage Characteristics of Synthetic Diamond under Pressure (original in Russian)," *Fiz. Tekh. Vys. Davlenii.*, vol. 9, pp. 62-65, 1982.

109. M. Aslam, I. Taher, A. Masood, M. A. Tamor, and T. J. Potter, "Piezoresistivity in Vapor Deposited Diamond Films," *Appl. Phys. Lett.*, vol. 60, pp. 2923-2925, 1992.

110. I. Taher, M. Aslam, M. A. Tamor, T. J. Potter, and R. C. Elder, "Piezoresistive Microsensors Using P-type CVD Diamond Films," *Sensors and Actuators: A*, vol. 45, pp. 35-43, 1994.

111. D. R. Wur, J. L. Davidson, W. P. Kang, and D. L. Kinser, "Polycrystalline Diamond Pressure Sensor," *J. of Microelectromechanical System*, vol. 4, no. 1, pp. 34-41, 1995.

112. S. Sahli, X. Hou, and M. Aslam, "Piezoresistive Gauge Factor of Polycrystalline Diamond Measured at Different Fields and Temperatures," *Applications of Diamond Films and Related Materials; Third International Conference*, Ed. A. Feldman, Y. Tzeng, W. A. Yarbrough, M. Yoshikawa, and M. Murakawa, NIST Special Publication, Washington D. C., pp. 95-98, 1995.

113. Y. Gurbuz, W. P. Kang, J. L. Davidson, D. V. Kerns, and B. Henderson, "High Sensitivity and Wide Temperature Tolerance Hydrogen Gas Sensors Utilizing PECVD Diamond Technology," *Applications of Diamond Films and Related Materials; Third International Conference*, Ed. A. Feldman, Y. Tzeng, W. A. Yarbrough, M. Yoshikawa, and M. Murakawa, NIST Special Publication, Washington D. C., pp. 87-90, 1995.

114. J. Zhang, B. Huang, D. K. Reinhard, and J. Asmussen, "An Investigation of The Effects of Electromagnetic Field Patterns on Microwave Plasma Diamond Thin Film Deposition," *J. Vac. Sci. and Technol. A*, vol. 8, pp. 2124-2128, 1990.

115. J. Zhang, "Diamond Thin Film Deposition by Microwave Plasma Enhanced Chemical Vapor Deposition," *Ph. D. dissertation*, Michigan State University, 1992.

116. M. J. Ulczynski, D. K. Reinhard, M. Prystajko, and J. Asmussen, "Low Temperature Deposition of Thin Film Diamond," *Advances in New Diamond Science and Technology*, Ed. S. Saito, N. Fujimori, O. Fukunaga, M. Kamo, K. Kobashi and M. Yoshikawa, MYU, Tokyo, pp. 41-44, 1994.

117. G. S. Yang, M. Asalm, K. P. Kuo, D. K. Reinhard, and J. Asmussem, "Effect of Ultrahigh Nucleation Density on Diamond Growth at Different Growth Rates and Temperatures," *J. Vac. Sci. and Technol. B*, vol. 13, no. 3, pp. 1030-1036, 1995.

118. The atomic force microscope unit is a Nano Scope III from Digital Instruments Corporation.

119. M. A. Tamor and M. P. Everson, "On the Role of Penetration Twins in the Morphological Development of Vapor-Grown Diamond Films," *Proceeding of SPIE Conference on Diamond-Film Semiconductors*, pp. 14-25, Los Angeles, CA, 1994.

120. K. Bekku, Y. Mori, N. Eimori, H. Makita, A. Hatta, T. Ito, and A. Hiraki, "Growth and Characterization of CVD Diamond Films Doped with Phosphorous," *Advances*

in New Diamond Science and Technology, Ed. S. Saito, N. Fujimori, O. Fukunaga, M. Kamo, K. Kobashi and M. Yoshikawa, MYU, Tokyo, pp. 701-704, 1994.

121. L. J. Giling, Y. S. Wang, G. Z. Cao, G. J. Bauhuis, and P. F. A. Alkemade, "Diamond Films Co-doped with Phosphorus and Nitrogen," *Advances in New Diamond Science and Technology*, Ed. S. Saito, N. Fujimori, O. Fukunaga, M. Kamo, K. Kobashi and M. Yoshikawa, MYU, Tokyo, pp. 359-362, 1994.

122. M. A. Plano, S. Zhao, C. F. Gardinier, M. I. Landstrass, D. R. Kania, H. Kagan, K. K. Gan, R. Kass, L. S. Pan, S. Han, S. Schnetzer, and R. Stone, "Thickness Dependence of the Electrical Characteristics of Chemical Vapor Deposited Diamond Films," *Appl. Phys. Lett.*, vol. 64, no. 2, pp. 193-195, 1994.

123. The definition of zero-power resistance is reprinted from MIL-T-23648A, the US Department of Defense general specification for thermistors.

124. G. S. Yang and D. M. Aslam, "Single-structure Heater and Temperature Sensor Using a p-type Polycrystalline Diamond Resistor," *IEEE Electron Device Letters*, vol. 17, no. 5, pp. 250-252, 1996.

125. M. Werner, O. Dorsch, H. U. Baerwind, E. Obermeier, L. Haase, W. Seifert, A. Ringhandt, C. Johnston, S. Romani, H. Bishop, and P. R. Chalker, "Charge Transport in Heavily B-doped Polycrystalline Diamond Films," *Appl. Phys. Lett.*, vol. 64, no. 5, pp. 595-597, 1994.

126. P. J. French and A. G. R. Evans, "Piezoresistance in Polysilicon and its Applications to Strain Gauges," *Solid State Electronics*, vol. 32, no. 1, pp. 1-10, 1989.

127. M. I. Landstrass and K. V. Ravi, "Resistivity of Chemical Vapor Deposited Diamond Films," *Appl. Phys. Lett.*, vol. 55, no. 10, pp. 975-977, 1989.

128. S. Albin and L.Watkins, "Electrical Properties of Thin Film and Bulk Diamond Treated in Hydrogen Plasma," *Diamond, Silicon Carbide, and Related Wide Bandgap Semiconductors*, Ed. J. T. Glass, R. Messier, and N. Fujimori, Materials Research Society Symposium Proceedings, vol. 162, pp. 303-308, 1990.

129. A. T. Collins, "The Optical and Electronic Properties of Semiconducting Diamond," *Philos. Trans. R. Soc. London A*, vol. 342, pp. 233-244, 1993.

130. S. Sahli and D. M. Aslam, "Effect of Post-deposition Anneal on the Resistivity of P-type Polycrystalline Diamond Films," in review by *Appl. Phys. Lett.*, 1996.

131. Y. Muto, T. Sugino, and J. Shirafuji, "Electrical Conduction in Undoped Diamond Films Prepared by Chemical Vapor Deposition," *Appl. Phys. Lett.*, vol. 59, no. 7, pp. 843-845, 1991.

132. H. Shiomi, K. Tanabe, Y. Nishibayashi, and N. Fujimori, "Epitaxial Growth of High Quality Diamond Film by the Microwave Plasma-Assisted Chemical-Vapor-Deposition Method," *Jap. J. Appl. Phys.*, vol. 29, pp. 34-40, 1990.

133. A. J. Chapman, *Heat Transfer*, Macmillan Co., New York, 1960.

134. A. I. Brown and S. M. Marco, *Introduction to Heat Transfer*, McGraw Hill Co., New York, 1958.


MICHIG
3